THE UNIVERSITY OF CHICAGO

EXPLORING THE INCLUSION OF DYNAMIC BONDS INTO ADAPTIVE LIQUID CRYSTALLINE FUNCTIONAL POLYMERS

A DISSERTATION SUBMITTED TO

THE FACULTY OF THE PRITZKER SCHOOL OF MOLECULAR ENGINEERING

IN CANDIDACY FOR THE DEGREE OF

DOCTOR OF PHILOSOPHY

BY

CHARLOTTE AUBRIE LINDBERG

CHICAGO, ILLINOIS

AUGUST 2025

Chapter 2 is adapted from: C. Lindberg et al. “Exploring the effect of dynamic bond placement in liquid crystal elastomers, *J. Polym. Sci.* **2024**, *62*, 907–915.

Chapter 3 is adapted from: C. Lindberg et al. “Should I stay or should I flow? An exploration of phase-separated liquid crystal polymers” *Chem. - A Eur. J.* **2025**, 2011854.

Chapter 4 is adapted from: C. Lindberg et al. “Stuck on repeat: Dynamic liquid crystal elastomers as (re)trainable adhesives *In prep.*

.

To the friends I made along the way. Thank you for everything.

“People speak of hope as if it is this delicate, ephemeral thing made of whispers and spider's webs. It's not. Hope has dirt on her face, blood on her knuckles, the grit of the cobblestones in her hair, and just spat out a tooth as she rises for another go.”

- Matthew (@CrowsFault)

TABLE OF CONTENTS

LIST OF FIGURES

ACKNOWLEDGEMENTS

I could fill another entire dissertation-sized document with the details of my undying gratitude for all the folks who I've crossed paths with on this journey. Your support has allowed me to make it all this way, and for that I am incredibly grateful.

To my family: Thank you for all your love and support these last eight years. It has meant the world to me to have you cheering me on from back home from the beginning all the way through to the end.

To Stuart: You have been one of the greatest teachers I could have asked for in an advisor. Even as I'm nearing the end of my time in the lab, I still find myself learning things from you in both scientific and professional contexts. The high standards you have for the work we perform and publish in the lab and your passion for "kick-ass science" are truly aspirational and things I will strive to emulate in my own future lab.

To Aaron Esser-Kahn and Sihong Wang: Thank you for serving on both my candidacy and dissertation committees. It has been an honor and a pleasure to have gotten to work with both of you through the different collaborative centers I've been a part of during my time at UChicago. I truly appreciate your feedback and guidance over the years.

To the Rowan group past and present: There's no one else I would have rather served with during the completion of this PhD. Words can't express how grateful I am to have found a group of people

as fun, supportive, and accepting as you all have been, and I couldn't imagine having a better environment to have figured myself out in. I wish you all nothing but the best, and keep on being respectful to daddy.

To Debbie: I've always truly admired your commitment to excellence for yourself and those around you, your no-b******* approach to science and life, and your compassionate approach to mentoring. Thank you for taking me under your wing during my first year as a scared, imposter syndrome riddled chemist playing engineer. Your willingness to answer my dumb questions without making me feel stupid singlehandedly kept me from leaving the program when I was not sure if grad school was somewhere I belonged, and for that I will be forever grateful.

To Alice, Sean, and Elina: Thank you all for being such amazing mentees and friends. Helping you three find your footing and watching you come into your own in lab have been without a doubt the most rewarding parts of my PhD and are honestly what swayed me toward pursuing a career in academia (in a good way I promise). Alice, keep dunking on haters with your limitless drive and tenacity. Sean, keep feeding your curiosity, and never let anything dim that shine of yours. Elina, never stop never stopping, and always keep an eye out for new opportunities that you'll crush. I am beyond proud of all three of you and can't wait to see where you all end up. Please never ever hesitate to reach out.

To Nick Macke: Thank you for being a most excellent and steadfast compatriot. Your ability to break down problems and view situations from new angles means you always offer the most measured and wisest of counsels (especially when I was on one). Our trips to Panera were always

a highlight of my day and offered the perfect opportunity for a breather to commiserate over L's or celebrate W's. Amidst a grad school experience that had its fair share of tumultuous moments, thank you for being a constant in my life and someone I could rely on.

To Kaden: Thank you for having good taste in music. I mean it. It was such a f****** treat to find someone at UChicago to bond with over music, and that was the moment I knew you had to be good people. Wandering over to your hood to hear about what you were working on whether it was science or music was always a welcome distraction. I know that whenever I ask you for advice it's going to come straight from the heart and you're going to mean every word you say. Thank you for always encouraging (read bullying) me to do things I don't want to (but should do for my own good) and believing in me more than I tend to myself.

To Lauryn: Thank you for always being down to go do a thing. Our adventures really remind me that there is so much more to Chicago than my apartment and the university. It's made me so much more appreciative of this city that we live in and made my time in grad school so much more enjoyable having a friend to explore it with. I appreciate you always pushing (read bullying) me to step out of my comfort zone and try something new as well as impressing upon me the importance of listening when the planets and universe are yelling at me because more often than not they know what they're talking about.

To Aaron and Chris: Thank you for being two of the best friends a girl could possibly ask for. The amount of love, acceptance, joy, and stupidity I experience around you two honestly feels like home and made it so much easier to bounce back on hard days. I never would've thought that

getting a septum piercing would be the catalyst (chemistry pun intended) for welcoming so many wonderful and loving people into my life starting with you two but here I am. I love you guys so much, and your unwavering support of me in whatever I do (in both the good and the questionable) means everything to me.

To Savannah: We did it comrade. We both know you have partial custody of this PhD because there's no way I would've gotten anywhere close to this far without you. Somehow, saying it's been a hell of a journey for the two of us doesn't come close to giving our story justice, but I think it does a pretty good job all things considered. Your expertise, experience, and passion as a teacher are truly inspirational and have undoubtedly shaped my perspectives on education in ways that will impact my future students for the better. I truly can't thank you enough for everything you've done for me. Love ya bud.

ABSTRACT

In Chapter 1, a review and background of stimuli-responsive materials is provided that identifies dynamic liquid crystal elastomers (LCEs) as a promising class of materials with avenues for potential study. In Chapter 2, a tailorable network design allows for the study of dynamic bond placement within disulfide containing LCEs as it pertains to thermomechanical, morphological, and relaxation properties. In Chapter 3, a linear phase-separated metallosupramolecular liquid crystal polymer (MSLCP) was developed to study the impact that phase separation and metallosupramolecular linkages have on liquid crystallinity as well as how these moieties can be leveraged to synthesize more processable LCP materials. In Chapter 4, disulfide containing LCEs are used as a platform for developing adaptive retrainable adhesive materials whose properties can be synthetically tailored through the bulkiness of the mesogen and the resulting control of the stability of the LC phase. Finally, Chapter 5 provides a summary of the work performed as well as some perspectives and outlooks for future research directions.

CHAPTER 1

INTRODUCTION

1.1 Summary

A new frontier in polymer science lies in the development of materials capable of responding and adapting to their environments. Developing materials with greater utility and therefore longevity is one route to challenge the paradigm of single use materials that currently plagues industrially relevant commodity polymers today. Liquid crystal elastomers (LCEs) are a class of stimuli-responsive materials that have been studied in this regard due to their ability to reversibly undergo macroscale physical changes in response to a variety of external environmental cues. The incorporation of dynamic bonds to create dynamic LCE materials has only further enhanced their utility, allowing them to be reprocessed, reprogrammed, and trained. By further incorporating additional stimuli-responsive moieties into these materials, the property profiles can be expanded far beyond what is currently possible into many untapped application spaces.

1.2 Stimuli Responsive Polymers

The idea that the everyday materials we create and interact with should do more and go further has pervaded the human imagination for generations. From Hollywood depictions of Flubber to the T1000, the idea of fantastical synthetic materials capable of doing incredible things is a captivating one that sits as a backdrop for the achievements that scientists today realize and strive toward. Closed loop plastics recycling, competitively performing bio-based commodity materials, and conductive polymers for soft electronics and sensors are just a few of the grand materials challenges[1] that polymer chemists and engineers devote their time and energy to addressing through the design and synthesis of next-generation polymeric materials. One class of materials with particular promise is that of stimuli-responsive polymers. The field of stimuli-responsive polymers is concerned with developing materials whose properties can be intentionally changed in response to a specific environmental condition.[2–4] These responses vary widely and include actions such as shape memory[5,6], color change[7,8], self-healing[9,10], and mechanical property changes.[11] The stimuli to trigger these behaviors can take many forms depending on the moieties

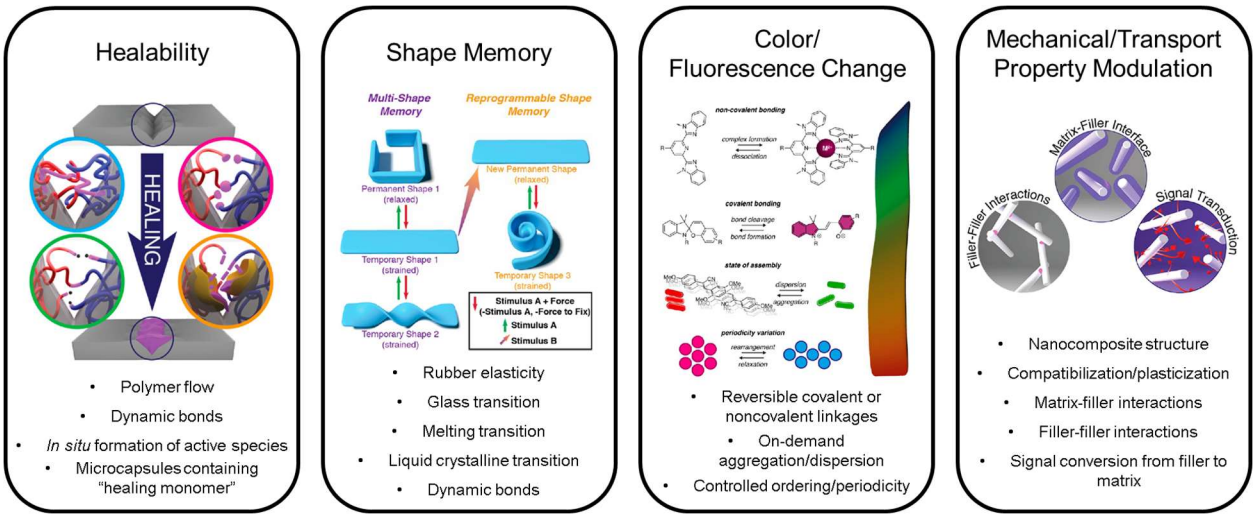

Figure 1.1: A summary of common stimuli-responses and the motifs used to produce them. Adapted from Ref 11. [11]

incorporated and include heat[12,13], light[14,15], pH[16,17], chemical[18,19], and humidity[20,21] to namea few. The acting species within stimuli-responsive materials are just as varied as the stimuli they can be activated with and include primarily include moieties such as phase transitions (melting, glass, liquid crystalline, LCST/UCST)[22,23] and reversible bonds (covalent and noncovalent interactions)[24–26]. Given the large space that stimuli-responsive materials span, they find applications in a range of application spaces including actuators[27], sensors[28], and photonics[29].

1.3 Liquid Crystal Elastomers

Liquid crystal elastomers (LCE) are a subclass of stimuli-responsive polymers characterized by their inclusion of mesogenic monomers into an elastomeric polymer network.[30–32] In 1975, renowned polymer physicist (and future 1991 Nobel laureate in physics) Pierre Gilles de Gennes proposed the existence of a unique class of materials comprised of an elastomeric polymer network containing liquid crystalline (LC) units.[33] He postulated that, in contrast to the highly confined glasses and compact gels comprised of LC monomers that had been previously studied[34], a material with more degrees of freedom in the polymer by way of the introduction of flexible segments would enable the formation of stable and thermally reversible nematic LC domains within the bulk material with the potential for remarkable non-linear elastic properties. It wasn't until five years later in 1981 that such systems were experimentally realized in the first work of its kind by Finkelmann et al.[35] To synthetically access these elastomeric LC systems, polysiloxane prepolymers functionalized with silyl hydride groups were reacted with alkene bearing LC moieties and a dialkene small molecule siloxane crosslinker. Following a careful washing and drying procedure, these materials were evaluated via differential scanning calorimetry where they exhibited low glass transitions in line with elastomeric materials and robust reversible LC transitions demonstrating the first successful incorporation of stable LC phases into a bulk

polymeric network introducing the first generation of liquid crystal elastomers (LCEs) to the polymer community. Notably, these materials were realized using hydrosilation chemistry and formed side chain LCEs where the mesogens were attached in a pendent fashion to the polymer strands of the network. Additionally, it was observed that the orientation of these phases could be facilely altered through simple strain of the bulk LCE film which was accompanied by an observable optical transition as the material transition from its opaque as-cast polydomain state, in which there is local order within the domains while the domains themselves are randomly oriented relative to one another, to a transparent strained monodomain state, in which the strain imposed on the material aligns the mesogens in the direction of strain. Notably, the syntheses of these materials resulted in networks whose equilibrium configuration at crosslinking was that of a polydomain structure and alignment was only achieved when an outside mechanical stress was applied to the material. It was also observed that one could strain these materials to alignment, and then, by thermally disrupting the interactions between the mesogens by heating the material through its LC transition, macroscopically return the material to its initial form factor as the entropy elasticity of the network was allowed to contract the network back to its most energetically favorable state. A follow up work by Kupfer et al.[36] explored materials they dubbed nematic liquid single crystal elastomers (LSCEs). While the first generation of LCEs were materials whose alignment had to be mechanically imposed each time, these LSCEs were partially crosslinked, mechanically aligned, and then fully crosslinked resulting in materials whose original form factor was one with mesogenic alignment. When these materials were heated through their LC transition, they contracted in a similar fashion to their one-way shape memory counterparts, however, upon cooling they returned to their as-crosslinked elongated state exhibiting reversible two-way shape memory behavior. The actuation performance of LCEs was further improved with the realization

of main-chain LCEs by Donnio et al.[37] where the mesogens were located in the backbone of the network strands producing a much more substantial effect on the network upon disordering. While other chemistries were subsequently employed to access main-chain LCEs, the use of thiol-Michael click chemistry became popular for two key reasons. The first is due to the high experimental accessibility of the method due to its facile setup and high conversion as well as the large number of commercially available acrylate-functionalized mesogens. The second reason came from work by Yakacki et al.[38] where they used thiol-Michael chemistry to demonstrate a highly tailorable method for producing LCEs with alignment programmed into them. This method used a base-catalyzed crosslinking to form a partially crosslinked yet robust network which could be strained to alignment followed by a photo-crosslinking step to polymerize any remaining acrylates and lock in the imposed alignment. As such, this method has seen much adoption in the literature since its introduction and is currently one of the most prevalent methods for synthesizing LCE materials.

1.4 Dynamic Liquid Crystal Elastomers

1.4.1 Dynamic Covalent Chemistries

As with conventional crosslinked polymeric materials, a major drawback of such systems is the inability to post-synthetically modify the topology of the network structure as efforts to thermally induce rearrangement ultimately result in the indiscriminate cleavage of chemical bonds and subsequent degradation of the material when high temperatures are applied. One advent to circumvent this shortcoming is the incorporation of dynamic chemistries into these materials as a means of providing linkages that can be selectively broken with a specific stimulus to induce

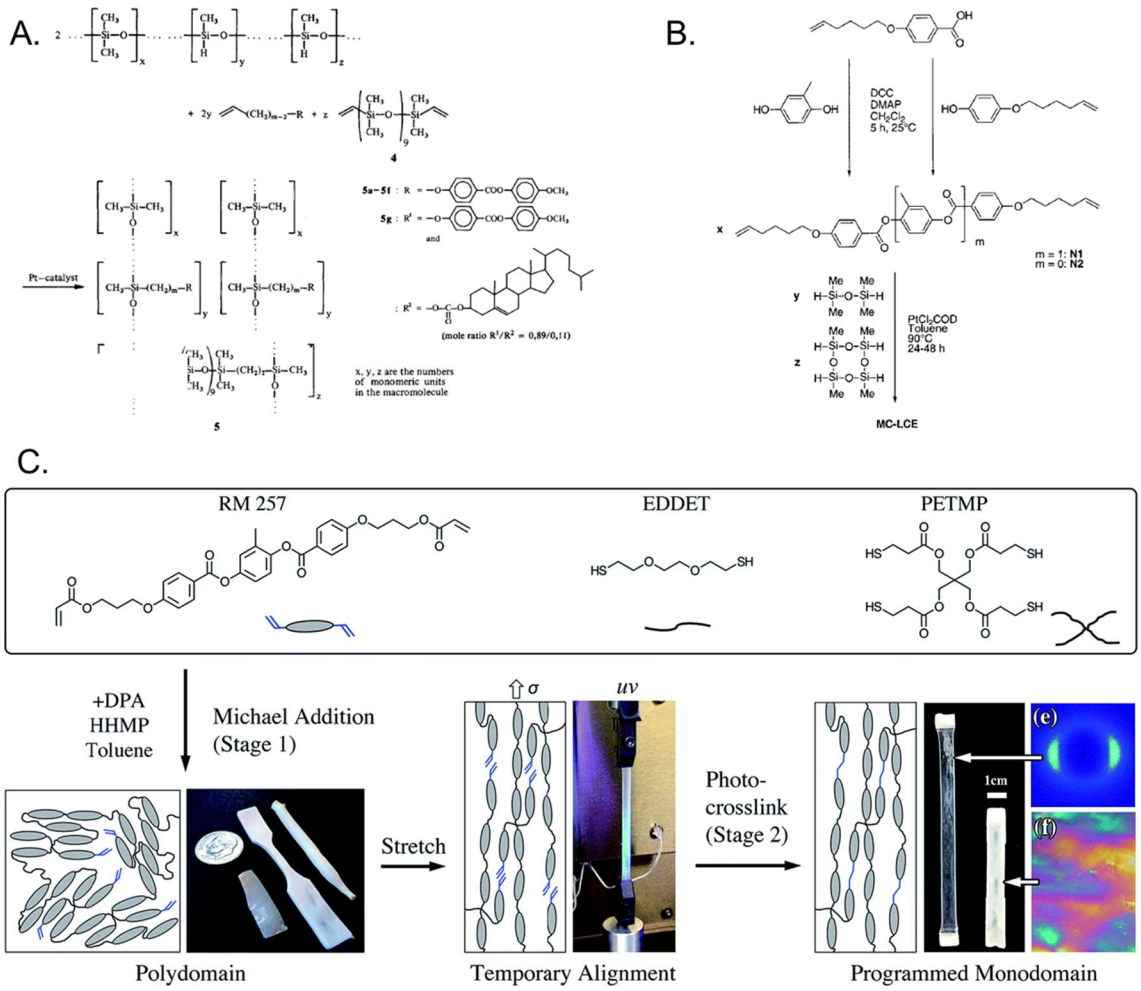

Figure 1.2: A. Synthetic scheme for side-chain LCEs using hydrosilation chemistry[35]; B. Synthetic scheme for main-chain LCEs using hydrosilation chemistry[37]; C. Synthetic formulation and alignment programming procedure enabled by a two-step thiol-Michael click chemistry[38]

network rearrangement and subsequently reformed upon removal of that stimulus. The first example of the implementation of this method into LCEs was from Pei et al.[39] where an LCE was prepared from an epoxy functionalized mesogen and a carboxylic acid bearing chain extender via the triazabicyclodecene (TBD) catalyzed epoxy ring-opening reaction. By allowing the TBD catalyst to remain in the material in the presence of the newly formed alcohol functional groups produced during the polymerization, it was possible to induce associative transesterification exchange reactions at high temperatures with the polymer's backbone ester groups (Figure 1.XX).

By activating these catalyzed reactions with high temperature (>160 °C) it became possible to reprocess and reprogram these materials allowing for the post-synthetic modification of the form factor of the bulk material as well as programming of the alignment of the mesogens. This implementation of exchangeable ester linkages with the mesogenic properties of the LCE opened the door for the incorporation of many dynamic chemistries including esters[40,41], disulfides[42–45], carbamates[46], addition fragmentation transfer adducts[47–49], aza-Michael bonds[50,51], and boronic esters[52]. The choice of dynamic chemistry ultimately depends on the desired pathway for the programming or reprocessing as each chosen chemistry will have its own specific set of equilibrium kinetics, required activation conditions, and environmental/chemical tolerances. One example of this is highlighted in work by Ghimire et al.[51] where the reaction and relaxation rates of an aza-Michael chemistry were tuned by the choice of catalyst employed. This allowed for both

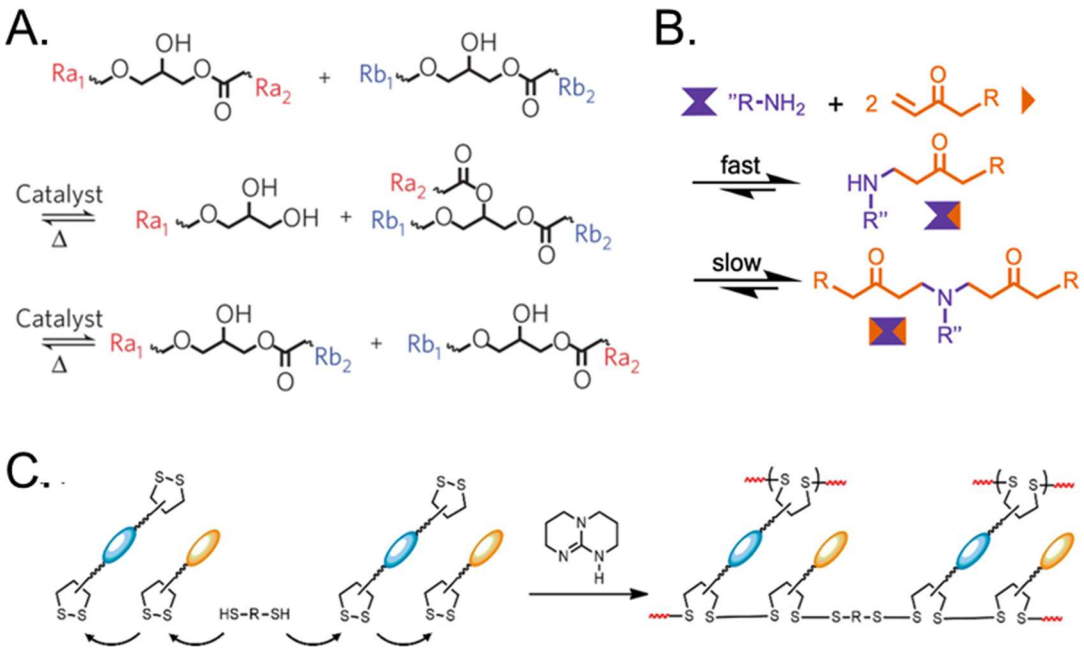

Figure 1.3: Examples of dynamic covalent chemistries employed in LCEs A. Catalyzed transesterification mechanism[53]; B. A mechanism for aza-Michael addition/rearrangement[51]; C. Scheme of disulfide incorporation into a dynamic LCE using a cyclic disulfide based feedstock[44]

control over the rate of formation of the network as well as the stress relaxation properties of the material if the catalyst was left in rather than removed. Another example of a dynamic linkage commonly used in dynamic LCEs is the disulfide bond. Disulfides are multi-responsive as they can be activated with heat[12], light, redox[54], or mechanical force[55] which gives an array of options for inducing their exchange within a material. One report by Huang et al. utilized cyclic disulfide containing mesogens that they ring-opened to form disulfide containing LCE networks (Figure 1.XX). These materials were highly reprocessable due to the high concentration and regular incorporation of the dynamic bond along the backbone of the material. These examples showcase the versatility of dynamic covalent interactions and their incorporation into LCEs thus far.

1.4.2 Noncovalent Interactions

Although less explored than dynamic covalent chemistries, noncovalent interactions also have been employed in LCEs as a crosslinking motif. While noncovalent interactions are typically weaker in strength, incorporating them at higher concentrations or coupling them with an additional structural mode such as phase separation allows for the formation of robust functional materials despite the inclusion of a much more active exchangeable moiety.[56–58] Some noncovalent interactions of note include hydrogen bonds[59,60], halogen bonds[61,62], and ionic interactions.[18,63–65] These weaker interactions allow for a more drastic transformation of the bulk phase of the material as the faster exchange of "load-bearing" linkages provides a mechanism by which rearrangement can occur at a much more substantial rate and extent. One example of noncovalent interactions being leveraged in LC polymers is work by Lugger et al.[66] incorporated thiourea moieties into linear LC polymers to form polythiourethane (PTU) LCEs crosslinked by hydrogen bonds. The PTU LCE materials were capable of being melt processed using an extrusion-

based 3D printer setup offering the ability to have a fully cured feedstock of printer material as well as the capacity for the direct recycling of the printed material post fabrication by thermally cleaving the supramolecular crosslinks. As such, due to the enhanced processing capability imparted through the use of noncovalent interactions instead of conventional crosslinking approaches, further study of this class of moiety in LC materials could be advantageous in future applications.

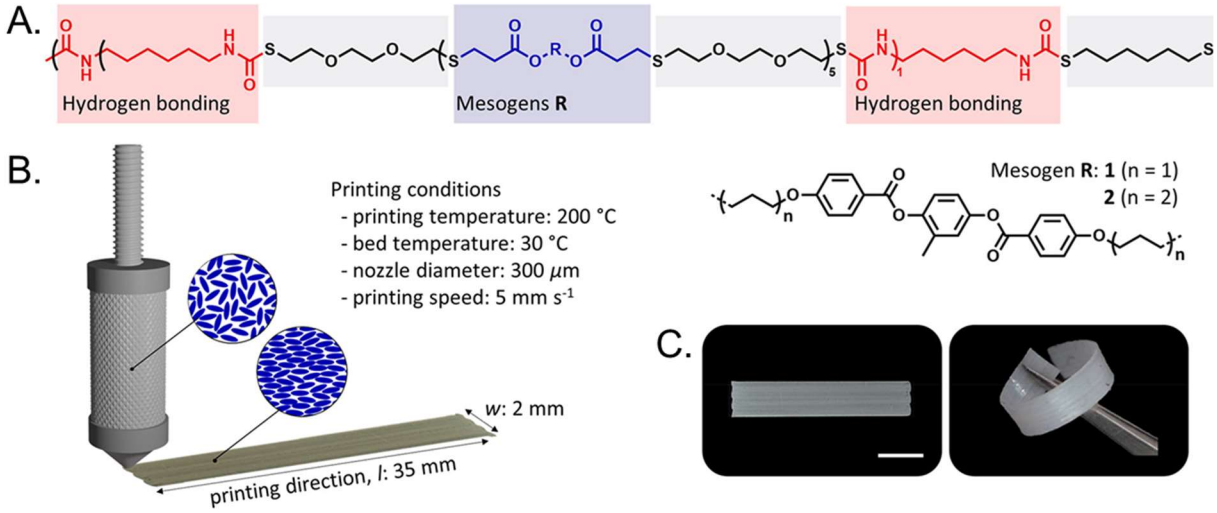

Figure 1.4: A. Chemical structure of a PTU LCE; B. 3D printer schematic with the conditions for printing; C. Optical images of a 3D printed piece of PTU LCE[66]

1.5 Applications of Polymeric Liquid Crystalline Polymers

Due to the versatile nature of their thermomechanical properties, polymeric LC materials can be tuned to have a wide range of properties. As such, the LC transition temperature has been controlled through a variety of methods including mesogen architecture[67], mesogen concentration[68], crosslink density[69,70], chain extender content[71,72], and the incorporation of additional interpolymer interactions[73] just to name a few. By controlling the stability of the LC

phase, one can directly tailor the material to have the desired LC transition temperature for a given application or environment. This ability to finely control these properties allows them to find use in a range of fields including biomedical applications, damping, and adhesives which despite being a rather disparate set of applications, each use case directly leverages the LC character of the materials.

1.5.1 Energy Dissipating Materials

Materials for dissipating energy or damping vibration are another application where LCEs have been utilized. Their ability to operate in this capacity stems from the rotational modes of the mesogens within the network. Depending on the magnitude of the strain imposed by the stress either the rotation of the nematic domains or the mesogens themselves provides a pathway by which this energy is transferred to overcoming the inertia of the domains or mesogens respectively before the polymer network itself is perturbed or distorted. Work by Luo et al.[74] explored using LCEs as a base material in 3D printed foam architectures. In traditional polymeric foams, it is the deformation and buckling of the foam architecture that imparts cushioning in the event of an impact. This work used 3D printing to fabricate similar structures comparing amorphous non-LC foams to foams printed with an LC feedstock. It was found that the LC foams had superior impact mitigation performance in terms deceleration achieved and energy dissipation. They further demonstrated this by dropping eggs from a set height onto amorphous and LC foam constructs (Figure 1.XX) resulting in breakage and survival respectively highlighting the additional dissipative character that the LC nature of the material provides. Work by Shaha et al.[75] utilized the damping ability of LCEs if a different way by applying it toward biomedical applications. In

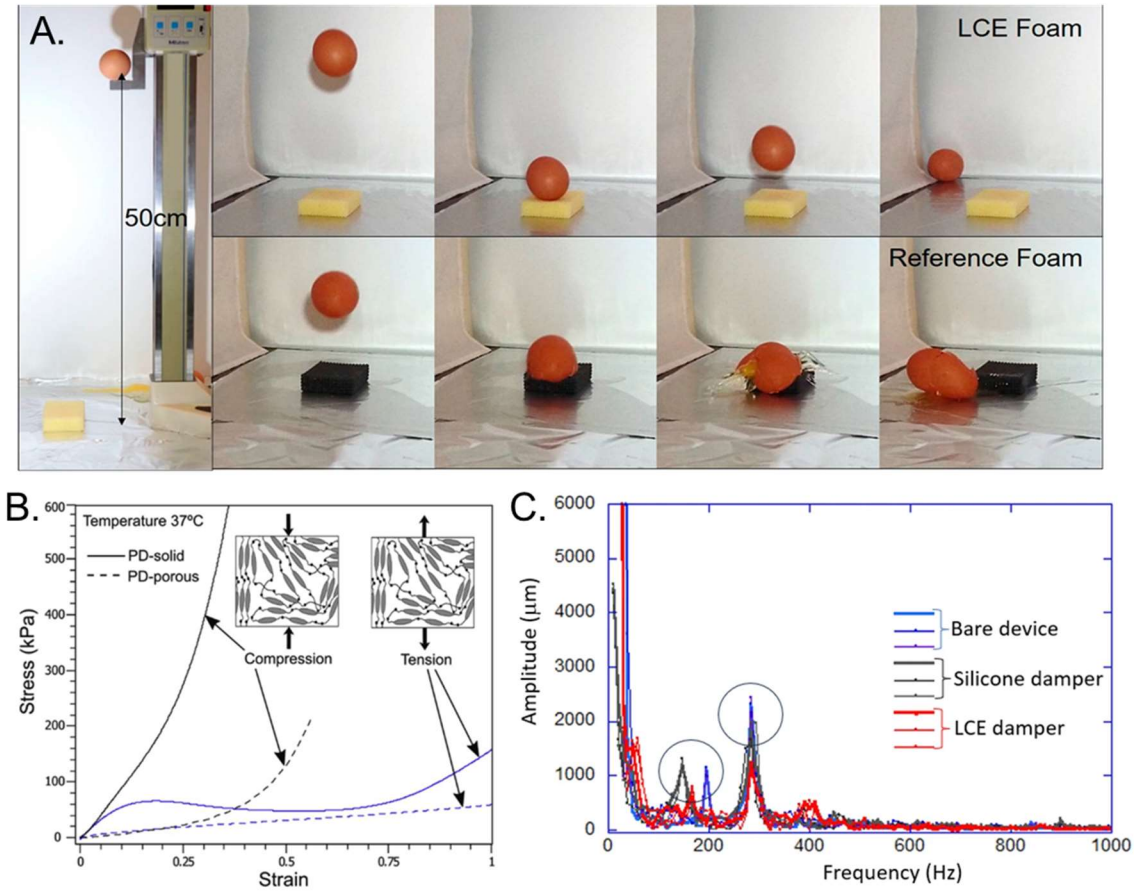

Figure 1.5 A. Impact drop testing of eggs onto 3D printed foams comprised of LCE (top) and an amorphous reference (bottom)[74]; B. Compression and tensile testing comparing porous and solid LCE monoliths[75]; C. Vibration spectra of a handheld drill demonstrating the difference between no damping layer, a silicone damper, and an LCE damper

this work a series of bulk and porous LCE scaffolds with different alignments were studied as load-bearing intervertebral disc implants in rats. In addition to proving the biocompatibility of the materials for *in vivo* use, mechanical characterization of the different materials demonstrated that porous polydomain LCE materials were significantly better at accommodating stress compared to the other structure/alignment combinations studied (Figure 1.XX). A more recent study by Elmadih et al.[76] showcased the use of LCEs as dissipative structures in equipment vibrational damping. A variety of damping materials including silicone and LCE were inserted into a handheld drill whose vibrational spectrum was measured to determine the amount of damping provided in each case.

The LCE materials exhibited an overdamping behavior greatly reducing the amplitude of vibration at a range of frequencies and outperforming the conventional silicone materials (Figure 1.XX) further demonstrating the potential that LCEs have in energy dissipating materials.

1.5.2 Adhesives

One of the more recent applications for liquid crystalline polymeric materials from the last decade or so is their use as adhesives. In 2013, work by Corbett et al.[77] proposed that LC networks should possess a high tack energy due to their dissipative character which would in theory make them excellent adhesive materials. It was not until 2019 that work by Ohzono et al.[78] experimentally verified this hypothesis and found that LCEs do in fact function as adhesives. This experimental work correlated the adhesive performance of the material to the stability of the LC phase by demonstrating that upon disordering the nematic phase of the LCE, a significant portion of the adhesive character of the material is lost. (Figure 1.XXA-B) A follow-up work by Ohzono et al.[15] extended this idea to photothermally-driven systems by imbibing an indocyanine green dye into LCEs and driving their adhesion with green light. Several additional works on studying the properties and different modes of LCE adhesion soon followed to develop a deeper understanding of the intricacies and mechanism of these systems. Work by Farre-Kaga et al.[79] sought to determine which viscoelastic parameters were important in producing adhesive behavior in LCEs. It was found that materials with higher loss factors (tan δ) at or around the adhesive testing temperature consistently had a superior tack performance (Figure 1.XXC) suggesting that the energy dissipation potential of the material is correlated to its adhesive behavior. Work by Pranda et al. looked at the effect of mesogen alignment on the peel test adhesion of LCEs to determine how alignment at the interface influenced adhesive character. This work determined that the more rotation a mesogen was able to experience over the course of the peel test, the higher its adhesive

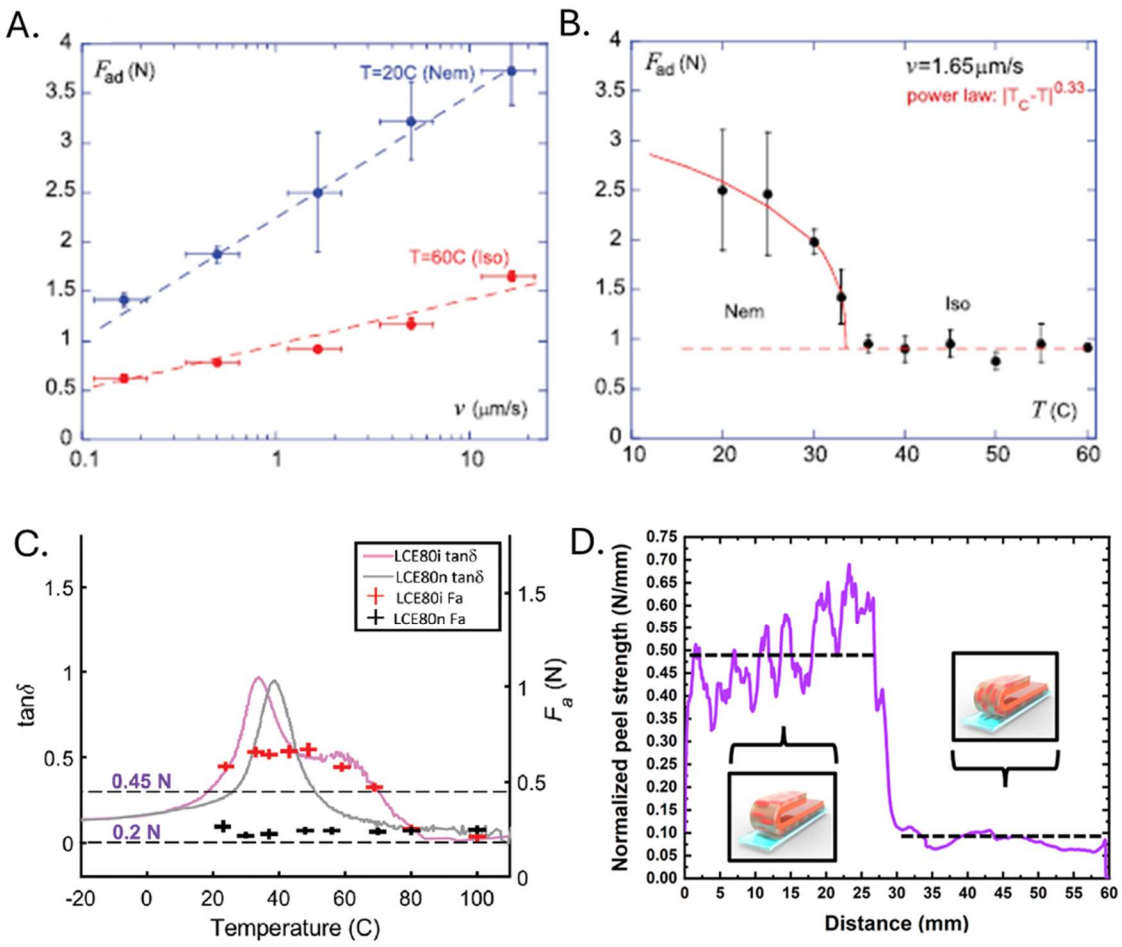

Figure 1.6 A. Adhesive force curves demonstrating the impact of removal rate on LCE adhesive performance[78]; B. Force vs temperature curves to illustrate the importance of the nematic state to LCE adhesive behavior[78]; C. Tan δ and adhesive force curves demonstrating the importance of energy dissipation as a function of temperature to the magnitude of adhesive performance[79]; D. Peel tests comparing the performance of differently aligned LCEs relative to the direction of peel[80]

performance would be. To test this, a bar of LCE was processed such that half of the strip was aligned parallel to long axis of the bar while the other half was aligned in the perpendicular direction. When the peel test was performed, relative to the direction of peel, the perpendicularly aligned half of the bar was found to have a significantly higher peel strength than the half aligned in parallel. (Figure 1.XXD) These works demonstrate the interplay between the energy dissipation potential and rotational freedom of the mesogens as they relate to adhesive performance in LCEs.

As such, there is further work to be done in the study of LCE adhesive systems as the incorporation of dynamic bonds should provide additional stress dissipation modes and rearrangement pathways which would result in enhanced adhesive performance.

1.6 References

[1] A. Jayaraman, H. A. Klok, *ACS Polym. Au* **2023**, *3*, 1–4.

[2] F. Liu, M. W. Urban, *Prog. Polym. Sci.* **2010**, *35*, 3–23.

[3] M. Wei, Y. Gao, X. Li, M. J. Serpe, *Polym. Chem.* **2017**, *8*, 127–143.

[4] Z. M. Png, C. G. Wang, J. C. C. Yeo, J. J. C. Lee, N. E. Surat'man, Y. L. Tan, H. Liu, P. Wang, B. H. Tan, J. W. Xu, X. J. Loh, Q. Zhu, *Mol. Syst. Des. Eng.* **2023**, *8*, 1097–1129.

[5] A. Lendlein, O. E. C. Gould, *Nat. Rev. Mater.* **2019**, *4*, DOI 10.1038/s41578-018-0078-8.

[6] Y. Xia, Y. He, F. Zhang, Y. Liu, J. Leng, *Adv. Mater.* **2021**, *33*, 1–33.

[7] W. Qiu, J. M. P. Scofield, P. A. Gurr, G. G. Qiao, *Macromol. Rapid Commun.* **2022**, *43*, 1–35.

[8] K. Imato, Y. Ooyama, *Polym. J.* **2024**, *56*, 1093–1109.

[9] S. Wang, M. W. Urban, *Nat. Rev. Mater.* **2020**, *5*, 562–583.

[10] B. Li, P. F. Cao, T. Saito, A. P. Sokolov, *Chem. Rev.* **2023**, *123*, 701–735.

[11] K. M. Herbert, S. Schrettl, S. J. Rowan, C. Weder, *Macromolecules* **2017**, *50*, 8845–8870.

[12] B. T. Michal, C. A. Jaye, E. J. Spencer, S. J. Rowan, *ACS Macro Lett.* **2013**, *2*, 694–699.

[13] B. T. Michal, W. A. Brenn, B. N. Nguyen, L. S. McCorkle, M. A. B. Meador, S. J. Rowan, *Chem. Mater.* **2016**, *28*, 2341–2347.

[14] H. Tsunoda, K. Kawasaki, T. Ube, T. Ikeda, *Mol. Cryst. Liq. Cryst.* **2018**, *662*, 61–67.

[15] T. Ohzono, Y. Norikane, M. O. Saed, E. M. Terentjev, *ACS Appl. Mater. Interfaces* **2020**, *12*, 31992–31997.

[16] I. K. Shishmanova, C. W. M. Bastiaansen, A. P. H. J. Schenning, D. J. Broer, *Chem. Commun.* **2012**, *48*, 4555–4557.

[17] H. Qian, I. Aprahamian, *Chem. Commun.* **2015**, *51*, 11158–11161.

[18] B. T. Michal, B. M. McKenzie, S. E. Felder, S. J. Rowan, *Macromolecules* **2015**, *48*, 3239–3246.

[19] B. M. Mckenzie, R. J. Wojtecki, K. A. Burke, C. Zhang, J. Antal, P. T. Mather, S. J. Rowan, **2011**, 3525–3533.

[20] L. T. De Haan, J. M. N. Verjans, D. J. Broer, C. W. M. Bastiaansen, A. P. H. J. Schenning, *J. Am. Chem. Soc.* **2014**, *136*, 10585–10588.

[21] Z. Wang, R. Lan, J. Bao, C. Shen, R. Huang, C. Song, L. Zhang, H. Yang, *ACS Appl. Mater. Interfaces* **2022**, *14*, 17869–17877.

[22] A. Lendlein, S. Kelch, *Angew. Chem. Int. Ed. Engl.* **2002**.

[23] M. H. P. de Heer Kloots, S. K. Schoustra, J. A. Dijksman, M. M. J. Smulders, *Soft Matter* **2023**, 2857–2877.

[24] S. J. Rowan, S. J. Cantrill, G. R. L. Cousins, J. K. M. Sanders, J. F. Stoddart, *Angew. Chemie - Int. Ed.* **2002**, *41*, 898–952.

[25] R. J. Wojtecki, M. A. Meador, S. J. Rowan, *Nat. Mater.* **2011**, *10*, 14–27.

[26] W. Lu, X. Le, J. Zhang, Y. Huang, T. Chen, W. Lu, **2017**, 1284–1294.

[27] S. Bonardd, M. Nandi, J. I. Hernández García, B. Maiti, A. Abramov, D. Díaz Díaz, *Chem. Rev.* **2023**, *123*, 736–810.

[28] M. W. Alam, S. I. Bhat, H. S. Al Qahtani, M. Aamir, M. N. Amin, M. Farhan, S. Aldabal, M. S. Khan, I. Jeelani, **2022**.

[29] I. Taghavi, M. Moridsadat, A. Tofini, S. Raza, N. A. F. Jaeger, L. Chrostowski, B. J. Shastri, S. Shekhar, **2022**, *11*, 3855–3871.

[30] M. Warner, E. M. Terentjev, *International Series of Monographs on Physics: Liquid Crystal Elastomers*, Oxford University Press, Oxford, **2007**.

[31] T. J. White, D. J. Broer, *Nat. Mater.* **2015**, *14*, 1087–1098.

[32] K. M. Herbert, H. E. Fowler, J. M. McCracken, K. R. Schlafmann, J. A. Koch, T. J. White, *Nat. Rev. Mater.* **2021**, *0123456789*, DOI 10.1038/s41578-021-00359-z.

[33] P. G. De Gennes, *C. R. Acad. Sci. B* **1975**, *281*, 101.

[34] Y. Bouligand, P. E. Cladis, L. Liebert, L. Strzelecki, *Mol Cryst Liq Cryst* **1974**, *25*, 233–252.

[35] H. Finkelmann, H.-J. Kock, G. Rehage, *Die Makromol. Chemie, Rapid Commun.* **1981**, *2*, 317–322.

[36] J. Kupfer, H. Finkelmann, *Makromol. Chem., Rapid Commun* **1991**, *12*, 717–726.

[37] B. Donnio, H. Wermter, H. Finkelmann, *Macromolecules* **2000**, *33*, 7724–7729.

[38] C. M. Yakacki, M. Saed, D. P. Nair, T. Gong, S. M. Reed, C. N. Bowman, *RSC Adv.* **2015**, *5*, 18997–19001.

[39] Z. Pei, Y. Yang, Q. Chen, E. M. Terentjev, Y. Wei, Y. Ji, *Nat. Mater.* **2014**, *13*, 36–41.

[40] K. Kawasaki, T. Ube, T. Ikeda, *Mol. Cryst. Liq. Cryst.* **2015**, *614*, 62–66.

[41] D. W. Hanzon, N. A. Traugutt, M. K. McBride, C. N. Bowman, C. M. Yakacki, K. Yu, *Soft Matter* **2018**, *14*, 951–960.

[42] C. A. Lindberg, E. Ghimire, C. Chen, S. Lee, N. D. Dolinski, J. M. Dennis, S. Wang, J. J. de Pablo, S. J. Rowan, *J. Polym. Sci.* **2024**, *62*, 907–915.

[43] Z. Wang, H. Tian, Q. He, S. Cai, *ACS Appl. Mater. Interfaces* **2017**, *9*, 33119–33128.

[44] S. Huang, Y. Shen, H. K. Bisoyi, Y. Tao, Z. Liu, M. Wang, H. Yang, Q. Li, *J. Am. Chem. Soc.* **2021**, *143*, 12543–12551.

[45] D. Tang, L. Zhang, X. Zhang, L. Xu, K. Li, A. Zhang, *ACS Appl. Mater. Interfaces* **2022**, *14*, 1929–1939.

[46] Z. Wen, M. K. McBride, X. Zhang, X. Han, A. M. Martinez, R. Shao, C. Zhu, R. Visvanathan, N. A. Clark, Y. Wang, K. Yang, C. N. Bowman, *Macromolecules* **2018**, *51*, 5812–5819.

[47] M. K. McBride, M. Hendrikx, D. Liu, B. T. Worrell, D. J. Broer, C. N. Bowman, *Adv. Mater.* **2017**, *29*, 1606509.

[48] M. K. McBride, A. M. Martinez, L. Cox, M. Alim, K. Childress, M. Beiswinger, M. Podgorski, B. T. Worrell, J. Killgore, C. N. Bowman, *Sci. Adv.* **2018**, *4*, eaat4634.

[49] E. C. Davidson, A. Kotikian, S. Li, J. Aizenberg, J. A. Lewis, *Adv. Mater.* **2019**, *1905682*, 1–6.

[50] J. Lee, J. Bae, J. H. Hwang, M. Choi, Y. S. Kim, S. Park, J. Na, D. Kim, S. Ahn, *Adv. Funct. Mater.* **2022**, *32*, 2110360.

[51] E. Ghimire, C. A. Lindberg, T. D. Jorgenson, C. Chen, J. J. de Pablo, N. D. Dolinski, S. J. Rowan, *Macromolecules* **2024**, *57*, 682–690.

[52] M. O. Saed, A. Gablier, E. M. Terentejv, *Adv. Funct. Mater.* **2019**, *1906458*, 1–8.

[53] Z. Pei, Y. Yang, Q. Chen, E. M. Terentjev, Y. Wei, Y. Ji, *Nat. Mater.* **2014**, *13*, 36–41.

[54] G. L. Grocke, H. Zhang, S. S. Kopfinger, S. N. Patel, S. J. Rowan, *ACS Macro Lett.* **2021**, *10*, 1637–1642.

[55] U. F. Fritze, M. Von Delius, *Chem. Commun.* **2016**, *52*, 6363–6366.

[56] M. Burnworth, L. Tang, J. R. Kumpfer, A. J. Duncan, F. L. Beyer, G. L. Fiore, S. J. Rowan, C. Weder, *Nature* **2011**, *472*, 334–337.

[57] J. R. Kumpfer, J. J. Wie, J. P. Swanson, F. L. Beyer, M. E. MacKay, S. J. Rowan, *Macromolecules* **2012**, *45*, 473–480.

[58] J. T. Carli, C. A. Lindberg, M. D. Heltne, E. C. Bornowski, E. A. John, K. N. Wiegel, *Mol. Cryst. Liq. Cryst.* **2017**, *656*, 83–88.

[59] L. Fang, H. Zhang, Z. Li, Y. Zhang, Y. Zhang, H. Zhang, *Macromolecules* **2013**, *46*, 7650–7660.

[60] S. J. D. Lugger, S. J. A. Houben, Y. Foelen, M. G. Debije, A. P. H. J. Schenning, D. J. Mulder, *Chem. Rev.* **2022**, *122*, 4946–4975.

[61] A. Priimagi, G. Cavallo, A. Forni, M. Gorynsztejn-Leben, M. Kaivola, P. Metrangolo, R. Milani, A. Shishido, T. Pilati, G. Resnati, G. Terraneo, *Adv. Funct. Mater.* **2012**, *22*, 2572–2579.

[62] A. Priimagi, G. Cavallo, P. Metrangolo, G. Resnati, *Acc. Chem. Res.* **2013**, *46*, 2686–2695.

[63] C. A. Lindberg, A. E. Roberson, E. Ghimire, J. E. Hertzog, N. R. Boynton, G. Liu, D. K. Schneiderman, S. N. Patel, S. J. Rowan, *Chem. - A Eur. J.* **2025**, 2011854.

[64] C. Zhang, G. Fei, X. Lu, H. Xia, Y. Zhao, *Adv. Mater.* **2024**, *36*, 2307210.

[65] S. J. A. Houben, S. J. D. Lugger, R. J. H. Van Raak, A. P. H. J. Schenning, *ACS Appl. Polym. Mater.* **2022**, *4*, 1298–1304.

[66] S. J. D. Lugger, R. M. C. Verbroekken, D. J. Mulder, A. P. H. J. Schenning, *ACS Macro Lett.* **2022**, *11*, 935–940.

[67] D. Martella, C. Parmeggiani, D. S. Wiersma, M. Piñol, L. Oriol, *J. Mater. Chem. C* **2015**, *3*, 9003–9010.

[68] M. Barnes, S. Cetinkaya, A. Ajnsztajn, R. Verduzco, *Soft Matter* **2022**, 5074–5081.

[69] Y. Yusuf, *Mater. Res.* **2017**, *20*, 1541–1547.

[70] H. J. Hong, S. Y. Park, *J. Ind. Eng. Chem.* **2022**, *110*, 424–433.

[71] H. H. Yoon, D. Y. Kim, K. U. Jeong, S. K. Ahn, *Macromolecules* **2018**, *51*, 1141–1149.

[72] Y. Lee, S. Choi, B.-G. Kang, S. Ahn, *Materials (Basel).* **2020**, *13*, 3094.

[73] M. O. Saed, R. H. Volpe, N. A. Traugutt, R. Visvanathan, N. A. Clark, C. M. Yakacki, *Soft Matter* **2017**, *13*, 7537–7547.

[74] C. Luo, C. Chung, N. A. Traugutt, C. M. Yakacki, K. N. Long, K. Yu, *ACS Appl. Mater. Interfaces* **2021**, *13*, 12698–12708.

[75] R. K. Shaha, D. R. Merkel, M. P. Anderson, E. J. Devereaux, R. R. Patel, A. H. Torbati, N. Willett, C. M. Yakacki, C. P. Frick, *J. Mech. Behav. Biomed. Mater.* **2020**, *107*, 103757.

[76] W. Elmadih, A. Terentjev, H. L. Liang, E. Terentjev, *Sci. Rep.* **2024**, *14*, 25860.

[77] D. R. Corbett, J. M. Adams, *Soft Matter* **2013**, *9*, 1151–1163.

[78] T. Ohzono, M. O. Saed, E. M. Terentjev, *Adv. Mater.* **2019**, *31*, 1902642.

[79] H. J. Farre-Kaga, M. O. Saed, E. M. Terentjev, *Adv. Funct. Mater.* **2022**, *32*, 2110190.

[80] P. A. Pranda, A. Hedegaard, H. Kim, J. Clapper, E. Nelson, L. Hines, R. C. Hayward, T. J. White, *ACS Appl. Mater. Interfaces* **2024**, *16*, 6394–6402.

CHAPTER 2

EXPLORING THE EFFECT OF DYNAMIC BOND PLACEMENT IN LIQUID CRYSTAL ELASTOMERS

2.1 Summary

Dynamic liquid crystal elastomers (LCEs) are a class of polymer networks characterized by the inclusion of both liquid crystalline monomers and dynamic covalent bonds. The unique properties realized through the combination of these moieties has produced a plethora of stimuli-responsive materials to address a range of emerging technologies. While previous works have studied the incorporation of different dynamic bonds in LCEs, few (if any) have studied the effect of the specific placement of the dynamic bonds within an LCE network. A series of dynamic LCE networks were synthesized using a generalizable approach that employs a tandem thiol-ene/yne chemistry which allows the location of the dynamic disulfide bond to be varied while maintaining similar network characteristics. When probing these systems in the LC regime, the thermomechanical properties were found to be largely similar. It is not until elevated temperatures (160–180 °C) that differences in the relaxation activation energies of these systems begin to materialize based solely on differences in placement of the dynamic bond throughout the network. This work demonstrates that through intentional dynamic bond placement, stress relaxation times can be tuned without affecting the LCE character. This insight can help optimize future dynamic LCE designs and achieve shorter processing times.

2.2 Introduction

Liquid crystal elastomers (LCEs) are a class of soft materials characterized by the incorporation of mesogenic monomers into a crosslinked polymer network.[1,2] Generally, the tethered mesogens form randomly-oriented but locally-aligned domains in what is referred to as a polydomain LCE. If the film is prepared in a manner that all the mesogens are aligned in the same direction, then the result is a "monodomain" LCE. Traversing the LC to isotropic transition, via stimuli such as heat,[3] light,[4] humidity,[5] or metal ions,[6] can result in responsive properties such as shape memory and optical responsivity. Another key feature of these materials is their "soft elasticity" which refers to their ability to dissipate stress through mesogenic rotational modes when an LCE is sufficiently stressed to strains outside of its specific linear viscoelastic regime.[7] Given these unique properties, LCEs have received much attention for emerging applications in soft robotics,[8,9] medical devices,[10,11] and adaptive optics.[12,13]

Traditionally, monodomain LCEs are accessed via either the alignment of the LC monomers prior to crosslinking or the utilization of a two-step crosslinking approach where materials are partially crosslinked, mechanically strained, and then fully crosslinked to lock in the aligned state as the permanent mesogenic configuration.[3,14–16] However, as these processes typically involve inducing alignment of viscous solutions or handling and manipulating fragile, still reactive materials, the scale and physical form that these LCEs can take is limited. Additionally, as is expected for a permanently crosslinked network, once the crosslinking reaction has been completed these materials are fixed with the alignment and shape they were crosslinked with and can no longer be reset or reprocessed.

A more recent development in LCEs has been the introduction of dynamic covalent chemistries into the structure of the network.[17–19] A dynamic covalent bond has the ability to be broken and reformed, ideally without any irreversible side reactions.[20,21] In addition to facilitating bulk reprocessability and enhancing stress relaxation / dissipation in LCEs, the dynamic bonds also provide a route to (re)program the LCEs after they have been crosslinked. By manipulating the mesogen alignment while simultaneously activating the dynamic bond, it is possible to utilize the dynamic exchange processes to promote network reorganization such that stable alignment is post-synthetically programmed upon bond reformation. A wide range of dynamic chemistries have been utilized in LCEs over the past decade including transesterification,[22–24] disulfide exchange,[25–27] and addition fragmentation transfer reactions[28–31] to name a few.

Of these dynamic bonds, disulfides stand out as a particularly useful dynamic chemistry for a multitude of reasons. The disulfide (Figure 2.1a), with a bond energy of around 60 kcal mol^{-1} (251 kJ mol^{-1}), is a well-studied multi-responsive dynamic bond, capable of being activated using a host of stimuli including heat,[32,33] UV light,[34,35] redox,[36] shear,[37] ultrasound,[38] and chemical catalysts.[39] The formed thiyl radicals (or thiolate ions) are also capable of exchanging with existing disulfide bonds through an associative process (Figure 2.1a) that occurs at a much faster rate than exchange mediated by the sequential breaking and reforming of disulfides.[40] Naturally, disulfides have been extended to LCEs, with a number of works incorporating disulfides into materials to achieve enhanced reprocessability and post-synthetic alignment capabilities.[13,25–27,41–44] However, among these reports, the routes for installing disulfides into LCEs vary greatly and include crosslinking through oxidizing thiols to disulfides,[25,27,42,43] incorporating monomers with preformed disulfide linkages,[26,41] or ring opening cyclic disulfides to form LCEs with polydisulfide backbones.[44] It is worth noting that in these dynamic LCEs the location of the

disulfide bond within the network is never expressly considered, and the disulfide is free to exist in the network anywhere the components or the chemistries permit. This ultimately produces systems where the disulfide placement is either random or hyper regular making it impossible to directly compare these systems from the perspective of dynamic LCE design. As topology is a critical factor when considering any polymer network, it stands to reason that dynamic topology, specifically the placement of the dynamic bond throughout the network, is also of critical importance when it comes to considering dynamic network materials and their properties. However, to properly test the impact of dynamic bond placement, the overall network characteristics must be held constant to isolate the impact of dynamic bond location.

A benefit of exploring the impact of dynamic bond location in LCEs comes from the ability to track programmed mesogen alignment, which directly correlates to the efficacy of network reorganization resulting from dynamic bond exchange. As such, the goal of this work was to design and synthesize a series of modular disulfide-containing LCEs to elucidate the effect that the topological placement of dynamic bonds plays on linear and nonlinear thermomechanical properties across different timescales. More specifically the use of a tandem thiol-ene/yne approach was explored to allow for locking in key network characteristics (glass transition temperature (T_g), nematic to isotropic transition temperature (T_{NI}), plateau modulus, etc.) while systematically varying the location of the dynamic moieties.

As click chemistries, thiol-ene and thiol-yne reactions have been well-studied in polymers, in large part for their rapid initiation and high efficiencies.[45–47] Given that both alkene and alkyne

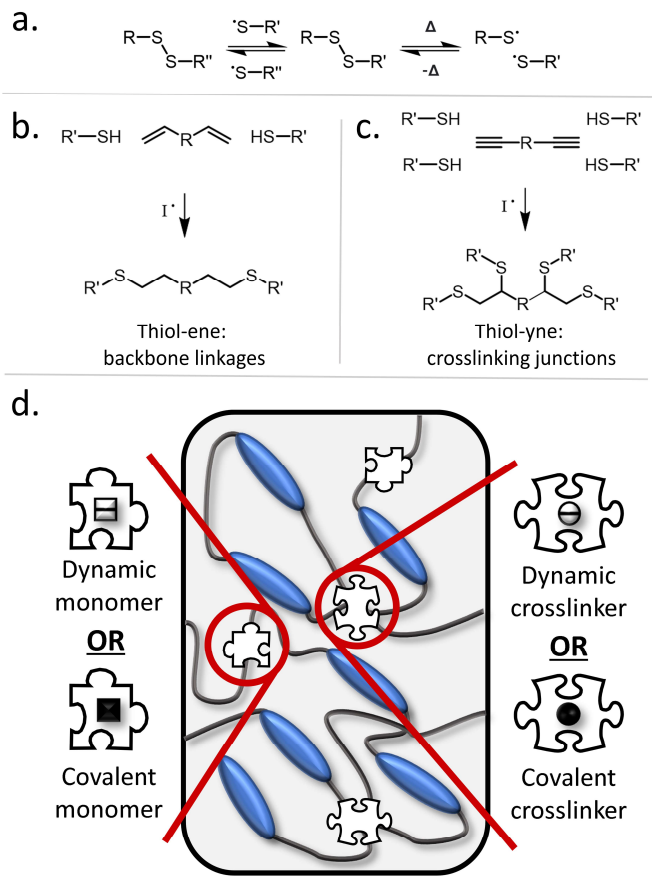

Figure 2.1: a. Dynamic exchange of disulfide bonds; b. Radical initiated reaction mechanism for a dialkene monomer with two thiols forming a linear backbone linkage; c. Radical initiated reaction mechanism for a dialkyne crosslinker with four thiols forming a crosslink; d. Schematic depicting the modular nature of this dynamic LCE system that allows for selective disulfide placement in backbone linkages, crosslinks, or both.

bonds are capable of reacting with thiols through a radically initiated pathway where one alkene can react with one thiol and one alkyne can react with two thiols, it follows that provided with a stoichiometric amount of thiol, both alkene and alkyne moieties can be incorporated into a single network using the same initiation process. As such, the current system consists of dialkene species that serve as linear components (Figure 2.2.1b) and dialkyne species that serve as crosslinkers (Figure 2.1c). Based on this concept, networks synthesized from a series of dynamic and covalent components based on thiol-alkene/alkyne chemistry would allow for the controlled placement of a dynamic bond within an otherwise identical LCE framework (Figure 2.1d). For this work, a

modular dynamic LCE system was devised using the disulfide bond as a multi-responsive dynamic linkage (Figure 2.1a), installed via a tandem thiol-ene/yne chemistry to allow for differentiation in bond placement based solely on component functionality.

2.3 Results and Discussion

2.3.1 Design and Synthesis

To best isolate the effect of dynamic bond location as a variable within a dynamic LCE material, a series of design criteria were followed that include 1) utilizing molecularly-similar monomers to minimize differences in intermolecular interactions between non-LC components; 2) thermally separating the LC transition temperature from the temperature where most disulfide bonds have been cleaved (>150 °C);[33] and 3) targeting a constant concentration of disulfide bonds within the network across the materials studied. The first criterion serves to minimize differences in the structure and properties of the networks outside of the placement of the dynamic bonds. The second criterion ensures that there is sufficient thermal isolation of the disulfide from the liquid crystalline transition so the similarity in LCE properties can be verified without convolution of relaxation events that occur on account of significant dynamic bond exchange. The final criterion ensures that the concentration of disulfide bonds present in any dynamic network studied is constant, so observed variations are decoupled from differences in the amount of dynamic character. To satisfy the first criterion, a series of components including a LC monomer (**1**), a dynamic monomer (**2D**), a covalent monomer (**2C**), a dynamic crosslinker (**3D**), and a covalent crosslinker (**3C**) were synthesized based on previously reported literature procedures (see Supporting Information for complete synthetic details).[48,49] For the design of the non-LC components, a constant number of atoms along the molecule's primary axis was targeted while ester linkages were used to maintain

similar polarity and secondary interactions. To satisfy the second criterion, the T_{NI} of the material system was tuned using the ratio of LC (**1**) to non-LC monomers (**2**) as it has been demonstrated previously in literature that the concentration of LC content in the feedstock can be used as a means of tuning the phase behavior for a given LCE.[50] A ratio of 3:1 was chosen for **1**:**2** as this ratio targets a material with a T_{NI} of around 70 °C which falls between ambient conditions and where there is significant cleavage of the dynamic bond (>150 °C) in order to limit the impact of thermally-induced disulfide cleavage on the LCEs' properties.

For the final criterion, it was necessary to find a ratio of components that allowed for the same amount of disulfide to be present in both the backbone as well as in the crosslinks. To achieve this, the molar ratio of non-LC alkene functionalized monomers (**2C** + **2D**) and alkyne functionalized crosslinkers (**3C** + **3D**) was set to be equivalent ensuring that the concentration of disulfide would be consistent across materials with different dynamic bond placements in addition to targeting a molecular weight between crosslinks of ca. 3,000 g mol^{-1}.

Using the components and design criteria outlined above, a series of networks were synthesized where only the location of the disulfide itself is varied within the network. Three different dynamic LCEs with a constant concentration of disulfide were targeted (Figure 2.2): a network where the disulfide is located in 25% of the repeat units within the backbone (**4B**, formed using **2D** and **3C**), a network where the disulfide is located in every crosslink (**4X,** formed using **2C** and **3D**), and a network where the concentration of disulfide is split between both the backbone and crosslinks (**4BX**, formed using half molar equivalents of **2D**, **2C**, **3D**, and **3C**). A nondynamic control LCE (**4N**, formed using **2C** and **3C**) that contains no dynamic bonds was also synthesized to determine the impact that incorporating disulfide bonds into these LCE networks has on their

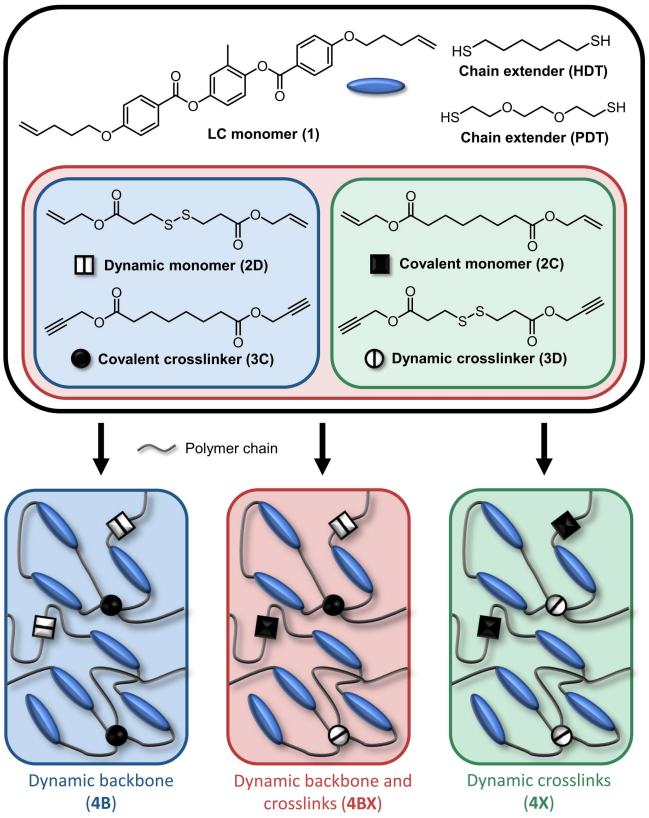

Figure 2.2: Component and network designs for a modular disulfide containing LCE network that allows for selective disulfide placement in backbone linkages, crosslinks, and a system containing both.

bulk thermomechanical properties. A mixture of the dithiol chain extenders 1,6-hexanedithiol (**HDT**) and 2,2′-(ethylenedioxy)diethanethiol (**PDT**) was selected to inhibit any potential aliphatic interactions between monomers as has been seen in previously studied systems.[51,52] To synthesize these materials, calculated quantities obtained through use of Carother's equation[53] of alkene functionalized monomers (**1**, **2C**, **2D**), dithiol chain extenders **HDT** and **PDT**, and alkyne functionalized crosslinker (**3C**, **3D**) were dissolved in tetrahydrofuran (THF) with a catalytic amount of the photoinitiator 2,2-dimethoxy-2-phenylacetophenone (DMPA). The reaction mixture was then cured though exposure to UV light (320–390 nm, 100 mW cm^{-2}, 2 x 30 s) to yield a solid film. While potential UV-induced cleavage of the disulfide can result in thiyl species capable of reacting with alkenes and alkynes, previous works have shown the effect of these reactions to be

minimal. For instance, Bongiardina *et al.* and Soars *et al.* both demonstrated a large difference in efficiency between reactions initiated by thiol generated radicals and those generated by cleaved disulfides for photo-mediated polymerizations.[54,55] Additionally, work by Kamps *et al.* demonstrated the low reactivity of aliphatic alkenes with photocleaved disulfides under ambient conditions in a study of the photodisulfidation of aliphatic alkenes.[56] To ensure the removal of any unreacted monomers from the dynamic LCEs, the films were then cut into pieces and washed with THF and methanol (MeOH) using a Soxhlet extractor. After drying under vacuum (16 h, 60 °C), the materials were melt processed under pressure (1 h, 180 °C, 4 tons) to homogenize the materials into films. Gel fractions were taken for the materials and ranged from 87–89 wt%. Thermogravimetric analysis was also performed to confirm the removal of solvent and unreacted starting materials (Figure S2.1).

2.3.2 Thermomechanical Characterization

To assess the thermal transitions of the prepared LCEs, differential scanning calorimetry (DSC) was employed (Figure 2.3a). Analysis of the DSC thermograms reveals only a minor effect in incorporating disulfide bonds into LCEs when comparing the non-dynamic **4N** to the disulfide-containing **4B**, **4BX**, and **4X** that manifests as a 3–6 °C decrease in both the glass T_g and T_{NI}. However, the T_gs and T_{NI}s as measured in DSC, ca. –33 °C and 71 °C respectively, for the dynamic LCEs **4B**, **4BX**, and **4X** fall within a few degrees of one another. This suggests that placement of the disulfide bond does not have a large impact on the liquid crystalline transition, implying that the bond placement does not strongly impact the packing stability of the mesogenic units. The similarity in thermal properties was corroborated by the small angle oscillatory shear (SAOS) rheology data (Figure 2.3b). The measured storage modulus (G') for all samples were found to nearly overlap across the entire temperature range probed (–50–180 °C). A steep decrease in the

G' curve as well as a peak in the tan(δ) curve corresponding to the T_g appears ca. –17 °C for all materials which further confirms that a consistent set of thermal properties was achieved. A shoulder from 10–70 °C in the tan(δ) curve is indicative of the nematic character of the networks and has been reported for previously studied LCEs.[57] Around 70 °C a minimum in the G' curve and a corresponding step in the tan(δ) curve (commonly ascribed to the T_{NI} for an LCE[57]) further demonstrate congruence in the liquid crystalline character of the dynamic materials and

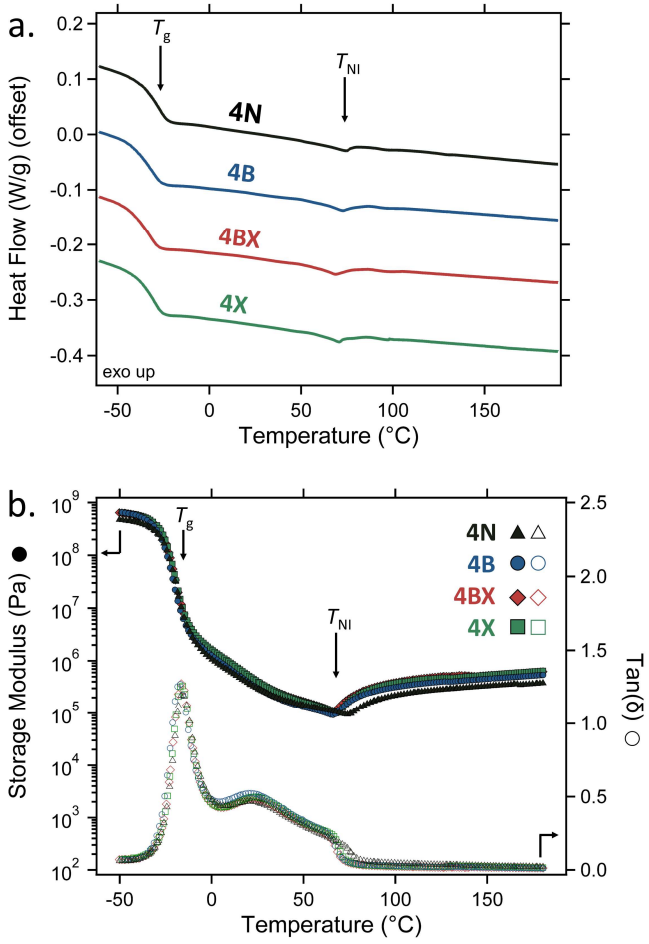

Figure 2.3: a. Differential scanning calorimetry thermograms of dynamic liquid crystal elastomer films; b. Shear rheology dynamic temperature ramps of storage modulus (solid shapes) and tan(delta) (empty shapes) for dynamic LCEs

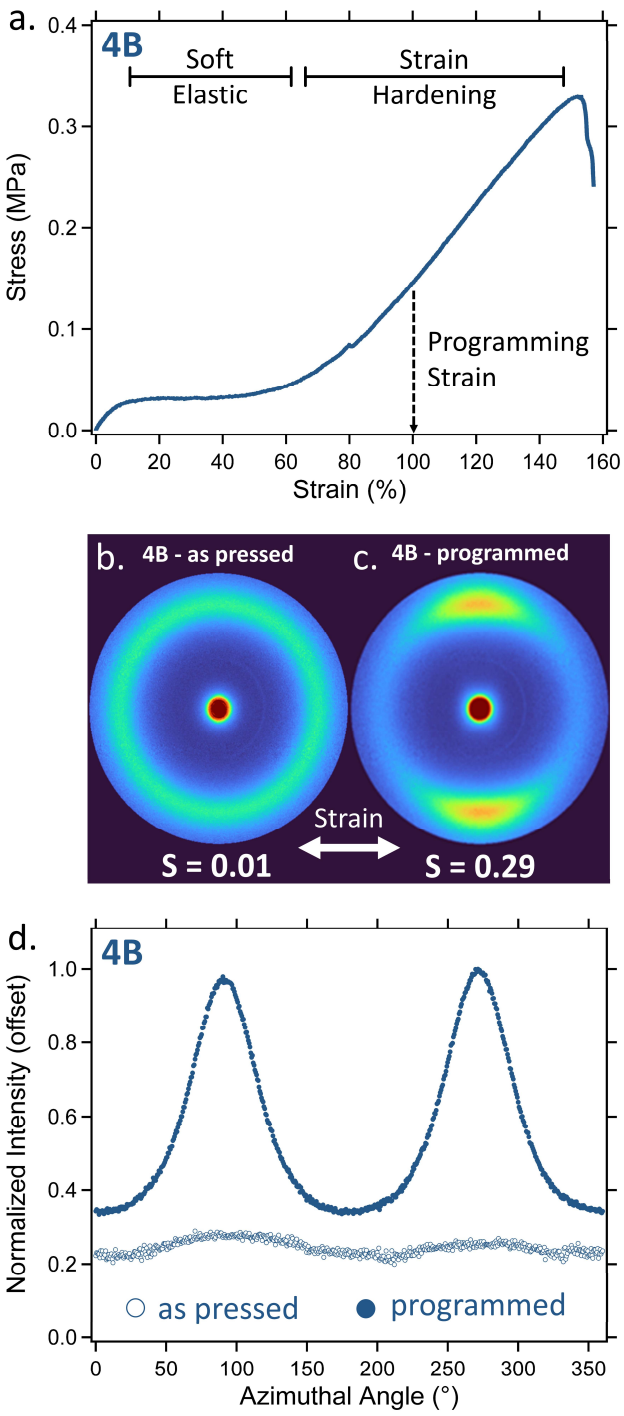

Figure 2.4: a. Stress-strain profile of an as pressed sample of **4B**; b. 2D WAXS image of an as pressed film of **4B**; c. 2D WAXS image of an aligned programmed film of **4B**; d. Plots of normalized intensity as a function of angle for both an as pressed and programmed aligned film of **4B**.

is in line with the trend observed in the DSC data. These data serve to establish the similarity of these materials despite their varied dynamic bond placement. To probe the nonlinear properties of the dynamic LCEs, tensile tests, dynamically programmed alignment, and wide-angle x-ray scattering (WAXS) experiments were performed on the series of dynamic materials to determine if dynamic bond placement alters the structural arrangement of the network in the nonlinear/high strain regime where LC alignment is induced.

To determine the programming strain conditions, tensile tests were performed under ambient conditions (22 °C) and on rectangular samples of **4B**, **4BX**, and **4X**, where the materials were elongated at a constant rate (5 mm min^{-1}) until failure. Much in line with the trends observed thus far, all measured tensile curves appear highly similar (Figure S2.2), suggesting that nonlinear tensile behavior under ambient conditions does not appear to be impacted by the placement of the disulfide bond within the network. A representative tensile curve of **4B** (Figure 2.4a) demonstrates the different mechanical regimes inherent to LCEs.[2] At low strains (0–10 % strain), the material possesses a primarily elastic response dominated by the LC domains. At intermediate strains (10–60 % strain) the material passes into a soft elastic state characterized by a plateau with a low change in stress, as stress is primarily being dissipated by mesogens rotating throughout the material. Once the majority of the mesogens are rotated such that their alignment is in the direction of the stress, the material enters a strain hardening regime (60–150 % strain) where the slope of the tensile curve begins to increase as the network increasingly resists alignment.

Utilizing the stress-strain profiles, a rectangular sample of each material was subjected to a programming process adapted from literature[25] to determine how dynamic network reorganization in the aligned nematic phase is affected by the location of the disulfide bond. In order to remain below T_{NI} and preserve mesogen alignment, UV light was used as a dynamic

stimulus to trigger disulfide exchange.[25,42] For this process, the samples were stretched to 100 % strain in the strain-hardening regime (to ensure rotation of the majority of mesogens had been induced). The samples were then fixed at this strain between two glass slides and then exposed to UV light (320–390 nm, 200 mW cm^{-2}) for 15 minutes on each side. Upon removing the samples from the slides, they were heated above their T_{NI} to induce a contraction to their initial state, and upon cooling, the materials adopted their new dynamically programmed elongated state.

To quantify the extent of alignment, WAXS measurements were taken on as pressed **4B**, **4BX**, and **4X** as well as their dynamically programmed counterparts. The as pressed **4B** displays an isotropic 2D WAXS pattern (Figure 2.4b) indicative of the statistical alignment of the domains in the polydomain material at every angle demonstrating the lack of overall alignment in the sample. For the dynamically aligned sample of **4B** (Figure 2.4c) the 2D pattern clearly changes to that of an anisotropic response with increased intensity of scattering in the vertical axis which indicates preferential alignment of the mesogens in the horizontal axis along which strain has been applied. Upon analyzing the plot of intensity as a function of azimuthal angle (Figure 2.4d), it becomes apparent that a significant change in alignment character has been imposed on the dynamically aligned sample. The fitting of these plots using the Kratky method[58] allows for the calculation of the Hermans order parameter (S)[59] for these systems where the as pressed material has an order parameter of $S = 0.01$ while dynamically programmed sample has an order parameter of $S = 0.29$. Critically, this trend holds true for the other materials as well with **4BX** (Figure S2.3) having order parameters of $S = 0.01$ and $S = 0.29$ for the as pressed and dynamically programmed respectively and **4X** (Figure S2.4) having order parameters of $S = 0.03$ and $S = 0.30$ for the as pressed and dynamically programmed respectively. This similarity in values not only suggests that the reorganization process under strain conditions can be achieved utilizing the multi-responsive

character of the disulfide bond, but also that under this set of ambient and active nonlinear conditions important for LCE actuation, the placement of the disulfide does not hinder the processes required for network reorganization. Up to this point, it has been demonstrated that the placement of the disulfide within the LCE network has seemingly not impacted the materials' properties. However, it is important to note that so far, the testing was done either in the nematic state where LC interactions are engaged or using methods that probe short relaxation timescales (at sufficiently low temperatures) within the material.

To isolate the impact of the location of the disulfide bonds, high temperature (i.e., well above the T_{NI} of ca. 70 °C) shear stress relaxation studies were performed on the dynamic LCEs. Figure 2.5 shows the stress relaxation behavior in the linear viscoelastic regime (Figure S2.5) for **4B**, **4BX**, and **4X** across a range of temperatures from 160–180 °C (3 % strain, 1 h), which represent an experimentally-active window (that maintains Arrhenius behavior[60,61]) for the disulfide exchange. A stretched exponential relaxation model was used to fit the data (fit parameters shown in Figure S2.6), which allowed for acquisition of characteristic relaxation times (τ^*) for these highly viscous systems where the characteristic relaxation time is defined as the time needed for the initial stress to decay to $1/e$ of its initial value. As shown in the insets for Figure 2.5, the fitted τ^* values across the measured range behave in an Arrhenius fashion. Interestingly, the activation energy of relaxation for **4B** and **4X** were found to be starkly different. The **4B** sample was found to have a considerably smaller activation energy of relaxation relative to **4X** (205 ± 15 vs 262 ± 8 kJ mol^{-1}). For reference the reported values of the activation energy of a disulfide bond is ca. 251 kJ mol^{-1}.[62] The activation energy of relaxation of **4BX** (188 ± 12 kJ mol^{-1}) was found to be within error of **4B** film, suggesting that the backbone-based relaxation processes dominate this film's overall relaxation behavior.

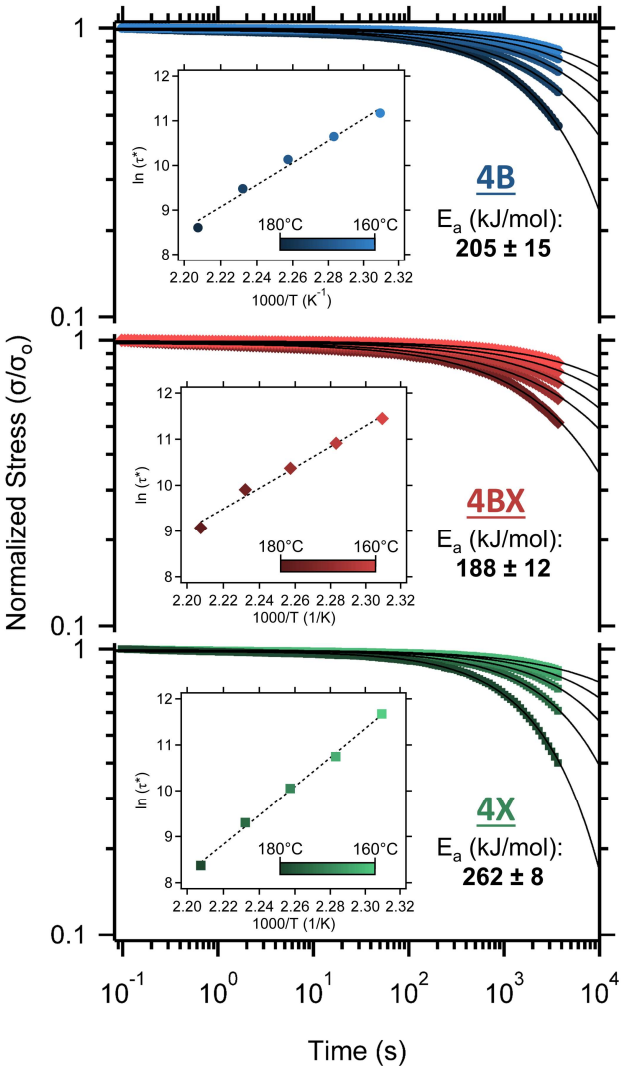

Figure 2.5: Temperature dependent stress relaxation curves for dynamic LCEs fitted to stretched exponential functions, with τ^* values determined by the fit. (inset) Arrhenius curves demonstrating the linear relationship between ln (τ^*) and temperature for a given sample. Errors for activation energies are derived from the linear fit of the data.

It is hypothesized that the observed differences in activation energies between systems with differing dynamic bond location stem from the ability of the disulfide to effectively exchange under these conditions. As demonstrated in recent work by Lessard *et al.*, diffusion of species has been shown to play an important role in the relaxation processes of dynamic covalent networks, where increases in molecular weight (and therefore lower diffusability) resulted in higher

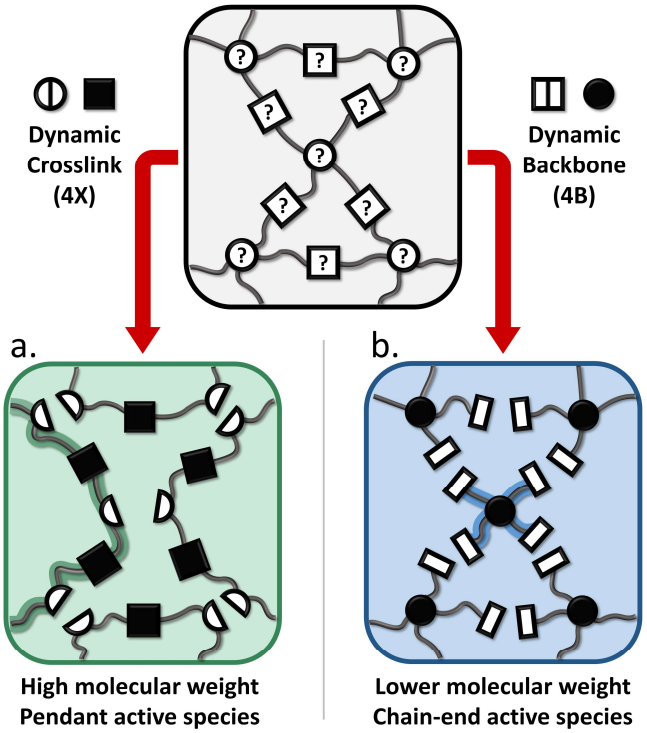

Figure 2.6: a. A schematic of the higher molecular weight, lower relative mobility pendant active species formed by the cleavage of a disulfide in a material with only dynamic crosslinks (**4X**); b. A schematic of the lower molecular weight, higher relative mobility chain-end active species formed by the cleavage of a disulfide in a material with only a dynamic backbone (**4B**).

activation flow energies, slower relaxations and lower recovery flow rates.[63] From a dynamic topology perspective, significant disulfide cleavage in the case of a material that is only dynamic at the crosslinks would result in very high molecular weight linear polymer species. The diffusion of this type of high molecular weight species and its ability to exchange are limited by the movement of the entire polymer chain resulting in lower mobility towards finding an exchange partner (Figure 2.6a). However, in the idealized case of significant disulfide bond cleavage in a material with backbone-placed disulfides, an unbound lower molecular weight species (~6 kg mol^{-1} 4-arm stars) should theoretically be formed free from the network where the active thiyl radicals exist at the free species' chain-ends (Figure 2.6b). This decrease in the molecular weight associated

with the free species would suggest a greater diffusability for the active thiyl radicals and a greater chance of finding a disulfide to exchange with. Therefore, it is possible to tune the activation energy for the relaxation processes in a dynamic LCE by controlling the architecture of the active species formed under conditions where the dynamic bond is active.

2.4 Conclusions

In this work, a tandem thiol-ene/yne strategy for synthesizing disulfide-containing LCEs was developed where the topological location of the dynamic bond was modified through targeted choice of network components with different functional handles. Characteristic thermal transitions such as the T_g and T_{NI} were found to be consistent between DSC and SAOS rheology. Additionally, the post-synthetic programming capability of these dynamic materials was found to be consistent between the different placements of the dynamic bond with the achieved order parameter being similar for the suite of dynamic materials. However, at higher temperatures, temperature-dependent stress relaxation experiments demonstrated a divergence in properties emerged where materials with disulfides only located in crosslinks (**4X**) have a markedly higher activation energy than materials that incorporate disulfides into backbone linkages (**4B** and **4BX**). These results suggest that designing dynamic species with high degrees of diffusability for the active species can result in lower activation energies for relaxation processes, and future works can adopt these design principles as a means of altering properties like processing time without changing other material properties or the chemistry being utilized. As such this provides an additional method of tuning the programmability of dynamic LCEs and the overall processing of other types of dynamic networks.

2.5 Materials and Methods

2.5.1 Materials

Potassium carbonate was purchased from Fisher Scientific. 5-Bromo-1-pentene was purchased from Combi-Blocks. All other chemicals were purchased from Millipore-Sigma and were used as received unless noted otherwise. All solvents were purchased from Fisher Scientific and were used as received unless noted otherwise.

2.5.2 Methods

Synthesis of 4'-(Pent-1-enyloxy)benzoic acid

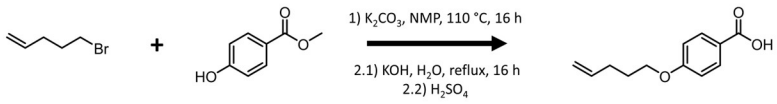

4′-(Pent-1-enyloxy)benzoic acid was synthesized using a modified version of previously published procedures.[1,2] 5-bromo-1-pentene (50 g, 0.336 mol, 1 eq), methyl-4-hyroxybenzoate (52.145 g, 0.342 mol, 1.02 eq), potassium carbonate (50.172 g, 0.362 mol, 1.08 eq) were all added to a flask containing N-methyl-2-pyrrolidone (150 mL, 3 vol). The flask was equipped with a condenser, and the reaction mixture was heated to 80°C while stirring. After observing an exotherm in the form of vigorous bubbling the temperature was raised to 110°C where the reaction was allowed to proceed for 16 h. The reaction mixture was then cooled to room temperature and added to a separatory funnel with toluene (300 mL) and water (100 mL). The organic layer was washed three times with water whereafter the solvent was removed under vacuum. To the resulting oil was added 300 mL of 10 wt% aqueous potassium hydroxide solution. The reaction mixture was then heated to 110 °C and allowed to proceed for 16 h with stirring. After cooling to room temperature, the reaction mixture was extracted with ethyl ether (50 mL) three times. The aqueous layer was then

diluted with water to a volume of 2 L while stirring whereupon concentrated sulfuric acid (25 mL) was added to adjust the solution to a pH of about 2. As the sulfuric acid is added, white solid began to precipitate from solution until the reaction mixture became a slurry that was difficult to stir magnetically. The solid was removed from the aqueous solution using a Buchner funnel and recrystallized three times in hot ethanol yielding white crystals. (61 g, 88% yield) ^{1}H NMR (400 MHz, $CDCl_3$) δ 8.16 – 7.97 (m, 2H), 7.00 – 6.88 (m, 2H), 5.98 – 5.74 (m, 1H), 5.17 – 4.94 (m, 2H), 4.04 (t, J = 6.4 Hz, 2H), 2.25 (qd, J = 7.4, 1.4 Hz, 2H), 2.03 – 1.82 (m, 2H).

Synthesis of liquid crystal monomer (1)

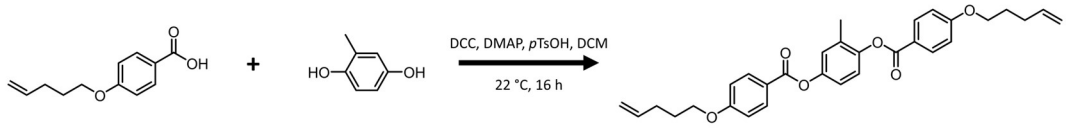

Liquid crystal monomer (**1**) was prepared using a previously reported procedure.[3] 4′-(Pent-1-enyloxy)benzoic acid (24.3 g, 0.118 mol, 1.95 eq), methylhydroquinone (7.5 g, 0.060 mol, 1 eq), dicyclohexylcarbodiimide (28.692g, 0.139 mol, 2.4 eq), 4-dimethylaminopyridine (14.050g, 0.115 mol, 1.9 eq), and *p*-toluenesulfonic acid monohydrate (21.875 g, 0.115 mol, 1.9 eq) were added to a flask containing 400 mL of dichloromethane. The reaction mixture was stirred at room temperature (22 °C) for 16 hours. A solid white urea byproduct was then filtered out of the reaction mixture, and the solvent was then removed from the filtrate under vacuum. The remaining solid was then recrystallized three times in hot ethanol to afford white powdery crystals. (44.25 g, 75% yield) ^{1}H NMR (400 MHz, $CDCl_3$) δ 8.29 – 8.04 (m, 4H), 7.22 – 7.04 (m, 3H), 7.04 – 6.92 (m, 4H), 5.96 – 5.77 (m, 2H), 5.17 – 4.97 (m, 4H), 4.07 (td, J = 6.4, 2.0 Hz, 4H), 2.35 – 2.20 (m, 7H), 2.01 – 1.87 (m, 4H).

Synthesis of dynamic monomer (2D)

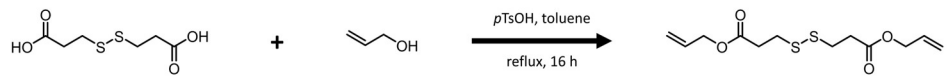

Dynamic monomer (**2D**) was prepared using a modified version of a previously reported procedure.[4] 3,3′-Dithiodipropionic acid (10 g, 0.048 mol, 1 eq), allyl alcohol (6.911 g, 0.119 mol, 2.5 eq), and *p*-toluenesulfonic acid (0.913 g, 0.005 mol, 0.1 eq) were added to a flask containing 200 mL of toluene. The flask was equipped with a Dean-Stark apparatus, and the reaction mixture was stirred under reflux for 16 h. Upon cooling to room temperature, the reaction mixture was transferred to a separatory funnel and washed with an aqueous solution saturated with sodium bicarbonate three times and then water three times. The organic layer was isolated and had the solvent removed from it under vacuum. The resulting product was a yellow oil. (12.824 g, 92% yield) ^{1}H NMR (400 MHz, $CDCl_3$) δ 5.92 (ddt, J = 17.1, 10.4, 5.8 Hz, 2H), 5.40 – 5.20 (m, 4H), 4.61 (dt, J = 5.8, 1.4 Hz, 4H), 2.94 (td, J = 7.2, 0.7 Hz, 4H), 2.77 (td, J = 7.1, 0.7 Hz, 4H).

Synthesis of covalent monomer (2C)

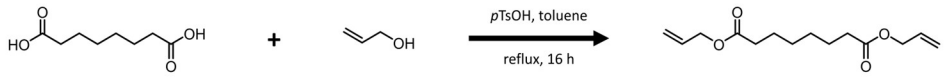

Covalent monomer (**2C**) was prepared using a modified version of a previously reported procedure.[4] Suberic acid (10 g, 0.057 mol, 1 eq), allyl alcohol (8.305 g, 0.143 mol, 2.5 eq), and *p*-toluenesulfonic acid (1.141 g, 0.006 mol, 0.1 eq) were added to a flask containing 200 mL of toluene. The flask was equipped with a Dean-Stark apparatus, and the reaction mixture was stirred under reflux for 16 h. Upon cooling to room temperature, the reaction mixture was transferred to a separatory funnel and washed with an aqueous solution saturated with sodium bicarbonate three

times and then water three times. The organic layer was isolated and had the solvent removed from it under vacuum. The resulting product was a yellow oil. (12.322 g, 85% yield) ^{1}H NMR (400 MHz, $CDCl_3$) δ 5.92 (ddt, J = 17.2, 10.4, 5.7 Hz, 2H), 5.37 – 5.15 (m, 4H), 4.57 (dt, J = 5.8, 1.4 Hz, 4H), 2.33 (t, J = 7.5 Hz, 4H), 1.73 – 1.54 (m, 4H), 1.43 – 1.28 (m, 4H).

Synthesis of dynamic crosslinker (3D)

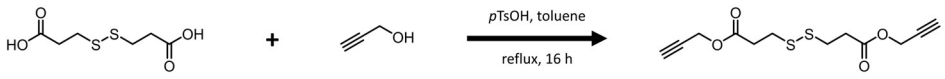

Dynamic crosslinker (**3D**) was prepared using a modified version of a previously reported procedure.[4] 3,3′-Dithiodipropionic acid (10 g, 0.048 mol, 1 eq), propargyl alcohol (6.671 g, 0.143 mol, 2.5 eq), and *p*-toluenesulfonic acid (0.913 g, 0.005 mol, 0.1 eq) were added to a flask containing 200 mL of toluene. The flask was equipped with a Dean-Stark apparatus, and the reaction mixture was stirred under reflux for 16 h. Upon cooling to room temperature, the reaction mixture was transferred to a separatory funnel and washed with an aqueous solution saturated with sodium bicarbonate three times and then water three times. The organic layer was isolated and had the solvent removed from it under vacuum. The resulting product was a pale-yellow oil. (11.958 g, 87% yield) ^{1}H NMR (400 MHz, $CDCl_3$) δ 4.71 (d, J = 2.5 Hz, 4H), 2.94 (td, J = 7.1, 0.9 Hz, 4H), 2.80 (td, J = 7.1, 0.9 Hz, 4H), 2.49 (t, J = 2.5 Hz, 2H).

Synthesis of covalent crosslinker (3C)

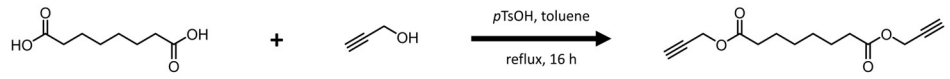

Covalent crosslinker (**3C**) was prepared using a modified version of a previously reported procedure.[4] Suberic acid (10 g, 0.048 mol, 1 eq), propargyl alcohol (8.017 g, 0.143 mol, 2.5 eq), and *p*-toluenesulfonic acid (1.141 g, 0.006 mol, 0.1 eq) were added to a flask containing 200 mL of toluene. The flask was equipped with a Dean-Stark apparatus, and the reaction mixture was stirred under reflux for 16 h. Upon cooling to room temperature, the reaction mixture was transferred to a separatory funnel and washed with an aqueous solution saturated with sodium bicarbonate three times and then water three times. The organic layer was isolated and had the solvent removed from it under vacuum. The resulting product was a pale-yellow oil. (10.211 g, 85% yield) ^{1}H NMR (400 MHz, $CDCl_3$) δ 4.67 (d, J = 2.5 Hz, 4H), 2.46 (t, J = 2.5 Hz, 2H), 2.35 (t, J = 7.5 Hz, 4H), 1.72 – 1.59 (m, 4H), 1.42 – 1.29 (m, 4H).

Preparation of dynamic LCE networks (4B, 4BX, 4X)

Dynamic LCE networks were prepared as follows utilizing a 1:1 ratio of thiol:(alkene + (alkyne/2)) to ensure a stoichiometric amount of functionalities. For example, synthesis of **4B** consisted of adding **1** (2.25 g, 0.005 mol), **HDT** (0.700 g, 0.005 mol), **PDT** (0.849 g, 0.005 mol), **2D** (0.436 g, 0.002 mol), **3C** (0.415 g, 0.002 mol), and a catalytic amount of photoinitiator 2,2-dimethoxy-2-phenylacetophenone (DMPA) (0.092 g, 0.0004 mol) to a vial containing tetrahydrofuran (4 mL). The reaction mixture was thoroughly mixed and sonicated until all components were well dissolved in solution. The reaction mixture was then transferred to a Teflon dish where it was

exposed to UV light (320-390 nm, 2 x 30 s, 50 mW cm^{-2}) to initiate the polymerization and form a solid LCE film.

Preparation of nondynamic LCE network (4N)

Nondynamic LCE network (4N) was prepared as follows utilizing a 1:1 ratio of thiol:(alkene + alkyne/2) to ensure a stoichiometric amount of functionalities. Synthesis of **4N** consisted of adding **1** (2.25 g, 0.005 mol), **HDT** (0.700 g, 0.005 mol), **PDT** (0.849 g, 0.005 mol), **2C** (0.381 g, 0.002 mol), **3C** (0.415 g, 0.002 mol), and a catalytic amount of photoinitiator 2,2-dimethoxy-2-phenylacetophenone (DMPA) (0.092 g, 0.0004 mol) to a vial containing tetrahydrofuran (4 mL). The reaction mixture was thoroughly mixed and sonicated until all components were well dissolved in solution. The reaction mixture was then transferred to a Teflon dish where it was exposed to UV light (320-390 nm, 2 x 30 s, 50 mW cm^{-2}) to initiate the polymerization and form a solid LCE film.

Processing of dynamic LCE networks

Freshly cured dynamic LCE networks were cut into pieces and washed in a Soxhlet extractor apparatus using a 50/50 mixture of tetrahydrofuran and methanol for 16 h. The washed LCE pieces were then dried under vacuum at 60 °C for 16 h. 0.5 mm thick Teflon was cut into 5 cm x 5 cm molds and used to set the thickness of the LCE films. Pieces of the washed and dried LCE were then thermally processed in the molds to make uniform films using a hot melt press at 180 °C for 1 h under 4 tons of pressure. The as-pressed films were then used as is for subsequent characterization.

Processing of Nondynamic LCE network

Freshly cured nondynamic LCE network was washed by allowing the as-cured film to swell in a gently stirring mixture of tetrahydrofuran and methanol that was changed once every hour for 6 hours. The film was then dried in a vacuum oven at 60 °C under vacuum for 16 h. The washed and dried film was then used for subsequent characterization.

2.5.3 Instrumentation

Nuclear magnetic resonance (NMR) spectra were collected on a Bruker Avance III HD nanobay 400 MHz spectrometer.

Differential scanning calorimetry (DSC) thermograms were collected on a TA Instruments Discovery 2500 differential scanning calorimeter. Experiments were run following a (22/200/-90/200) ramp using heating and cooling rates of 10 °C min^{-1}. All curves shown are from the second heating.

Shear mechanical testing including dynamic temperature ramps and stress relaxation data were collected on TA Instruments ARES-G2 shear rheometer. Shear rheology experiments were performed on discs (diameter = 8 mm, thickness = 0.43 mm)

Tensile mechanical testing were collected on films (~ 5mm x 0.45mm x 10mm) using a Zwick-Roell zwickiLine Z0.5 materials testing instrument. Tensile tests were performed on at 22 °C at a strain rate of 5 mm/min until failure.

Wide-angle x-ray scattering (WAXS) data were collected on a SAXSLAB GANESHA 300XL utilizing a Cu Kα source (λ = 0.154 nm) at a voltage and power of 40 kV and 40 mA, respectively.

Films were affixed to a stage with Kapton tape and shot directly and measured for 5 min at q = 0.05 – 0.25.

Processing of WAXS Data

To capture the whole 2D scattering pattern, four individual WAXS patterns are acquired with shifted detector location. Polar transformation is performed to align and average the four scattering patterns. The final scattering pattern is computed by the inverse transformation of the averaged plot. The samples show peak intensity around $q = 1.45 \sim 1.5 Å^{-1}$, indicating an average spacing of $d = 4.27$ Å between the mesogens. To compute the order parameter, the 1D azimuthal data is calculated by integrating the 2D data between $q = 0.97$ $Å^{-1}$ and $q = 1.90$ $Å^{-1}$. The background is subtracted by a linear fit and the order parameter is calculated by the Kratky method as described previously.[5]

2.6 Supporting Information

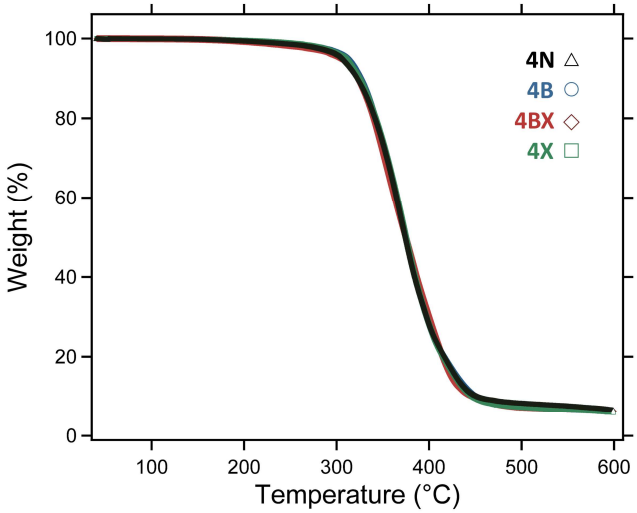

Figure S2.1: Stacked thermal degradation profiles for **4N, 4B**, **4BX**, and **4X**.

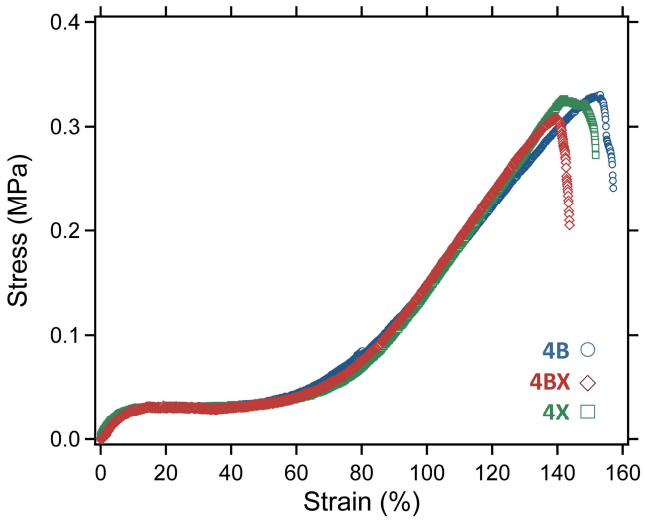

Figure S2.2: Stacked stress-strain profiles for the representative tensile curves for **4B**, **4BX**, and **4X**.

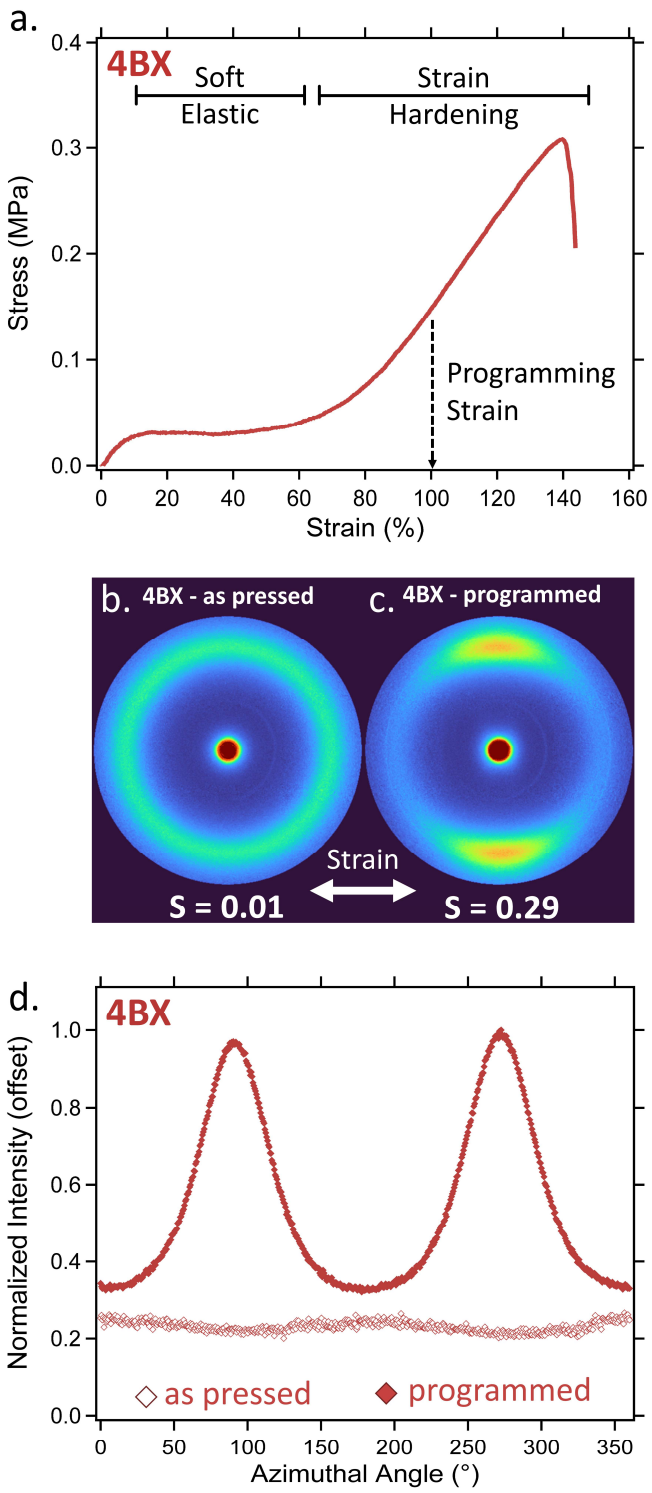

Figure S2.3: a. Stress-strain profile of an as pressed sample of **4BX**; b. 2D WAXS image of an as pressed film of **4BX**; c. 2D WAXS image of an aligned programmed; d. Plots of normalized intensity as a function of angle for both an as-pressed and aligned programmed film of **4BX**.

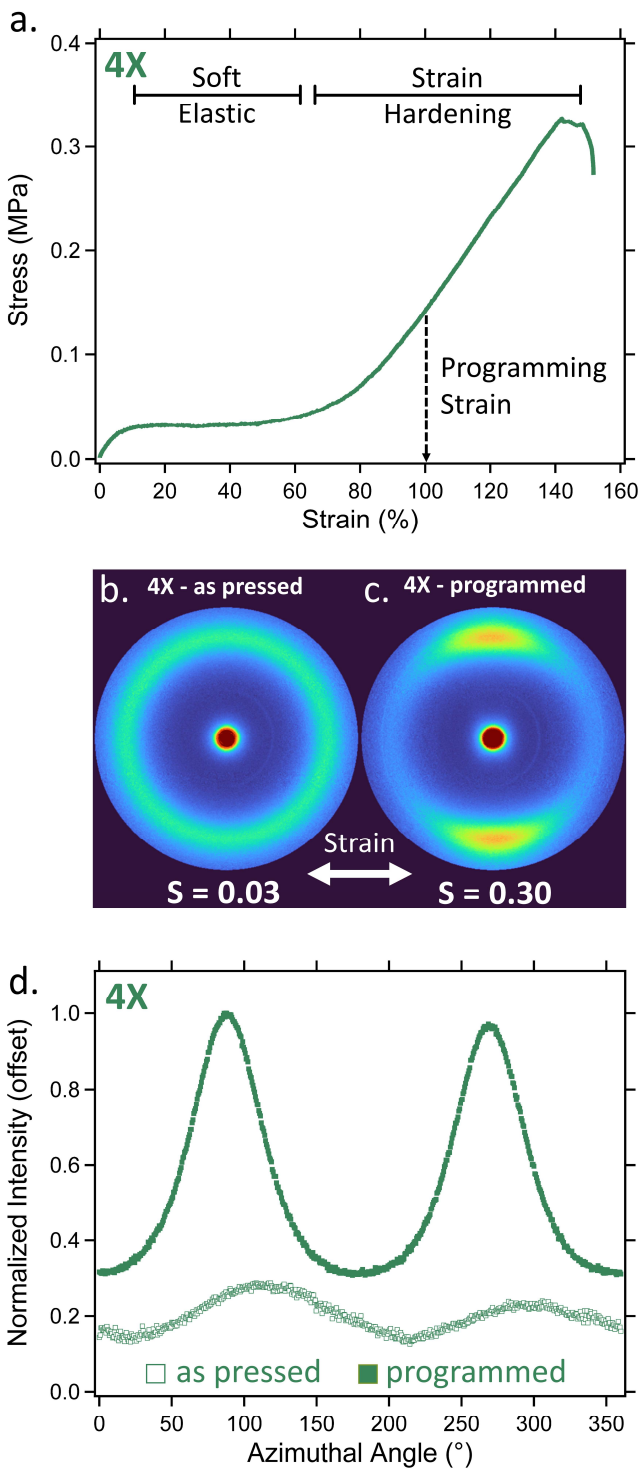

Figure S2.4: a. Stress-strain profile of an as pressed sample of **4X**; b. 2D WAXS image of an as pressed film of **4X**; c. 2D WAXS image of an aligned programmed; d. Plots of normalized intensity as a function of angle for both an as-pressed and aligned programmed film of **4X**.

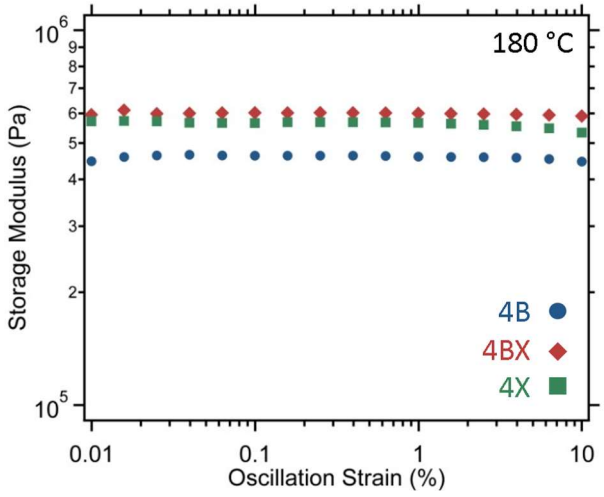

Figure S2.5: Amplitude sweeps showing storage modulus versus oscillation strain at 180 °C for **4B**, **4BX**, and **4X** to illustrate the linear viscoelastic regime for these materials.

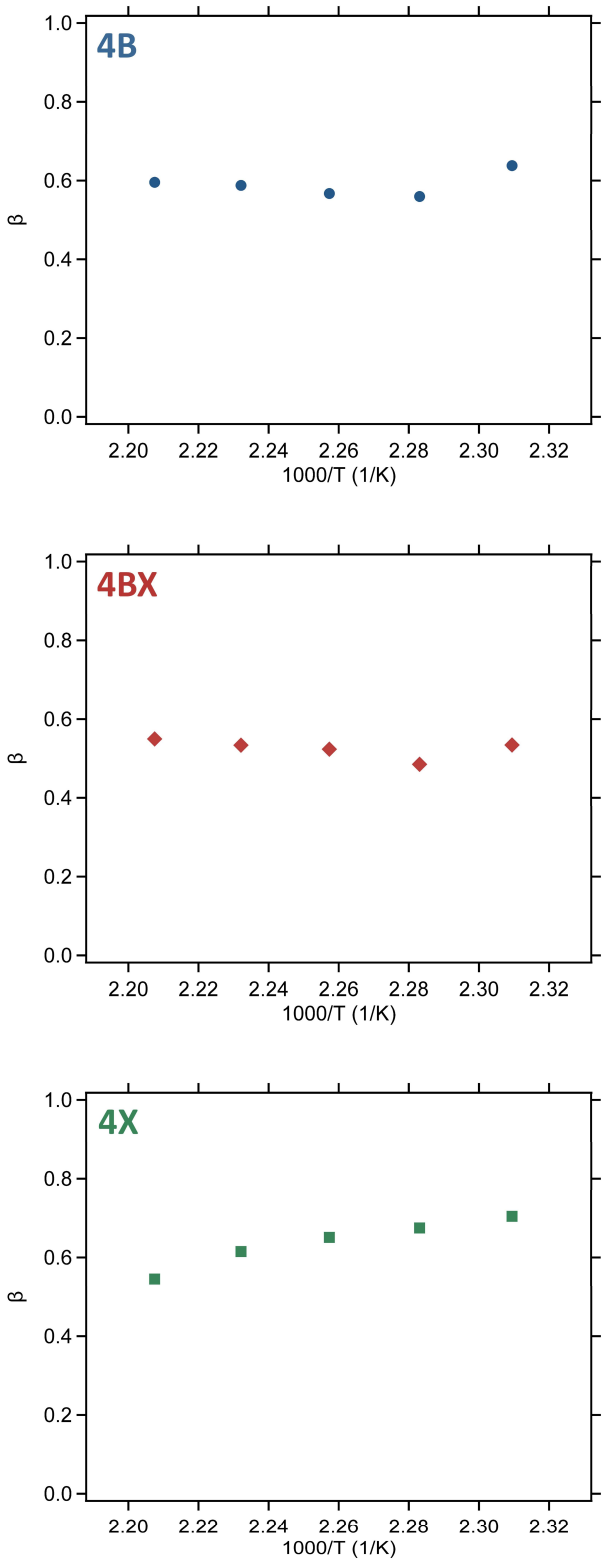

Figure S2.6: Plots of β parameters as a function of temperature for stretched exponential fits of stress relaxation measurements.

2.7 References

[1] P. G. De Gennes, *C. R. Acad. Sci. B* **1975**, *281*, 101.

[2] M. Warner, E. M. Terentjev, *International Series of Monographs on Physics: Liquid Crystal Elastomers*, Oxford University Press, Oxford, **2007**.

[3] J. Kupfer, H. Finkelmann, *Makromol. Chem., Rapid Commun* **1991**, *12*, 717.

[4] T. Ube, K. Kawasaki, T. Ikeda, *Adv. Mater.* **2016**, *28*, 8212.

[5] L. T. De Haan, J. M. N. Verjans, D. J. Broer, C. W. M. Bastiaansen, A. P. H. J. Schenning, *J. Am. Chem. Soc.* **2014**, *136*, 10585.

[6] B. T. Michal, B. M. McKenzie, S. E. Felder, S. J. Rowan, *Macromolecules* **2015**, *48*, 3239.

[7] M. Warner, P. Bladon, E. M. Terentjev, *J. Phys. II* **1994**, *4*, 93.

[8] A. Kotikian, C. McMahan, E. C. Davidson, J. M. Muhammad, R. D. Weeks, C. Daraio, J. A. Lewis, *Sci. Robot.* **2019**, *4*, eaax7044.

[9] Q. He, Z. Wang, Y. Wang, A. Minori, M. T. Tolley, S. Cai, *Sci. Adv.* **2019**, *5*, eaax574.

[10] R. H. Volpe, D. Mistry, V. V. Patel, R. R. Patel, C. M. Yakacki, *Adv. Healthc. Mater.* **2020**, *9*, 1901136.

[11] N. A. Traugutt, D. Mistry, C. Luo, K. Yu, Q. Ge, C. M. Yakacki, *Adv. Mater.* **2020**, *32*, 2000797.

[12] M. T. Brannum, A. M. Steele, M. C. Venetos, L. T. J. Korley, G. E. Wnek, T. J. White, *Adv. Opt. Mater.* **2019**, *7*, 1801683.

[13] S. Hussain, S. Y. Park, *ACS Appl. Mater. Interfaces* **2021**, *13*, 59275.

[14] T. H. Ware, Z. P. Perry, C. M. Middleton, S. T. Iacono, T. J. White, *ACS Macro Lett.* **2015**, *4*, 942.

[15] T. Guin, B. A. Kowalski, R. Rao, A. D. Auguste, C. A. Grabowski, P. F. Lloyd, V. P. Tondiglia, B. Maruyama, R. A. Vaia, T. J. White, *ACS Appl. Mater. Interfaces* **2018**, *10*, 1187.

[16] C. M. Yakacki, M. Saed, D. P. Nair, T. Gong, S. M. Reed, C. N. Bowman, *RSC Adv.* **2015**, *5*, 18997.

[17] Z. Wang, S. Cai, *J. Mater. Chem. B* **2020**, *8*, 6610.

[18] M. O. Saed, A. Gablier, E. M. Terentjev, *Chem. Rev.* **2022**, *122*, 4927.

[19] C. Valenzuela, Y. Chen, L. Wang, W. Feng, *Chem. – A Eur. J.* **2022**, *28*, e202201957.

[20] S. J. Rowan, S. J. Cantrill, G. R. L. Cousins, J. K. M. Sanders, J. F. Stoddart, *Angew. Chemie - Int. Ed.* **2002**, *41*, 898.

[21] R. J. Wojtecki, M. A. Meador, S. J. Rowan, *Nat. Mater.* **2011**, *10*, 14.

[22] Z. Pei, Y. Yang, Q. Chen, E. M. Terentjev, Y. Wei, Y. Ji, *Nat. Mater.* **2014**, *13*, 36.

[23] H. Tsunoda, K. Kawasaki, T. Ube, T. Ikeda, *Mol. Cryst. Liq. Cryst.* **2018**, *662*, 61.

[24] D. W. Hanzon, N. A. Traugutt, M. K. McBride, C. N. Bowman, C. M. Yakacki, K. Yu, *Soft Matter* **2018**, *14*, 951.

[25] Z. Wang, H. Tian, Q. He, S. Cai, *ACS Appl. Mater. Interfaces* **2017**, *9*, 33119.

[26] L. Chen, M. Wang, L. X. Guo, B. P. Lin, H. Yang, *J. Mater. Chem. C* **2018**, *6*, 8251.

[27] D. Tang, L. Zhang, X. Zhang, L. Xu, K. Li, A. Zhang, *ACS Appl. Mater. Interfaces* **2022**, *14*, 1929.

[28] M. K. McBride, M. Hendrikx, D. Liu, B. T. Worrell, D. J. Broer, C. N. Bowman, *Adv. Mater.* **2017**, *29*, 1606509.

[29] M. K. McBride, A. M. Martinez, L. Cox, M. Alim, K. Childress, M. Beiswinger, M. Podgorski, B. T. Worrell, J. Killgore, C. N. Bowman, *Sci. Adv.* **2018**, *4*, eaat4634.

[30] Z. S. Davidson, H. Shahsavan, A. Aghakhani, Y. Guo, L. Hines, Y. Xia, S. Yang, M. Sitti, *Sci. Adv.* **2019**, *5*, eaay0855.

[31] E. C. Davidson, A. Kotikian, S. Li, J. Aizenberg, J. A. Lewis, *Adv. Mater.* **2020**, *32*, 1905682.

[32] L. Zhang, S. J. Rowan, *Macromolecules* **2017**, *50*, 5051.

[33] L. Imbernon, E. K. Oikonomou, S. Norvez, L. Leibler, *Polym. Chem.* **2015**, *6*, 4271.

[34] B. T. Michal, C. A. Jaye, E. J. Spencer, S. J. Rowan, *ACS Macro Lett.* **2013**, *2*, 694.

[35] B. T. Michal, E. J. Spencer, S. J. Rowan, *ACS Appl. Mater. Interfaces* **2016**, *8*, 11041.

[36] G. L. Grocke, H. Zhang, S. S. Kopfinger, S. N. Patel, S. J. Rowan, *ACS Macro Lett.* **2021**, *10*, 1637.

[37] J. M. A. Carnall, C. A. Waudby, A. M. Belenguer, M. C. A. Stuart, J. J.-P. Peyralans, S. Otto, *Science (80-.).* **2010**, *327*, 1502.

[38] U. F. Fritze, M. Von Delius, *Chem. Commun.* **2016**, *52*, 6363.

[39] Z. Q. Lei, H. P. Xiang, Y. J. Yuan, M. Z. Rong, M. Q. Zhang, *Chem. Mater.* **2014**, *26*, 2038.

[40] M. Pepels, I. Filot, B. Klumperman, H. Goossens, *Polym. Chem.* **2013**, *4*, 4955.

[41] Y. Li, Y. Zhang, O. Rios, J. K. Keum, M. R. Kessler, *RSC Adv.* **2017**, *7*, 37248.

[42] Z. Wang, Q. He, Y. Wang, S. Cai, *Soft Matter* **2019**, *15*, 2811.

[43] Q. He, Z. Wang, Y. Wang, Z. Song, S. Cai, *ACS Appl. Mater. Interfaces* **2020**, *12*, 35464.

[44] S. Huang, Y. Shen, H. K. Bisoyi, Y. Tao, Z. Liu, M. Wang, H. Yang, Q. Li, *J. Am. Chem. Soc.* **2021**, *143*, 12543.

[45] B. D. Fairbanks, T. F. Scott, C. J. Kloxin, K. S. Anseth, C. N. Bowman, *Macromolecules* **2009**, *42*, 211.

[46] A. B. Lowe, C. E. Hoyle, C. N. Bowman, *J. Mater. Chem.* **2010**, *20*, 4745.

[47] C. E. Hoyle, C. N. Bowman, *Angew. Chemie Int. Ed.* **2010**, *49*, 1540.

[48] S. V. Arehart, C. Pugh, *J. Am. Chem. Soc.* **1997**, *119*, 3027.

[49] Y.-K. Lee, K. Onimura, H. Tsutsumi, T. Oishi, *Polym. J.* **2000**, *32*, 395.

[50] M. Barnes, S. Cetinkaya, A. Ajnsztajn, R. Verduzco, *Soft Matter* **2022**, 5074.

[51] H. Kim, J. M. Boothby, S. Ramachandran, C. D. Lee, T. H. Ware, *Macromolecules* **2017**, *50*, 4267.

[52] M. O. Saed, R. H. Volpe, N. A. Traugutt, R. Visvanathan, N. A. Clark, C. M. Yakacki, *Soft Matter* **2017**, *13*, 7537.

[53] W. H. Carothers, *Trans. Faraday Soc.* **1936**, *32*, 39.

[54] N. J. Bongiardina, S. M. Soars, M. Podgorski, C. N. Bowman, *Polym. Chem.* **2022**, *13*, 3991.

[55] S. M. Soars, N. J. Bongiardina, B. D. Fairbanks, M. Podgórski, C. N. Bowman, *Macromolecules* **2022**, *55*, 1811.

[56] J. T. Kamps, S. M. Soars, N. J. Bongiardina, B. D. Fairbanks, C. N. Bowman, *Tetrahedron* **2022**, *109*, 10.

[57] M. O. Saed, A. H. Torbati, C. A. Starr, R. Visvanathan, N. A. Clark, C. M. Yakacki, *J. Polym. Sci. Part B Polym. Phys.* **2017**, *55*, 157.

[58] M. T. Sims, L. C. Abbott, R. M. Richardson, J. W. Goodby, J. N. Moore, *Liq. Cryst.* **2019**, *46*, 11.

[59] J. J. Hermans, P. H. Hermans, D. Vermaas, A. Weidinger, *Recl. des Trav. Chim. des Pays-Bas* **1946**, *65*, 427.

[60] L. Zhang, L. Chen, S. J. Rowan, *Macromol. Chem. Phys.* **2017**, *218*, 1.

[61] B. R. Elling, W. R. Dichtel, *ACS Cent. Sci.* **2020**, *6*, 1488.

[62] S. Patai, Z. Rappoport, *Sulphur-Containing Functional Groups (1993)*, John Wiley & Sons, Inc., Chichester, UK, **1993**.

[63] J. J. Lessard, K. A. Stewart, B. S. Sumerlin, *Macromolecules* **2022**, *55*, 10052.

CHAPTER 3

SHOULD I STAY OR SHOULD I FLOW? AN EXPLORATION OF PHASE-SEPARATED METALLOSUPRAMOLECULAR LIQUID CRYSTAL POLYMERS

3.1 Summary

Dynamic liquid crystalline polymers (dLCPs) incorporate both liquid crystalline mesogens and dynamic bonds into a single polymeric material. These dual functionalities impart order-dependent thermo-responsive mechano-optical properties and enhanced reprocessability/programmability enabling their use as soft actuators, adaptive adhesives, and damping materials. While many previous works studying dynamic LCPs utilize dynamic covalent bonds, metallosupramolecular bonds provide a modular platform where a series of materials can be accessed from a single polymeric feedstock through the variation of the metal ion used. A series of dLCPs were prepared by addition of metal salts to a telechelic 2,6-bisbenzimidazolylpyridine (Bip) ligand endcapped LCP to form metallosupramolecular liquid crystal polymers (MSLCPs). The resulting MSLCPs were found to phase separate into hard and soft phases which aids in their mechanical robustness. Variation of the metal salts used to access these materials allowed for control of the thermomechanical, viscoelastic, and adhesive properties with relaxations that can be tailored independent of the mesogenic transition. This work demonstrates that by accessing phase separation through the incorporation of metallosupramolecular moieties, highly processable yet robust MSLCP materials can be realized. This class of materials opens the door to LCPs with bulk flow behavior that can also be utilized as multi-level adhesives.

3.2 Introduction

Liquid crystal polymers (LCPs) are a class of materials characterized by the covalent incorporation of liquid crystalline moieties (mesogens) into a polymeric structure.[1,2] LCP materials include traditional linear polymeric species as well as crosslinked systems such as liquid crystal networks (LCNs) and liquid crystal elastomers (LCEs).[3–5] By selectively manipulating the orientation of these mesogens and/or disrupting the liquid crystalline phase via an external stimulus (e.g. heat or light), it is possible to induce functional responses in these materials such as complex optical transformations,[6–8] thermally-induced shape memory,[9–11] and "soft elastic" damping behavior stemming from the mesogens' rotational modes.[12–14] Due to the interplay between the entropic elasticity afforded by the network structure and the reversible assembly of the liquid crystal (LC) domain structure, crosslinked LCPs have been studied for use in a wide array of application spaces including reversible actuators,[15,16] biomedical devices,[17,18] and adaptive adhesives.[19–21]

One drawback of many permanently crosslinked polymer networks is the inability to undergo further reprocessing once crosslinking has occurred, making reprogramming and reprocessing efforts futile. One advent to circumvent this shortcoming has been the incorporation of dynamic covalent chemistries into the network structure as a means of providing linkages that can reversibly cleave to induce structural reorganization.[22–24] Dynamically crosslinked LCP materials have also been studied in this regard, demonstrating that the incorporation of dynamic bonds can facilitate both reprocessability as well as post-synthetic programmability.[25–27] However, while reprocessability is achievable for many of these systems, it often requires rather harsh processing conditions[28–31] due to the inherent tradeoff between stability and processability in dynamic polymer systems and the need to balance the two.[32,33]

One potential route to enhance the processability of dynamic materials is the use of more labile linkages to facilitate network exchange under more moderate conditions. An obvious drawback to this approach is the diminishing stability that comes with the incorporation of a more labile dynamic linkage. However, there are a number of examples of dynamic polymer systems that utilize weak dynamic bonds in combination with phase separation[34–37] to yield robust materials.[38–41] Supramolecular polymers formed from (macro)monomers polymerized through noncovalent interactions, such as ionic bonds, hydrogen bonding, or host-guest interactions, are a class of dynamic polymers that have been used to access robust functional materials.[42–47] A subclass of supramolecular polymers are the metallosupramolecular polymers (MSPs), in which metal-ligand coordination is the driving force to form the polymers.[48–54] MSPs are particularly interesting as there are a wide range of accessible bond strengths and connectivities based on different metal ion/ligand pairs.[55–62] Metallosupramolecular interactions have been previously incorporated into crosslinked LCP materials as an modality for introducing new adaptive/functional properties such as chemo-based actuation,[63] shape fixing,[64] and programmability.[65] However, little work has been conducted in the utilization of metallosupramolecular interactions as the driving force to form LCPs from lower molecular weight (macro)monomers. Work by Liang et al.[66] took inspiration from the protein chemistry of mussels and created catechol-terminated liquid crystalline polymers which were crosslinked with an Fe (III) salt. The use of these strong metallosupramolecular linkages resulted in materials that formed tough, processable films capable of shape-memory behavior. That work showed that metal-ligand linkages could be successfully incorporated into LCPs without significantly disrupting the LC phase. Work reported herein focuses on the design, synthesis and characterization of metallosupramolecular liquid crystal polymers (MSLCPs) with the goal of exploring how altering

the nature of the metal-ligand interactions can be used to impact the thermomechanical, viscoelastic, and adhesive properties of these materials. More specifically, the target telechelic LCP macromonomers will bear terminal bis(benzimidazolyl)pyridine (Bip) ligands (Figure 3.1A). It has previously been shown that the Bip ligand is capable of binding to a variety of metal ions and has been studied extensively in the context of metallosupramolecular polymers (MSPs).[39,58,67–71] Importantly for this study it has been shown that Bip can bind to Zn(II) ions in a 2:1 ratio and to lanthanides, such as Eu(III), in a 3:1 ratio (Figure 3.1B, Figure S3.1-3).[69]

3.3 Results and Discussion

3.3.1 Design and Synthesis

A dialkene mesogenic monomer (**1**) was reacted with a dithiol chain extender (**2**) and an alkene bearing Bip ligand (**3**) using photoinitiated thiol-ene chemistry to synthesize the telechelate LCP (**4**) (Figure 3.1C). Using Carother's equation, the ratio of **1** and **2** was calculated to target a polymer with a molecular weight of around 10,000 g/mol with thiol end groups. The monomers were dissolved in methylene chloride (DCM) with a catalytic amount of the photoinitiator 2,2-dimethoxy-2-phenylacetophenone (DMPA).

The reaction solution was then exposed to UV light (320-390 nm, 3 mW cm^{-2}) for 15 minutes to initiate the polymerization. Full conversion of the alkene moieties was confirmed via ^{1}H-NMR spectroscopy via the disappearance of the signal corresponding to the alkene protons (Figure S3.4). A stoichiometric amount of **3** (relative to thiol chain ends of the polymer) and a catalytic amount of DMPA was then added to the reaction solution, which was then irradiated by UV light to initiate this thiol-ene coupling of the ligand to the polymer chain ends. As before, full conversion was confirmed by the disappearance of the alkene protons signals in the ^{1}H-NMR

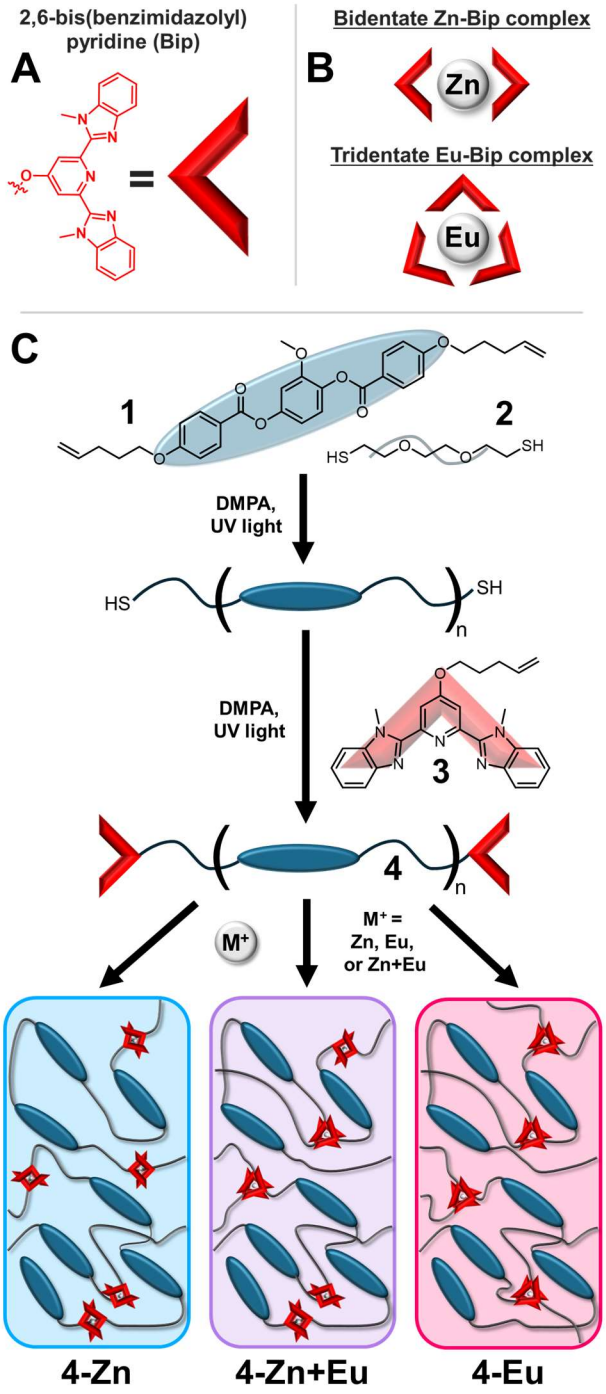

Figure 3.1 : A. Chemical structure of the 2,6-bis(benzimidazolyl)-pyridine ligand; B. Diagrams of the different connectivities that the Bip ligand can adopt depending on the metal center is Zn(II) or Eu(III); C. Component and polymeric architectures for a modular MSLCP material that allows for selective metallosupramolecular connectivities based on the metal adding where Zn(II) provides linear linkages, Eu(III) provides crosslinks, and mixture of Zn(II) and Eu(III) provides both

(Figure S3.4). The telechelate polymers (**4**) were then purified via precipitation in methanol (MeOH). ^{1}H-NMR of the purified polymer confirmed a number-average molecular weight (M_n) of approximately 10,000 g mol^{-1}, as calculated by comparing the chain end and mesogenic proton signals (Figure S3.5). Gel permeation chromatography (GPC) versus polystyrene standards further verified the molecular weight of the LCPs with an M_n of 8,500 g mol^{-1}, and a $Đ$ of 1.3 (Figure S3.6). To access the desired MSLCPs, **4** was mixed with the metal salts zinc di[bis(trifluoromethylsulfonyl)imide] ($Zn(NTf_2)_2$) and europium tri[bis(trifluoromethylsulfonyl)imide] ($Eu(NTf_2)_3$).[69]

These metal ions not only bind in different stoichiometries with the Bip ligand but also exhibit significantly different binding strengths - the formed Zn:Bip complex (~10^6 M^{-2}) and Eu:Bip complex (~10^3-10^4 M^{-3}).[49,72,73] To form the MSLCPs, **4** was dissolved in chloroform ($CHCl_3$) with a stoichiometric amount (such that each Zn(II) ion would complex to two Bip ligands and each Eu(III) ion would complex to three Bip ligands) of $Zn(NTf_2)_2$ (**4-Zn**), $Eu(NTf_2)_3$) (**4-Eu**), or a 50/50 mixture of $Zn(NTf_2)_2$ and $Eu(NTf_2)_3$ (**4-Zn+Eu**). The resulting solutions were cast into films and dried under vacuum (16 h, 60 °C) to remove any residual solvent. The films were then melt processed (5 min, 130 °C, 4 tons) to form homogeneous films for testing (Figure S3.7A). As a confirmation of the formation of stable metal ligand complexes in the bulk material, the films were imaged under UV light (Figure S3.7B). The color of the observed fluorescence directly corresponds to the nature of the complex formed with the Zn:Bip complex fluorescing blue, the Eu:Bip complex fluorescing red, and the mixed system fluorescing purple as a combination of the two. Thermogravimetric analysis (TGA) was performed on the materials to determine the materials' thermal stability with all materials exhibiting a primary degradation onset temperature

between 325-335 °C (Figure S3.8) which is well above any temperature accessed for any further characterization in this work.

3.3.2 Thermomechanical and Morphological Characterization

The thermal transitions of the prepared MSLCPs were then studied using differential scanning

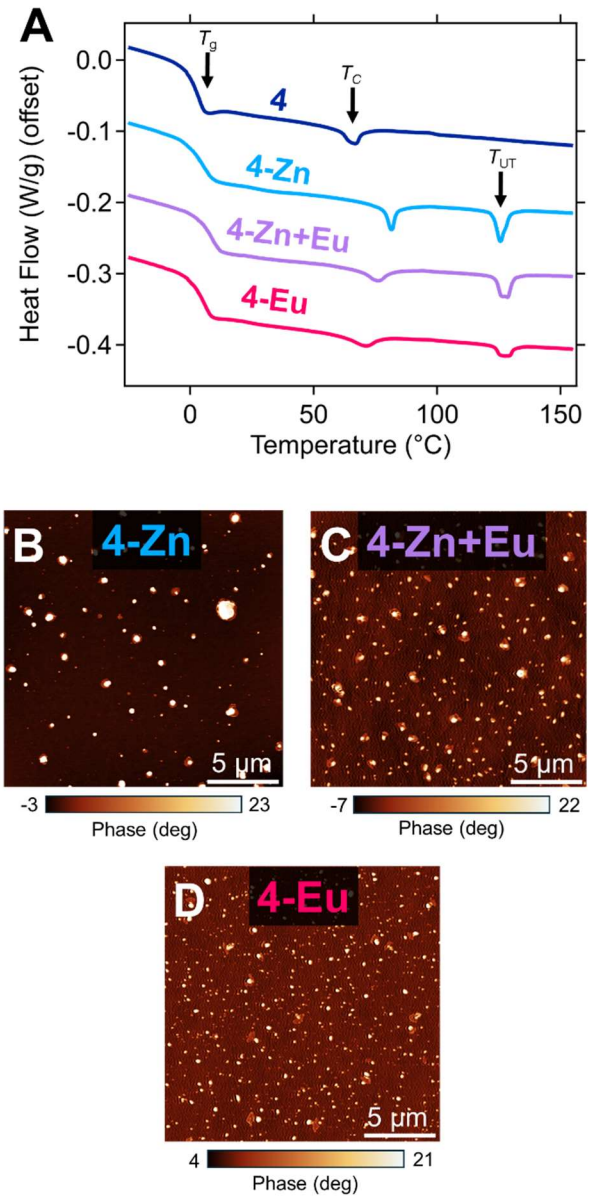

Figure 3.2: A. Differential scanning calorimetry thermograms of MSLCP materials; B. A representative atomic force microscopy phase image of **4-Zn**; C. A representative atomic force microscopy phase image of **4-Zn+Eu** D. A representative atomic force microscopy phase image of **4-Eu**.

calorimetry (DSC). The DSC thermograms revealed the existence of two transitions in the parent telechelate polymer **4** and three transitions for each of the MSLCPs (Figure 3.2A). Each material exhibits a glass transition temperature (T_g) below room temperature with **4**, **4-Zn**, **4-Zn+Eu**, and **4-Eu** possessing T_g's of 2 °C, 4 °C, 8 °C, and 4 °C, respectively (measured by the midpoint of the step present in the DSC thermogram). Every material also displays an endotherm peak indicative of the clearing temperature (T_C) inherent to the liquid crystalline domains formed in the material where **4**, **4-Zn**, **4-Zn+Eu**, and **4-Eu** have T_C's of 66 °C, 81 °C, 76 °C, and 72 °C, respectively. Additionally, the width of the T_C appears to broaden as the amount Eu(III) in the material increases with **4-Zn** having the narrowest T_C and **4-Eu** having the broadest, which follows literature precedent of more crosslinked LCPs displaying broader T_C's.[74] As mentioned above, the MSLCP materials exhibit an additional higher temperature third transition consistent with what has been seen previously in metallosupramolecular polymers.[58,68,75,76] This third transition which is not present in the parent telechelate polymer is assigned as an upper transition (T_{UT}) potentially corresponding to a hard phase formed in the material. **4-Zn**, **4-Zn+Eu**, and **4-Eu** displayed T_{UT}'s of 126 °C, 128 °C, and 128 °C, respectively. Interestingly, this transition consists of two peaks (Figure S3.9) that shift to slightly higher temperatures and decrease in intensity when replacing the Zn(II) ions with the Eu(III) ions. Variable temperature polarized optical microscopy (POM) was also performed to determine the liquid crystalline character of the metallated samples at different temperatures relative to the endotherms observed in DSC (Fig S3.10A-C). All metallated samples exhibit a birefringent liquid crystalline phase at temperatures below their respective T_C's that clears to an isotropic state above T_C, as evidenced by disappearance of the birefringence. No further changes to the images are observed at higher temperatures on either side of the T_{UT} suggesting that any change corresponding to the upper endotherm is occurring at length scales not

observable by optical microscopy. To confirm the presence of a phase separated structure in the MSLCP materials as suggested by the DSC thermograms, atomic force microscopy (AFM) was employed to ascertain the morphology of the materials. AFM measurements were performed on as cast samples of **4**, **4-Zn**, **4-Zn+Eu**, and **4-Eu** at 25 °C (above the glass transition for all materials). While the AFM height images do not show a large contrast indicative of features in **4-Zn** (Figure S3.11A), smaller features can be made out in the case of **4-Zn+Eu** and **4-Eu** (Figure S3.11B-C). The phase images for the metallated materials on the other hand clearly illustrate the

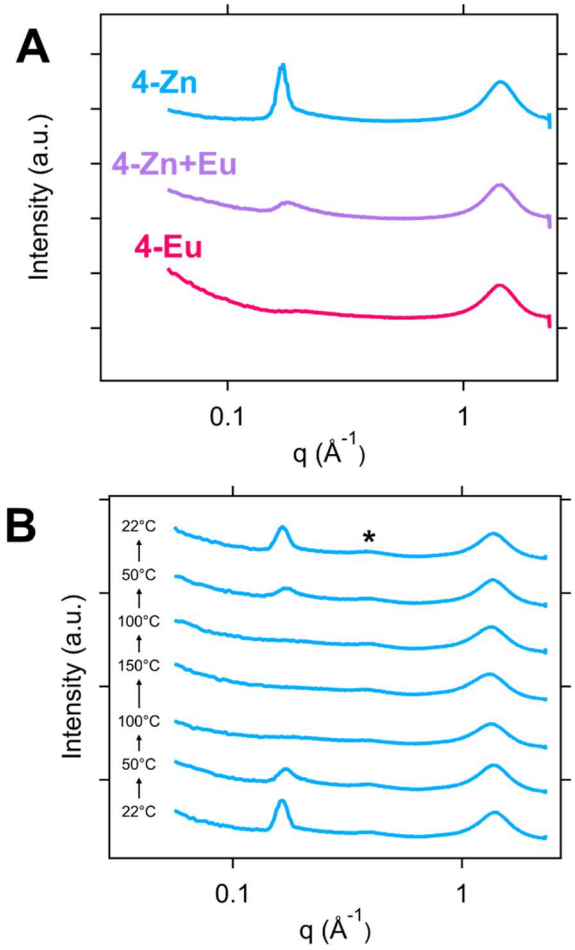

Figure 3.3: A. Room temperature wide-angle x-ray scattering spectra of **4-Zn**, **4-Zn+Eu**, and **4-Eu**; B. Temeprature-dependent wide angle x-ray scattering spectra of **4-Zn** heated across a range of temperature from 22 °C to 150 °C and back to 22 °C. The feature at q = 0.38 $Å^{-1}$ (d = 16.5 Å) indicated by an asterisk corresponds to the polyimide tape used to seal the samples.

presence of a hard and soft phase in each of the materials with larger hard phases in **4-Zn** (Figure 3.2B), smaller hard phases in **4-Eu** (Figure 3.2C), and a mixture of the two sizes in **4-Zn+Eu** (Figure 3.2D) while the phase image of **4** (Figure S3.12) shows no features.To determine the impact of metal-ligand stoichiometry on the formation of the phase separated architecture, two additional off-stoichiometry materials were synthesized, **4-Zn$_{80}$** and **4-Zn$_{95}$**, which possessed ratios of Zn(II) metal binding site to Bip ligand of 0.8:1 and 0.95:1, respectively. DSC thermograms (Figure S3.13A) show the absence of T_{UT}'s in both **4-Zn$_{80}$** and **4-Zn$_{95}$** suggesting that stoichiometry is important in the formation of a phase that exhibits a bulk endotherm. Interestingly, AFM images taken of films of these materials (Figure S3.13B-D) reveal that while **4-Zn$_{80}$** lacks a phase-separated structure, **4-Zn$_{95}$** does appear to exhibit some phase-separation albeit not to the extent of that present in **4-Zn**, as evidenced by the lower contrast between the phases in the **4-Zn$_{95}$** image. Both the DSC and AFM data imply a dependence on stoichiometry on the formation of robust hard phases in MSLCP materials. Temperature dependent wide-angle x-ray scattering (WAXS) experiments were performed across a range of temperatures to elucidate any ordering at smaller length scales. Room temperature measurements of each of the MSLCP materials displayed two signals in the WAXS regime (Figure 3.3A), a signal at a q-value of 1.4 Å^{-1} (d = 0.4 nm) corresponding to an amorphous polymer scattering distance between mesogens on neighboring polymer chains and a signal at a q-value of 0.16 Å^{-1} (d = 3.8 nm) that is consistent with the mesogen to mesogen distance along the backbone of the same polymer chain. The strength of the room-temperature signal at q = 0.16 Å^{-1} decreases with an increase in Eu(III) content which falls in line with the subsequent decrease in locally aligned character of the samples possibly as a result of the formation of branching points. A series of temperature sweeps were also performed to determine the thermoreversibility of the structures present in the materials. From room

temperature (22 °C), the samples were heated to 50 °C, 100 °C, and 150 °C and cooled back through those same temperatures to relate any structural changes to the thermal transitions observed in DSC. In all the materials the signal at q = 1.4 showed no significant change in peak shape or location at any of the temperatures tested. For **4-Zn** and **4-Zn+Eu** (Figure 3.3B, Figure S3.14), the peak at q = 0.16 $Å^{-1}$ decreases in intensity at 50 °C and disappears by 100 °C. This coincides with the DSC peak assigned to the T_C suggesting the WAXS peak at q = 0.16 $Å^{-1}$ is related to the liquid crystalline ordering of the material. Upon equilibration at 50 °C during cooling, this peak reappears in both samples, demonstrating the reversibility of the mesogenic ordering with temperature. For **4-Eu**, a weaker intensity signal at q = 0.16 $Å^{-1}$ is present (Figure 3.3A) at room temperature, which suggests that the increase in Eu(III) content diminishes local LC ordering. This is hypothesized to be a consequence of an increase in the number of potential branching points resulting from formation of the Eu:Bip_3 complex. As with the other samples at elevated temperatures this weak peak disappears (Figure S3.15).

To probe the temperature-dependent short time scale mechanical properties of the MSLCP materials, small angle oscillatory shear (SAOS) rheology experiments were performed (Figure 3.4A). The measured storage moduli (G') for all samples display three characteristic transitions. The first transition at approximately 12 °C for **4-Zn**, **4-Zn+Eu**, and **4-Eu** corresponds to T_g, appears as a stepwise drop in the G' and a peak in the tan(δ) suggesting that variations in the metal content and subsequent supramolecular architecture have little effect on the T_g for these materials. The second transition is assigned to the T_C and manifests as a local minimum in the G' and a step in the tan(δ) appearing at 81 °C, 80 °C, and 70 °C for **4-Zn**, **4-Zn+Eu**, and **4-Eu** respectively. These data are consistent with the T_C trend observed in the DSC when replacing the Zn(II) ions with Eu(III) ions in these MSLCP materials. The third transition manifests as a downward slope

in G' and a sharp increase in tan(δ) indicating the onset of bulk flow in the materials. In all three MSLCPs, this transition occurs immediately after the T_C suggesting that the LC interactions play a large part in the robustness of the materials as the films lose cohesion once the material enters the isotropic state. Additionally, there does not appear to be an observable change in the rheology indicative of the T_{UT} which further suggests that the LC character is responsible for the majority of the mechanical properties. The MSLCPs were also tested for their nonlinear mechanical properties using tensile testing at ambient conditions. Rectangular bars of **4-Zn**, **4-Zn+Eu**, and **4-Eu** were elongated at a constant strain rate (5 mm min^{-1}) until failure or reaching the maximum testing length of the instrument (Figure 3.4B). **4-Eu** displayed a curve shape representative of a soft and extensible material with a relatively low yield stress (σ_y) of 0.3 MPa and a maximum measured strain of around 5500% while the stress gradually decayed to zero stress across the strain range. **4-Zn** displayed a curve shape more consistent with a yielding plastic, with a higher σ_y of 0.6 MPa and yield strain (ε_y) of 40% while decaying out to a stress of 0.1 MPa and a maximum measured strain of >5500%. It is important to note that none of the tested samples of **4-Zn** or **4-Eu** could be strained to failure with the specified sample geometry and testing apparatus. Interestingly, the **4-Zn+Eu** film exhibited a very different behavior that deviates significantly from the stress decays and high extensions observed in the **4-Zn** and **4-Eu** samples. These films exhibited a strain hardening behavior and a much larger maximum stress before failing around 1000%. One hypothesis for this behavior is that the mixture of both a strong and a weak binder in the Zn:Bip and Eu:Bip complexes enable rearrangement while maintaining structure which allows the network to reorganize while strengthening.

Spent tensile samples were then collected to characterize the alignment of the resulting materials post straining. This was probed using polarized optical microscopy (POM) imaging and

wide-angle X-ray scattering (WAXS) experiments. For POM measurements, samples were cut from the center of the spent tensile bar and placed on glass slides after being allowed to and wide-angle x-ray scattering (WAXS) experiments. For POM measurements, samples were relax at room temperature for five minutes. The samples were then imaged at both 0° and 45° relative to the direction of the polarizer to visually determine the coherence of the strain-induced alignment imparted to the materials. All samples exhibited high levels of alignment (Figure 3.5A) as evidenced by the stark contrast in the transmitted brightness between the 0° and 45° images for each sample tested. To better quantify this behavior, WAXS experiments (Figure 3.5B) were performed on the previously strained MSLCP materials as to determine the amount of alignment

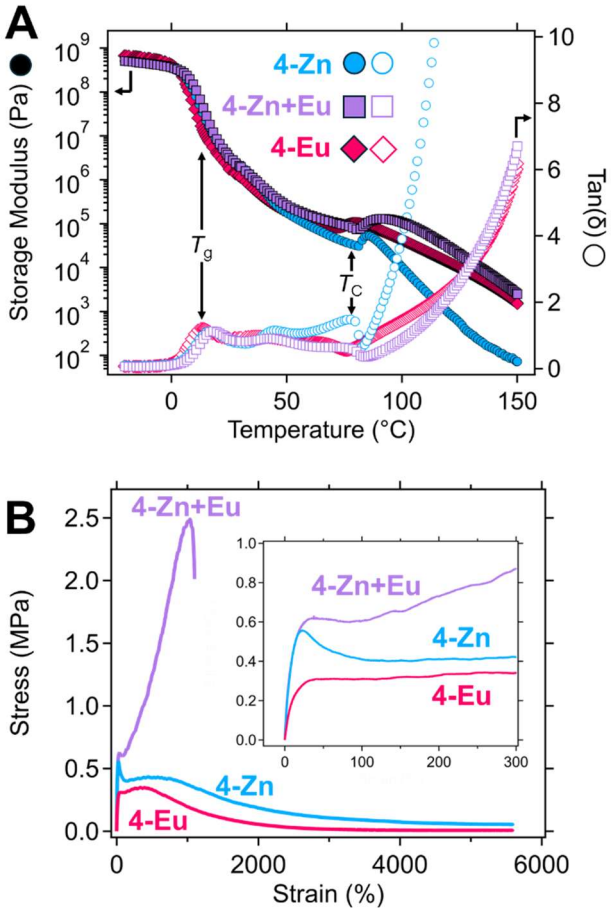

Figure 3.4: A. Shear dynamic rheology temperature ramps of storage modulus (solid shapes) and tan(delta) (empty shapes) for MSLCPs; B. Stress-strain profiles for MSLCPs

that can be achieved. As expected, the strained samples of **4-Zn**, **4-Zn+Eu**, and **4-Eu** exhibit an anisotropic 2D WAXS pattern (Figure 3.5B) with regions of intensity along the horizontal axis corresponding to alignment of mesogens in the direction of applied strain along the vertical axis. By converting these images into plots of scattering intensity versus azimuthal angle (Figure 3.5C), fitting them using the Kratky method[77], and calculating the Hermans order parameter (S)[78] for the aligned materials, it is possible to compare the overall alignment in the MSLCP samples. The samples of **4-Zn**, **4-Zn+Eu**, and **4-Eu** possessed order parameter values of $S = 0.39$, $S = 0.34$, and $S = 0.30$ respectively. This decrease in S value with increasing amount of Eu(III) ions may be

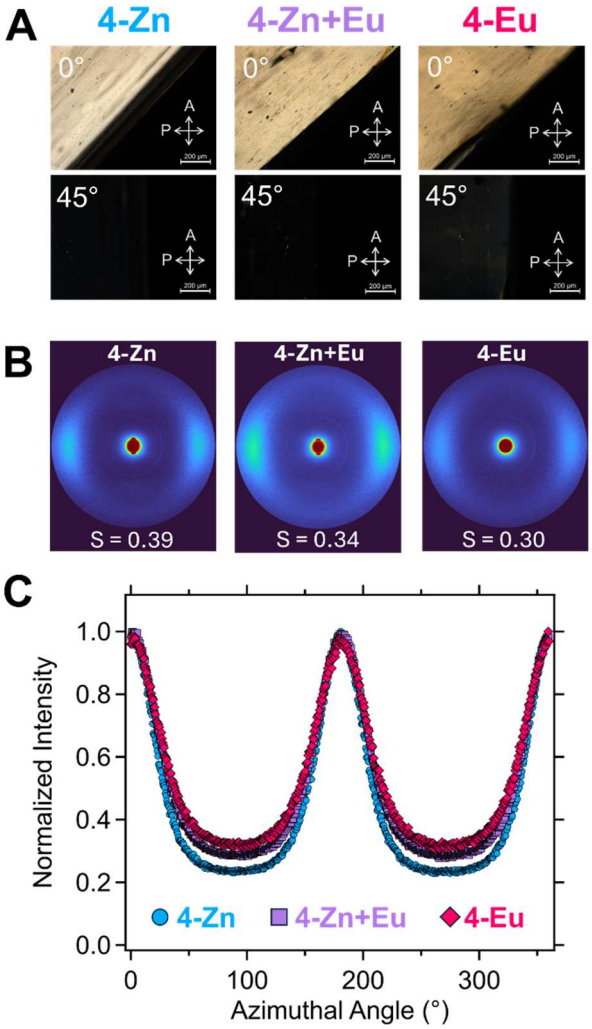

Figure 3.5: A. Polarized optical microscopy images at 0° and 45° B. 2D WAXS images of strained MSLCPs; C. Plots of normalized intensity as a function of azimuthal angle for strained MSLCPs

related to the weaker binding of the Eu(III) and/or an increase in the potential branching points at the Eu(III) metal center that results in less strain induced mesogenic alignment. As both LCPs[79] and supramolecular polymers[80,81] have been studied as adhesive materials, the room temperature stress relaxation and pressure sensitive probe tack behavior of the MSLCPs were also evaluated. Room temperature (22 °C) shear stress relaxation experiments (3% strain, 1 hr) (Figure 3.6A) were performed to determine how the different metal ions impact the dissipative nature of the MSLCPs. Akin to what is observed in recent studies on LCE adhesives[20,79,82], all the MSLCP materials rapidly dissipate stress, with **4-Zn**, **4-Zn+Eu**, and **4-Eu** dropping to 14%, 14%, and 7% of their initial applied stress value over the course of 60 seconds. As the majority of the applied stress (> 90%) had dissipated in the first 60 seconds, this time point was used to perform probe tack tests (Figure 3.6B) where a stainless-steel fixture was pressed into a disk of MSLCP at a constant force and time (1 N, 60 s) after which the probe was retracted at a constant rate (0.1 mm s^{-1}), and the pull-off force required to break contact with the sample was measured (Figure 3.6C). For **4-Zn**, **4-Zn+Eu**, and **4-Eu** the sample required pull-off forces of 6.4 N, 6.0 N, and 19.4 N which are comparable to other LCP PSAs that have been studied.[20,79,83] The probe tack results also trend with the stress relaxation data in that at 60 s, **4-Zn** and **4-Zn+Eu** both have similar stress dissipations and pull-off forces while **4-Eu** has a higher stress dissipation correlating to a higher pressure-sensitive adhesive response.

3.3.3 Adhesive Testing

Hot melt adhesive (HMA) testing was then performed to demonstrate the utility of the bulk flow behavior exhibited by the MSLCP materials. As previously demonstrated in the temperature-dependent rheology data, the onset of bulk flow for all MSLCP materials occurs upon reaching T_C. However, the highest thermal transition (T_{UT}) based on the DSC thermograms does not occur

until 130 °C, so in pursuit of a robust adhesive joint, 3 mm diameter disk-shaped samples of each of the MSLCPs were placed between two aluminum I-bar fixtures, fixed in place with quarter inch binder clips, heated to 130 °C for two minutes, and allowed to cool to room temperature. The adhesive strength of these fixtures was then measured via uniaxial tensile testing where the adhesive strength was taken as the maximum stress achieved prior to failure (Figure 3.7A). For **4-**

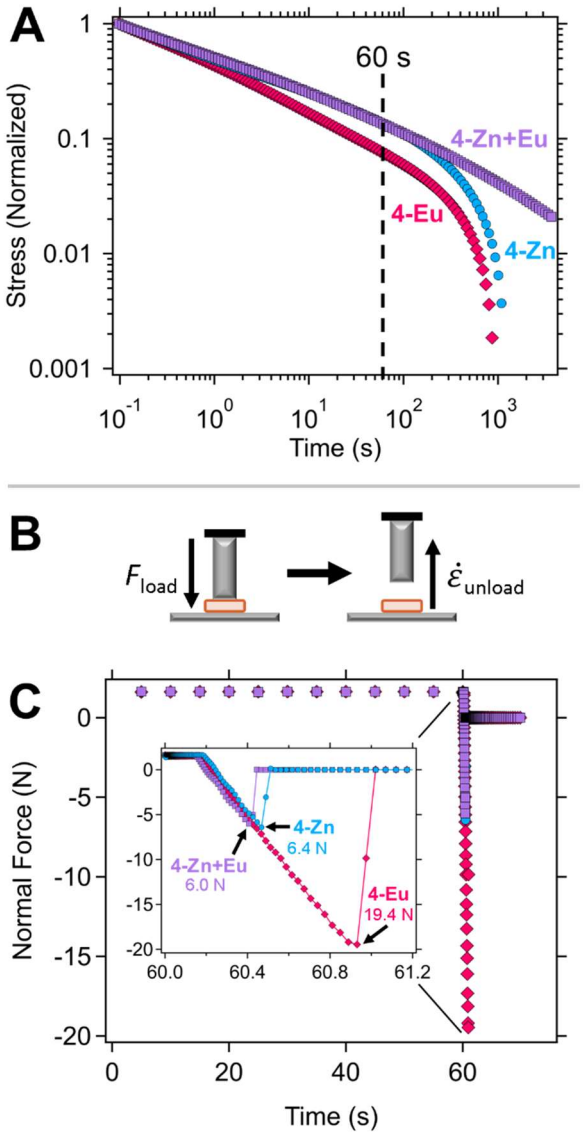

Figure 3.6: A. Room temperature stress relaxation curves for MSLCPs; B. General schematic for the probe tack test; C. A representative force curve as a function of time for a single probe tack test; (inset) zoomed in view of debonding event.

Zn, **4-Zn+Eu**, and **4-Eu** the materials demonstrated respectable adhesive strengths of 4.5 ± 0.6 MPa, 8.5 ± 1.3 MPa, and 7.6 ± 1.1 MPa respectively. As evidenced by the representative images displayed in Figures 3.7B-D, all these materials present regions of material on each of I-bars used to form the adhesive joint consistent with cohesive failure. To further contextualize the utility of this enhanced hot melt adhesive strength, a 5 mm disk (thickness = 0.43 mm, mass = ~10 mg)

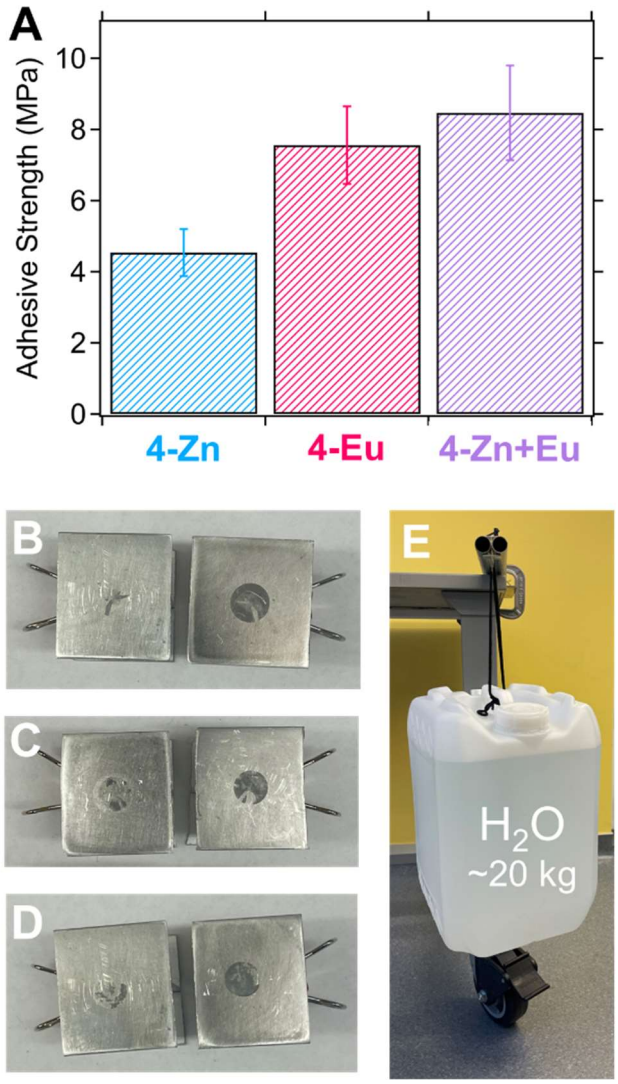

Figure 3.7: A. Adhesive strength comparison of **4-Zn**, **4-Eu**, and **4-Zn+Eu**; B. Representative sample of **4-Zn** after testing to failure; C. Representative sample of 4-Zn+Eu after testing to failure; D. Representative sample of **4-Eu** after testing to failure; E. Demonstration of a sample of **4-Zn+Eu** supporting the weight of a 20 kg carboy filled with water

of **4-Zn+Eu** was used to form an adhesive joint between two aluminum I-bars which was capable of fully supporting a carboy filled with ~20 kg of water (Figure 3.7C).

3.4 Conclusions

In this work, metal-ligand interactions were utilized to develop a series of phase-separated metallosupramolecular liquid crystal polymers (MSLCPs) whose thermomechanical, viscoelastic, and morphological properties were tailored through selection of the linking metal ion. The choice of metal ion impacted the dynamic connectivity of the polymer architecture

and subsequently altered the materials' characteristic thermal transitions, namely the T_g, T_C, and T_{UT} as measured by DSC and SAOS rheology techniques. Additionally, the nonlinear mechanical properties studied via tensile testing of these materials were found to depend drastically on the identity of the incorporated metal ion with a strain hardening phenomenon only observed in the system with a mixture of metals (**4-Zn+Eu**). As the materials studied herein displayed high stress dissipation and terminal flow behavior, these materials were studied for their adhesive character in both PSA and HMA contexts. The MSLCPs displayed robust PSA adhesive behavior that could be tailored through the nature of the metallosupramolecular bond, while HMA behavior trended with the modulus of the bulk material. These results demonstrate that tunable phase-separated MSLCPs are capable of forming tough (re)processable materials with potential applications as multi-level adhesives.

3.5 Materials and Methods

3.5.1 Materials

Potassium carbonate was purchased from Fisher Scientific. 5-Bromo-1-pentene was purchased from Combi-Blocks. All other chemicals were purchased from Millipore-Sigma and were used as received unless noted otherwise. All solvents were purchased from Fisher Scientific and were used as received unless noted otherwise. 2,6-Bis(1H-benzimidazolyl)-4-hydroxypyridine (HOBip) was

prepared following literature precedent.[1] Europium tri[bis(trifluoromethylsulfonyl)imide] ($Eu(NTf_2)_3$) was prepared following literature precedent.[2]

3.5.2 Methods

Synthesis of 4'-(Pent-1-enyloxy)benzoic acid

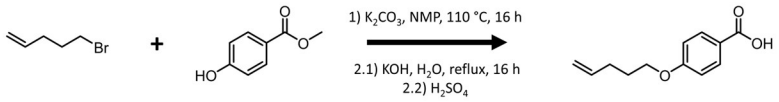

4′-(Pent-1-enyloxy)benzoic acid was synthesized using a modified version of previously published procedures.[3,4] 5-bromo-1-pentene (50 g, 0.336 mol, 1 eq), methyl-4-hyroxybenzoate (52.145 g, 0.342 mol, 1.02 eq), potassium carbonate (50.172 g, 0.362 mol, 1.08 eq) were all added to a flask containing N-methyl-2-pyrrolidone (150 mL, 3 vol). The flask was equipped with a condenser, and the reaction mixture was heated to 80°C while stirring. After observing an exotherm in the form of vigorous bubbling the temperature was raised to 110°C where the reaction was allowed to proceed for 16 h. The reaction mixture was then cooled to room temperature and added to a separatory funnel with toluene (300 mL) and water (100 mL). The organic layer was washed three times with water whereafter the solvent was removed under vacuum. To the resulting oil was added 300 mL of 10 wt% aqueous potassium hydroxide solution. The reaction mixture was then heated to 110 °C and allowed to proceed for 16 h with stirring. After cooling to room temperature, the reaction mixture was extracted with ethyl ether (50 mL) three times. The aqueous layer was then diluted with water to a volume of 2 L while stirring whereupon concentrated sulfuric acid (25 mL) was added to adjust the solution to a pH of about 2. As the sulfuric acid is added, white solid began to precipitate from solution until the reaction mixture became a slurry that was difficult to stir magnetically. The solid was removed from the aqueous solution using a Buchner funnel and

recrystallized three times in hot ethanol yielding white crystals. (61 g, 88% yield) ^{1}H NMR (400 MHz, $CDCl_3$) δ 8.16 – 7.97 (m, 2H), 7.00 – 6.88 (m, 2H), 5.98 – 5.74 (m, 1H), 5.17 – 4.94 (m, 2H), 4.04 (t, J = 6.4 Hz, 2H), 2.25 (qd, J = 7.4, 1.4 Hz, 2H), 2.03 – 1.82 (m, 2H).

Synthesis of liquid crystal monomer (1)

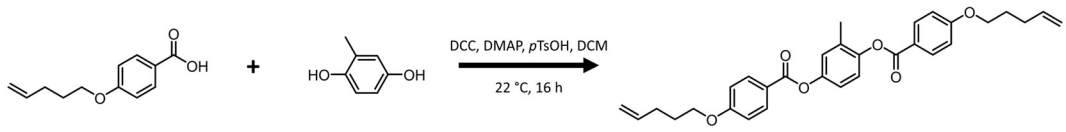

Liquid crystal monomer (**1**) was prepared using a previously reported procedure.[5] 4′-(Pent-1-enyloxy)benzoic acid (24.3 g, 0.118 mol, 1.95 eq), an 2-methoxyhydroquinone (8.44 g, 0.060 mol, 1 eq), dicyclohexylcarbodiimide (28.69g, 0.139 mol, 2.4 eq), 4-dimethylaminopyridine (14.050g, 0.115 mol, 1.9 eq), and *p*-toluenesulfonic acid monohydrate (21.88 g, 0.115 mol, 1.9 eq) were added to a flask containing 400 mL of dichloromethane. The reaction mixture was stirred at room temperature (22 °C) for 16 hours. A solid white urea byproduct was then filtered out of the reaction mixture, and the solvent was then removed from the filtrate under vacuum. The remaining solid was then recrystallized three times in hot ethanol to afford white powdery crystals. (44.25 g, 75% yield) ^{1}H NMR (400 MHz, $CDCl_3$) δ 8.29 – 8.04 (m, 4H), 7.22 – 7.04 (m, 3H), 7.04 – 6.92 (m, 4H), 5.96 – 5.77 (m, 2H), 5.17 – 4.97 (m, 4H), 4.07 (td, J = 6.4, 2.0 Hz, 4H), 2.35 – 2.20 (m, 7H), 2.01 – 1.87 (m, 4H).

Synthesis of alkene functionalized 2,6-bisbenzyimidazolylpyridine (Bip) ligand (3)

5-bromo-1-pentene (5 g, 0.034 mol, 1 eq), 2,6-Bis(1H-benzimidazolyl)-4-hydroxypyridine (HOBip) (12.162 g, 0.034 mol, 1.02 eq), potassium carbonate (5.075 g, 0.037 mol, 1.08 eq) were all added to a flask containing N-methyl-2-pyrrolidone (25 mL, 5 vol). The flask was equipped

with a condenser, and the reaction mixture was heated to 80°C while stirring. After observing an exotherm in the form of vigorous bubbling the temperature was raised to 110°C where the reaction was allowed to proceed for 16 h. The reaction mixture was then cooled to room temperature and extracted with toluene (100 mL) and water (25 mL) collecting the organic fraction. The solvent was removed in vacuo and the remaining solid was triturated with hot ethanol and filtered until the filtrate was colorless leaving a light pink fluffy solid. (11.07 g, 77% yield) ^{1}H NMR (500 MHz, CDCl3) δ 7.94 (s, 2H), 7.87 (d, J = 6.3 Hz, 2H), 7.46 (m, 2H), 7.40 – 7.33 (m, 4H), 5.86 (m, 1H), 5.13 – 5.00 (m, 2H), 4.27-4.22 (m, 8H), 2.31 – 2.25 (m, 2H), 1.98 (dt, J = 8.0, 6.5 Hz, 2H).^{13}C NMR (126 MHz, CDCl3) δ 166.67, 151.22, 150.33, 142.63, 137.43, 137.30, 123.64, 122.91, 120.26, 115.77, 111.89, 110.02, 67.87, 32.63, 29.99, 28.20. MALDI-MS: 446.9 ([M]+Na^{+}).

Synthesis of Bip-terminated telechelate LCP (4)

To form the Bip-terminated telechelate LCP with a targeted molecular weight of 10,000 g/mol, **1** (1.032 g, 0.002 mol), 2,2-(ethylenedioxy)diethanethiol (0.281 mL, 0.0017 mol), and a catalytic amount of 2,2-dimethoxy-2-phenylacetophenonec (DMPA) (0.031 g, 0.00012 mol) were added to 3 mL of methylene chloride. The reaction mixture was stirred until all components were well dissolved in solution and then exposed to UV light while stirring (320-390 nm, 60 min, 3 mW cm^{-2}) to initiate the polymerization. A stoichiometric amount of **3** (relative to the thiol chain ends of the polymer) (0.114 g, 0.00027 mol) and a catalytic amount of DMPA (0.0041 g, 0.000016 mol) was dissolved in 1 mL of chloroform and added to the polymer reaction mixture and well mixed. The polymer and ligand reaction mixture was then exposed to UV light (320-390 nm, 600 s, 3 mW cm^{-2}) after which another equivalent of DMPA was then added to the reaction mixture and the UV light exposure was repeated. This telechelate polymer mixture was then precipitated into 100 mL

of methanol and placed into a freezer (8 °C) for 2 hours after which the methanol was decanted and the polymer was dried in an oven at 60°C under vacuum for 16 hours.

Synthesis of Metallosupramolecular LCPs (MSLCPs) (4-Zn, 4-Zn+Eu, 4-Eu)

MSLCPs were synthesized by adding a stoichiometric amount of **4** with the appropriate metal such that each Bip ligand has a metal binding site. For example, **4-Zn** was prepared via the mixture of a solution of **4** (1.347 g, 0.00013 mol) in 3 mL of chloroform with a solution of zinc di[bis(trifluoromethylsulfonyl)imide] ($Zn(NTf_2)_2$) (0.084 g, 0.00013 mol) dissolved in 1 mL of a 4:1 chloroform:acetonitrile mixture. The resulting mixture was stirred at room temperature until well-mixed and then poured into a PTFE dish and heated to 50°C under ambient conditions for two hours. The dish was then placed in an oven at 60°C under vacuum for 16 hours to remove residual solvent. The resulting material was then collected and melt processed in a hot compression molder (Carver) (130°C, 4 tons, 10 minutes) inside a mold (50 mm x 50 mm x 0.5 mm) to make films of homogeneous thickness for further testing.

3.5.3 Instrumentation

All nuclear magnetic resonance (NMR) spectra were collected on a Bruker Avance III HD nanobay 400 MHz spectrometer.

All differential scanning calorimetry (DSC) thermograms were collected on a TA Instruments Discovery 2500 differential scanning calorimeter. Experiments were run following a (22/200/-90/200) ramp using heating and cooling rates of 10 °C min^{-1}. All curves shown are from the second heating.

All shear mechanical testing including dynamic temperature ramps and stress relaxation data were collected on TA Instruments ARES-G2 shear rheometer. Shear rheology experiments were performed on discs (diameter = 8 mm, thickness = 0.43 mm)

All tensile mechanical testing of rectangular samples of MSLCPs and stud-pull adhesive joints were collected on a Zwick-Roell zwickiLine Z0.5 materials testing instrument. Tensile tests were performed at 22 °C at a strain rate of 5 mm/min until failure.

All probe-tack testing was performed on a TA Instruments ARES-G2 shear rheometer. Tests were performed at 22 °C on discs (diameter = 8 mm, thickness = 0.43 mm)

All wide-angle x-ray scattering (WAXS) data were collected on a SAXSLAB GANESHA 300XL utilizing a Cu Kα source (λ = 0.154 nm) at a voltage and power of 40 kV and 40 mA, respectively. Films were affixed to a stage with Kapton tape and shot directly and measured for 5 min at q = 0.05 – 0.25. For the variable temperature studies, samples were sealed inside Kapton tape.

All polarized optical microscopy images were collected on an Leica DM2700P polarized optical microscope equipped with MC170 HD 5 camera.

All gel permeation chromatography (GPC) data were collected on a Shimadzu HPLC LC20-AD outfitted with a Wyatt Optilab T-rEX differential refractive index detector running tetrahydrofuran as the eluent. Samples were prepared at a concentration of 1.5 mg/mL in tetrahydrofuran and passed through a 200 μm syringe filter prior to sample injection. Molecular weights were measured against a calibration curve created from polystyrene standards.

All UV-Vis spectroscopy data was collected on a Shimadzu UV-3600 Plus UV-VIS-NIR spectrophotometer.

All atomic force microscopy (AFM) images were collected using an Asylum Research Cypher ES AFM with BlueDrive. Tapping-mode imaging was performed using Asylum Research FS-1500-AuD cantilevers with resonant frequencies of 1.5 MHz. Images were collected at a scan rate of 4.88 Hz with a 950 mV set point in the repulsive mode (to prevent tip-induced damage of the sample surface). Samples were equilibrated for 15 min at the desired temperature prior to imaging. Images were processed using Gwyddion 2.61. First, a polynomial (3rd degree horizontal, 3rd degree vertical) background was removed before aligning rows via the median method. Using Gwyddion software, any horizontal scars were removed, and samples were colored using the default Gwyddion palette.

WAXS Data Processing

To capture the whole 2D scattering pattern, four individual WAXS patterns are acquired with shifted detector location. Polar transformation is performed to align and average the four scattering patterns. The final scattering pattern is computed by the inverse transformation of the averaged plot. The samples show peak intensity around $q = 1.45 \sim 1.5$ Å^{-1}, indicating an average spacing of d=4.27 Å between the mesogens. To compute the order parameter, the 1D azimuthal data is calculated by integrating the 2D data between $q = 0.97$ Å^{-1} and $q=1.90$ Å^{-1}. The background is subtracted by a linear fit and the order parameter is calculated by the Kratky method as described previously.

3.6 Supporting Information

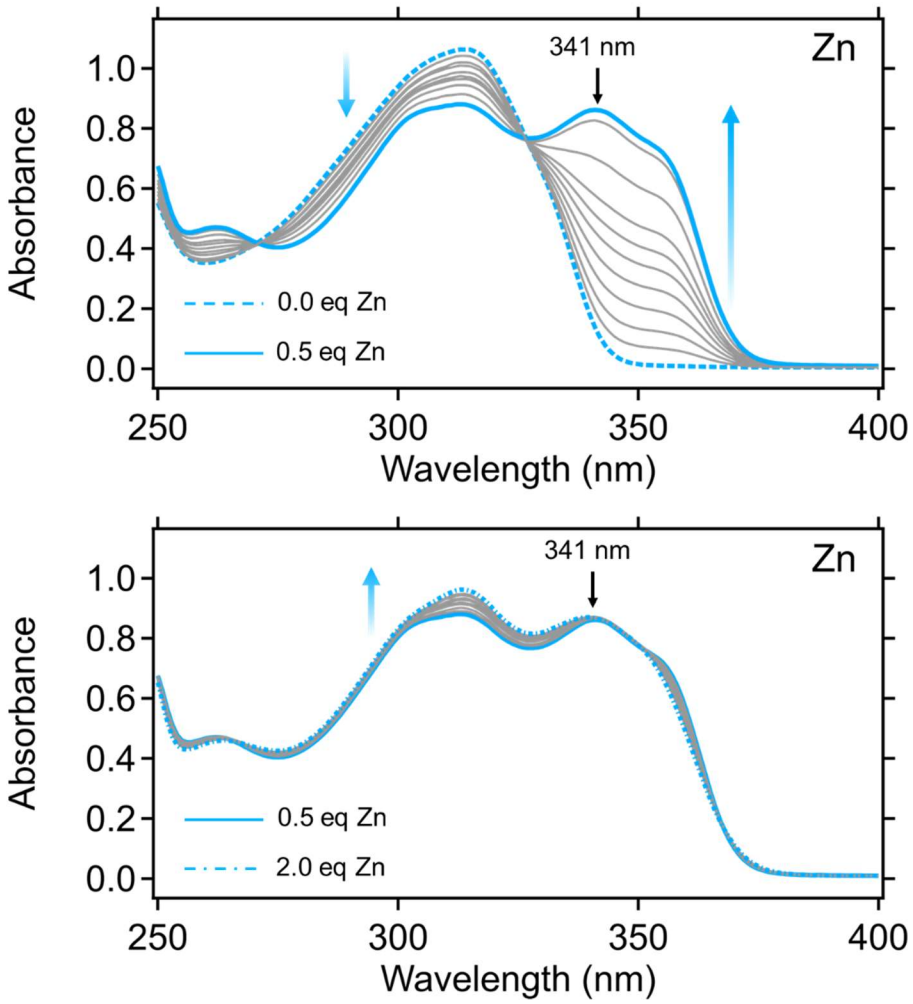

Figure S3.1: UV-Vis titrations of $Zn(NTf_2)_2$ against **3** from no metal ion to an excess of metal ions.

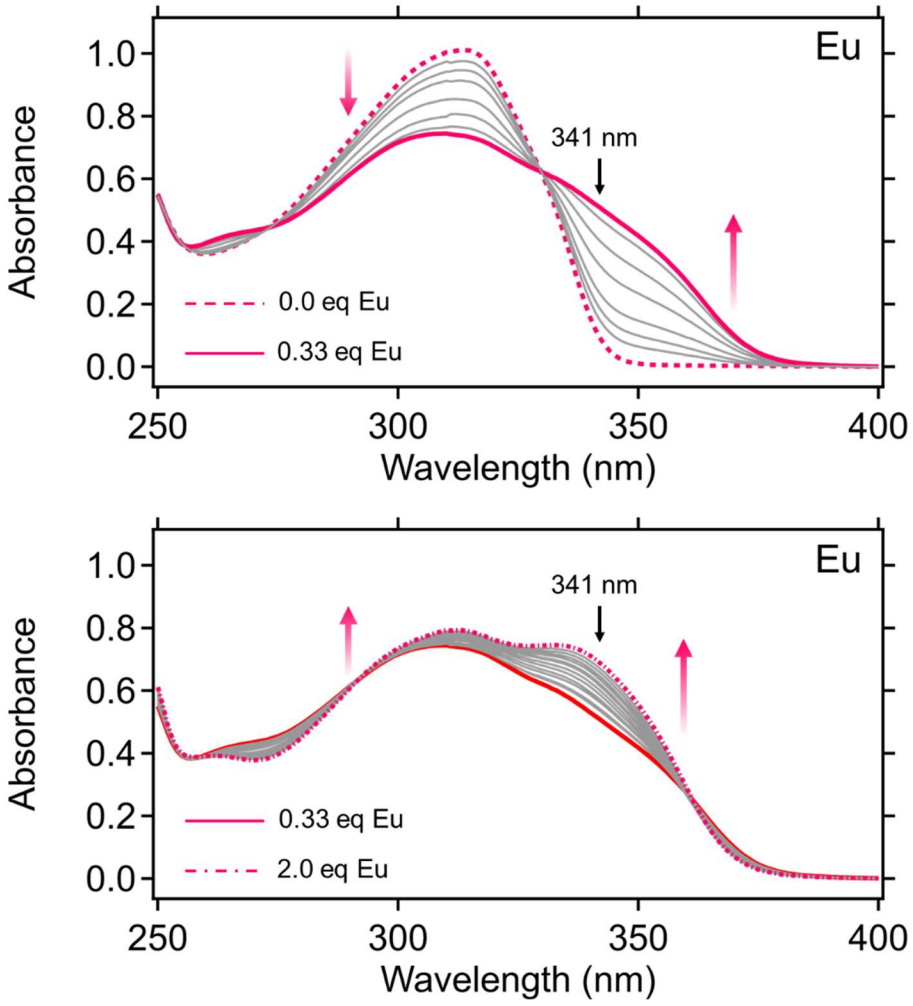

Figure S3.2: UV-Vis titrations of $Eu(NTf_2)_3$ against **3** from no metal ion to an excess of metal ions.

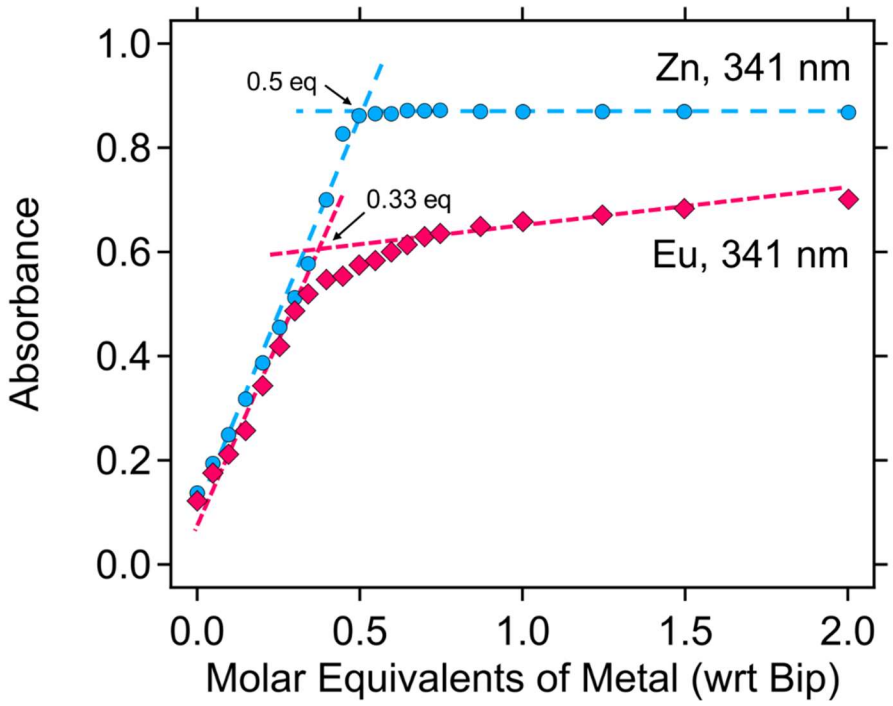

Figure S3.3: Compiled UV intensity at 341 nm vs molar equivalents of metal ion plots for both the Zn ion and Eu ion titrations

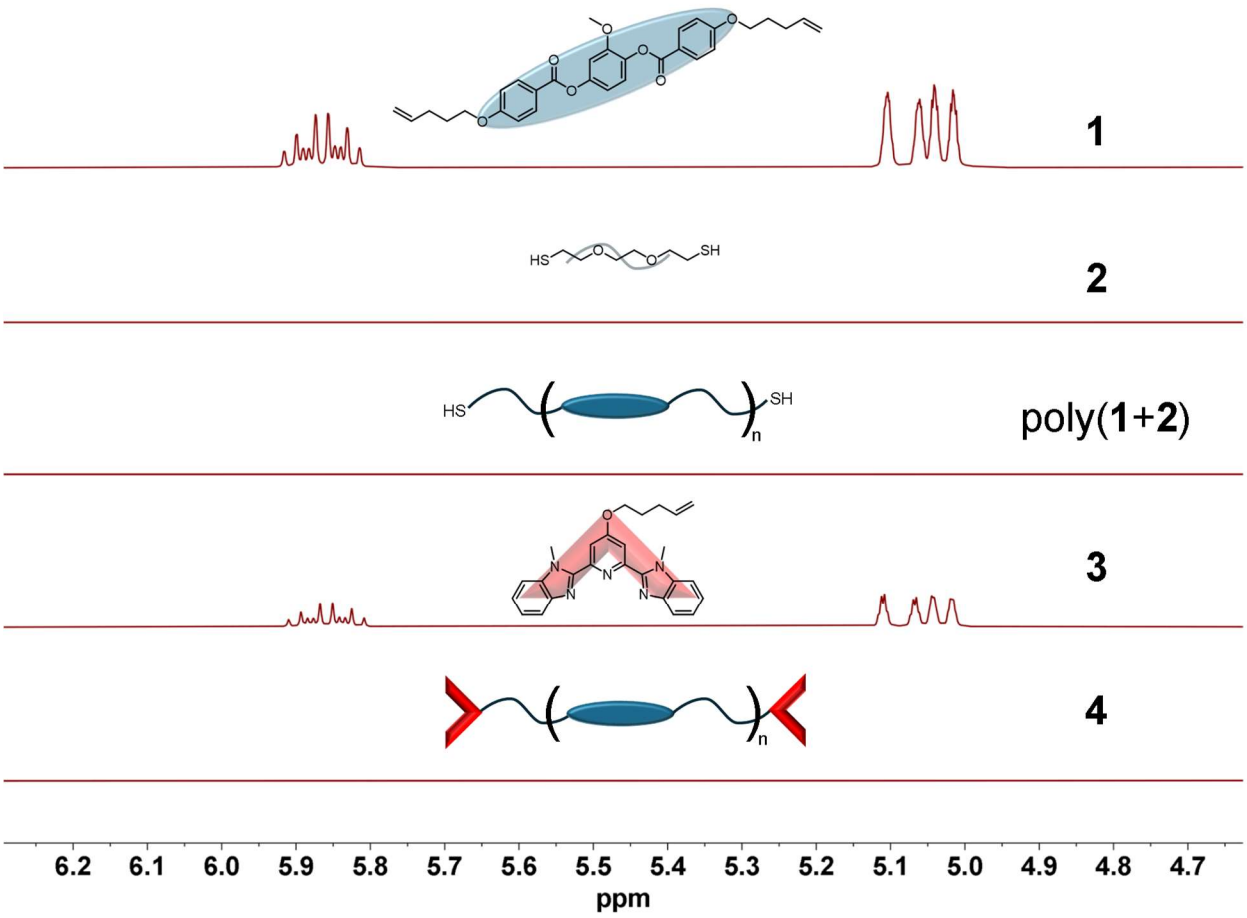

Figure S3.4: ^{1}H-NMR ($CDCl_3$, 400 MHz, 22 °C) spectra zoomed in on the alkene signals illustrating the disappearance of alkene protons from both the polymerization of **1** and **2** to **poly(1+2)** and the reaction of **poly(1+2)** and **3** to form **4** demonstrating the full conversion of alkene functional groups for these thiol-ene reactions.

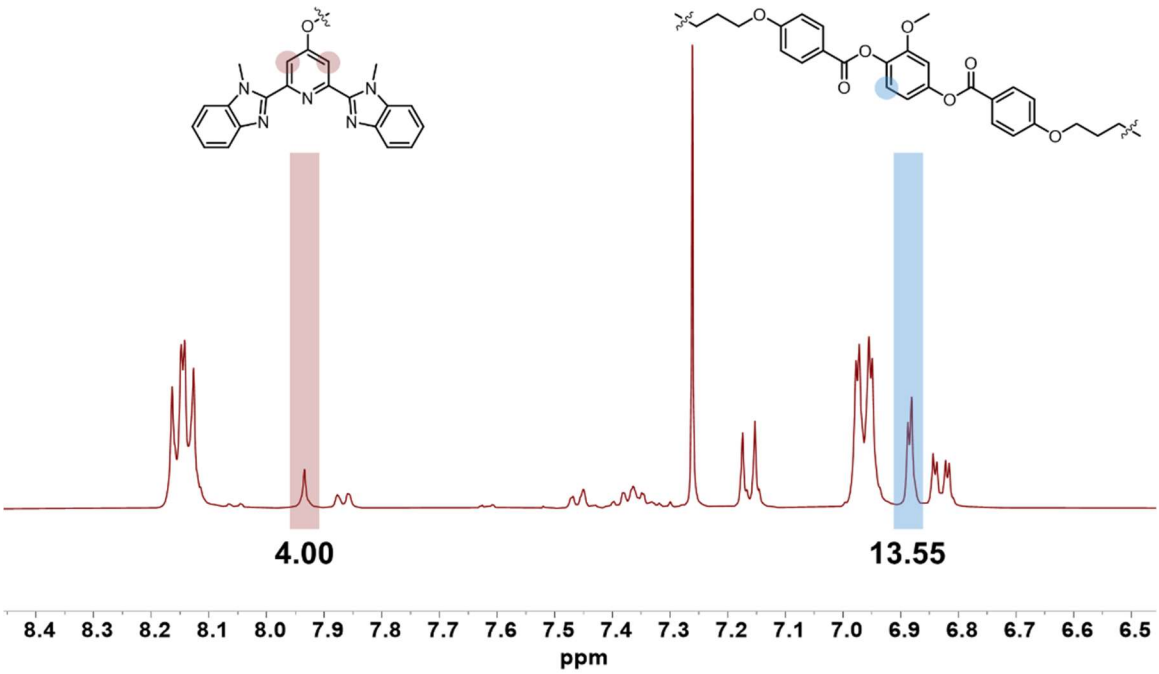

Figure S3.5: ^{1}H-NMR spectrum ($CDCl_3$, 400 MHz, 22 °C) of the aromatic signals of **4** showing the ratio of chain end protons (left) to repeat unit protons (right)

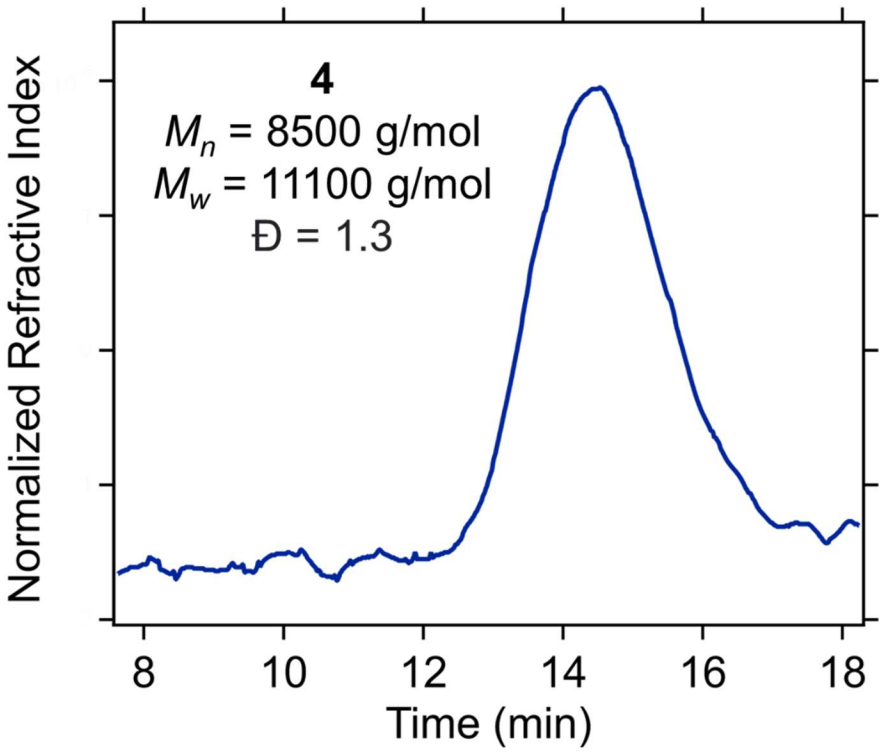

Figure S3.6: Gel permeation chromatography curve for **4** in tetrahydrofuran with molecular weights calculated against polystyrene standards

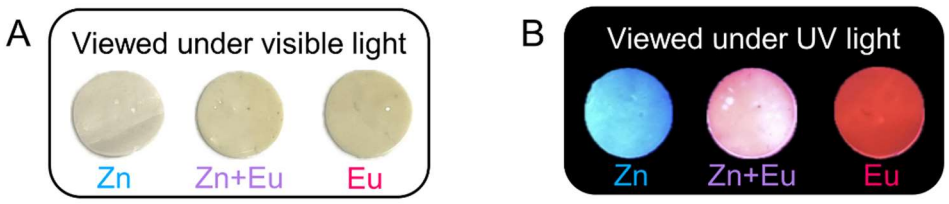

Figure S3.7: A. Optical images of each of the MSLCP materials; B. Optical images under UV light (365 nm) of each of the MSLCP materials.

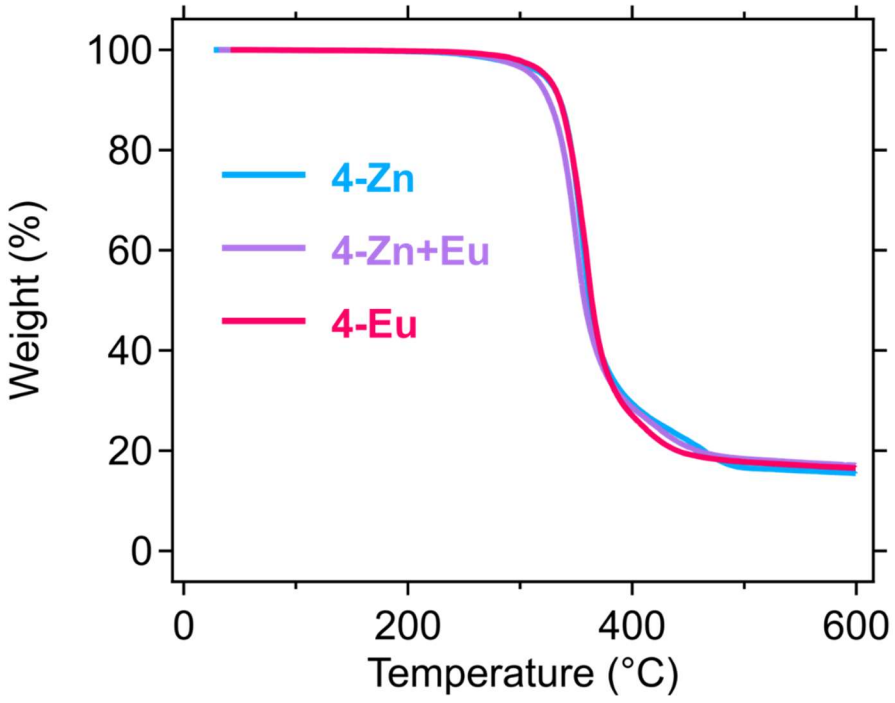

Figure S3.8: Thermogravimetric analysis of the MSLCP materials performed at a heating rate of 10 °C min^{-1} to 600 °C.

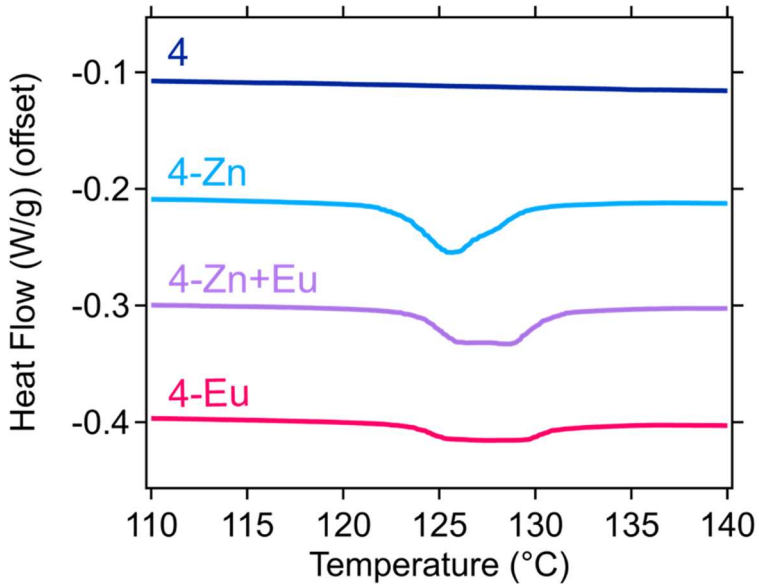

Figure S3.9: Differential scanning calorimetry heating curve performed at 10 °C min^{-1} zoomed in on T_{UT} showing the bimodal nature the signal.

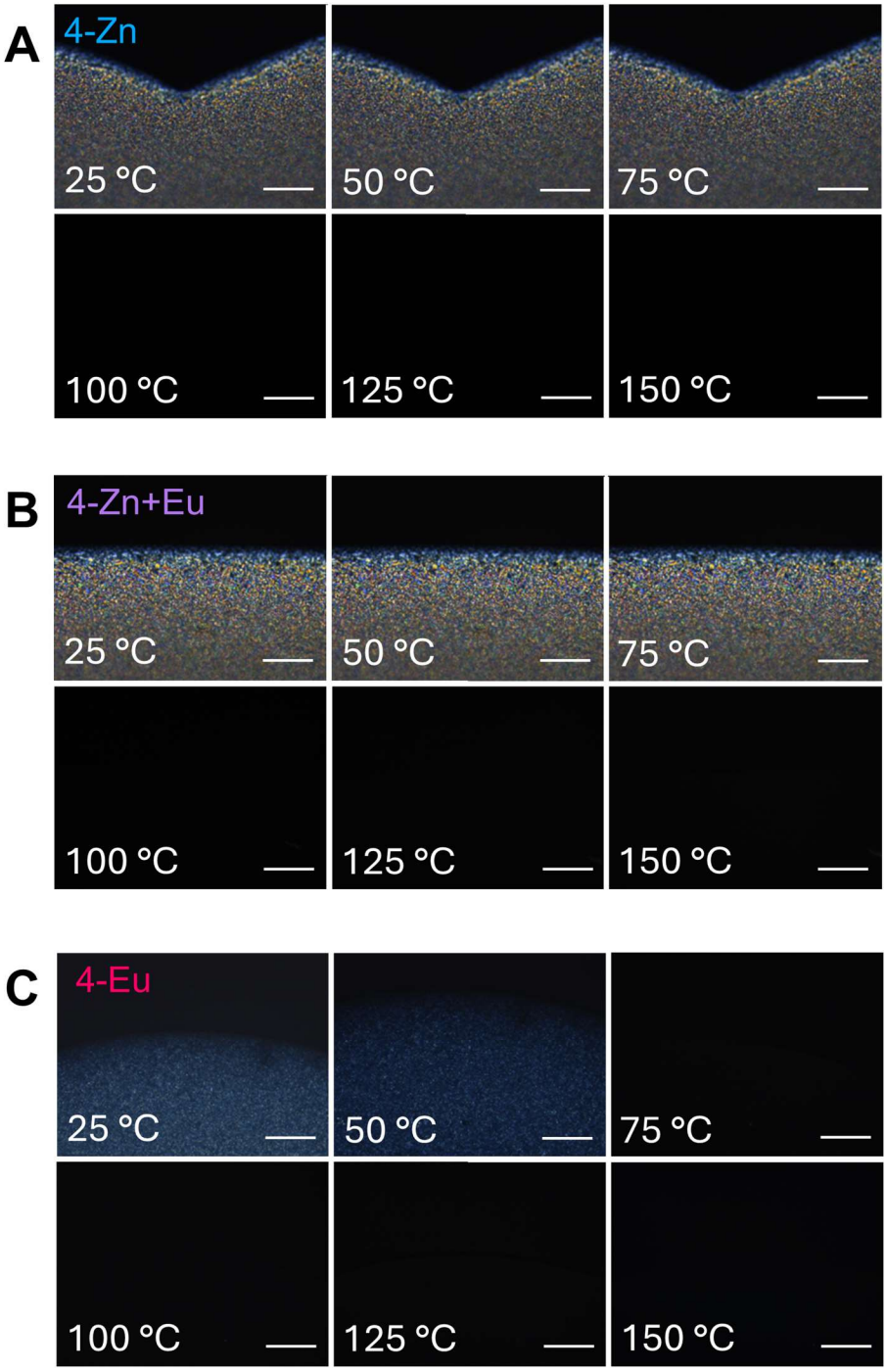

Figure S3.10: Variable temperature polarized optical microscopy images for: A. **4-Zn**, B. **4-Zn+Eu** and C. **4-Eu**. Scale bar is representative of 50 μm

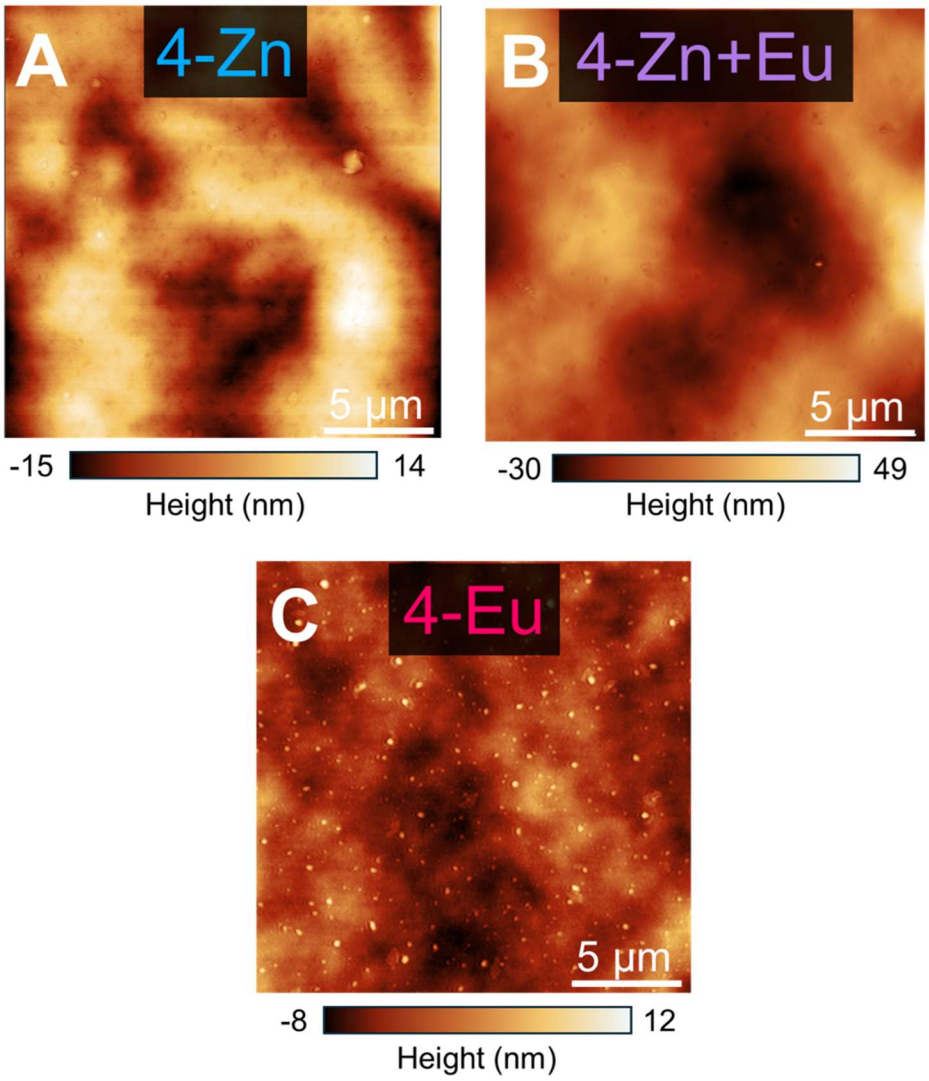

Figure S3.11: Atomic force microscopy height images for A. **4-Zn**; B. **4-Zn+Eu**; C. **4-Eu**

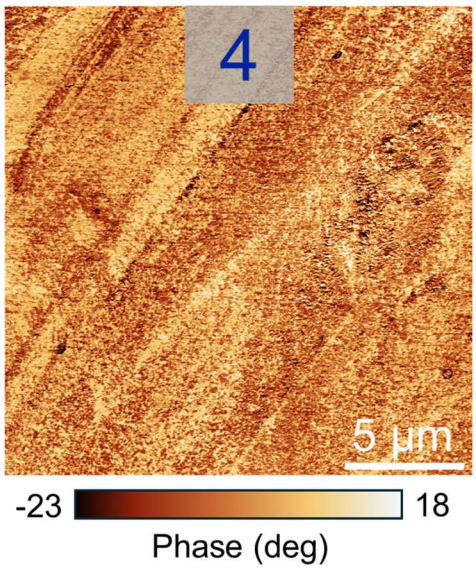

Figure S3.12: Atomic force microscopy phase image for **4**.

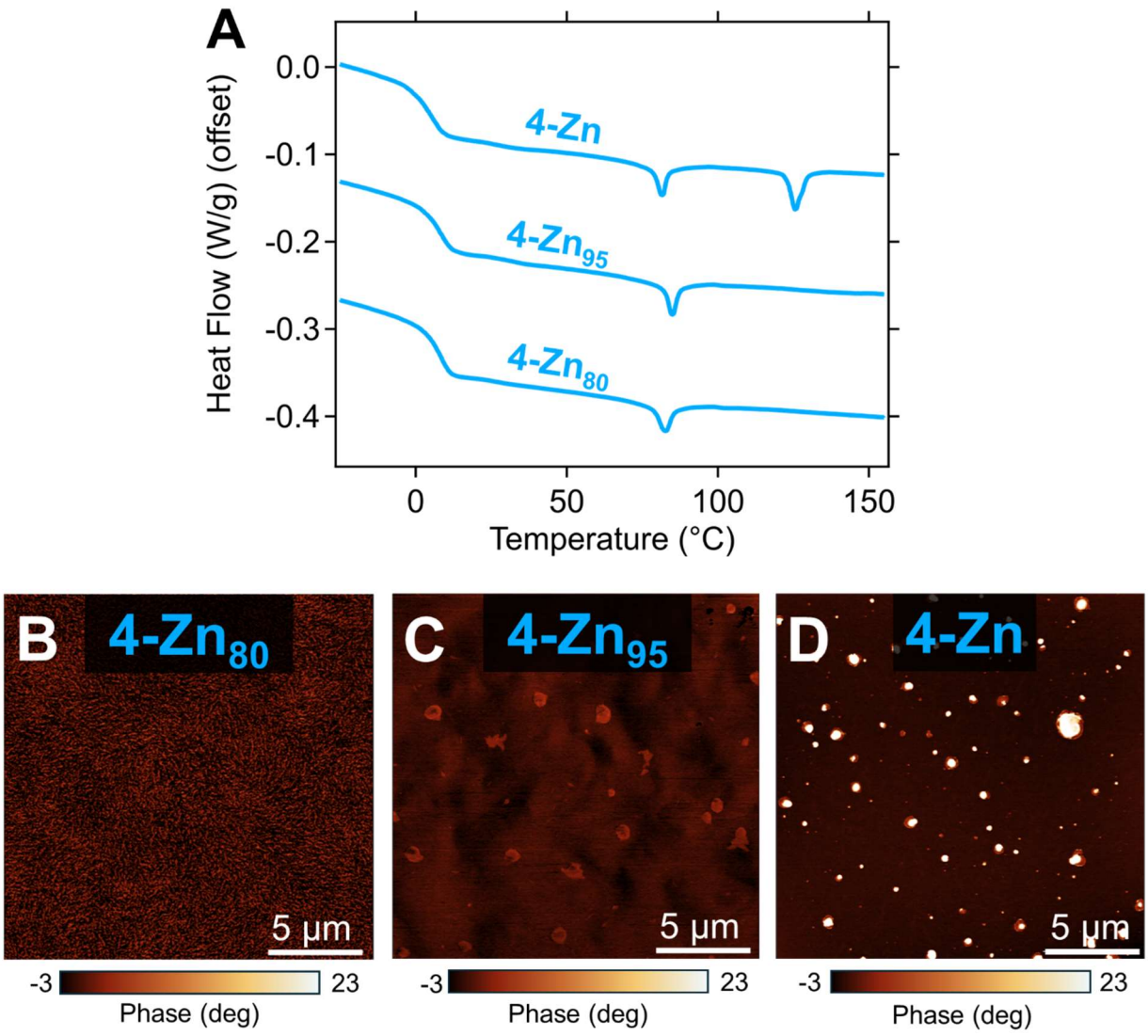

Figure S3.13: A. Differential scanning calorimetry heating curve performed at 10 °C min^{-1} of **4-Zn**, **4-Zn$_{95}$**, and **4-Zn$_{80}$**, Atomic force microscopy phase images for B. **4-Zn$_{80}$**; C. **4-Zn$_{95}$**; D. **4-Zn**

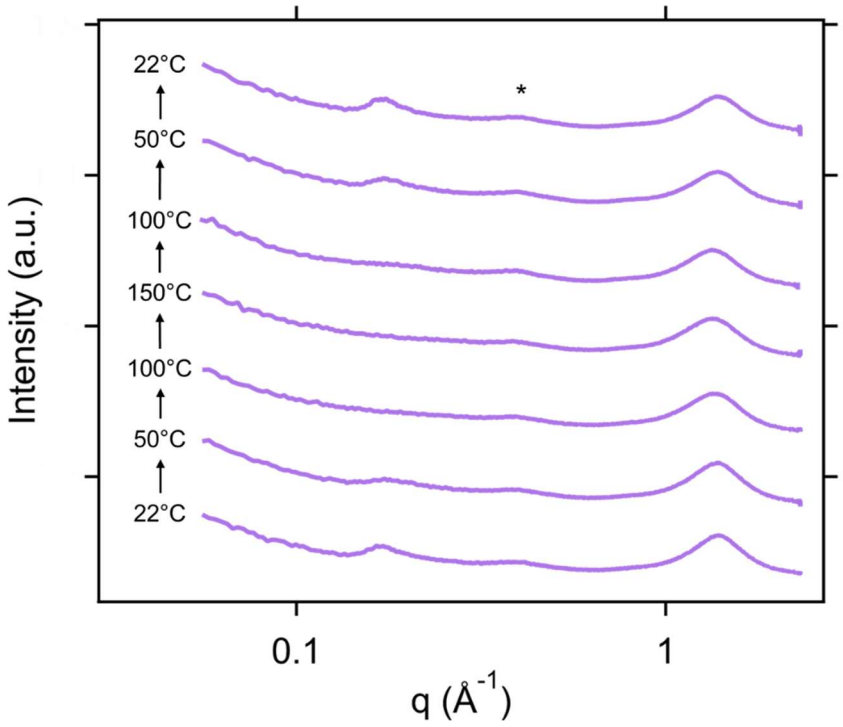

Figure S3.14: Temperature-dependent wide angle x-ray scattering spectra of **4-Zn+Eu** heated across a range of temperature from 22 °C to 150 °C and back to 22 °C. The feature at q = 0.38 Å^{-1} (d = 16.5 Å) indicated by an asterisk corresponds to the polyimide tape used to seal the samples.

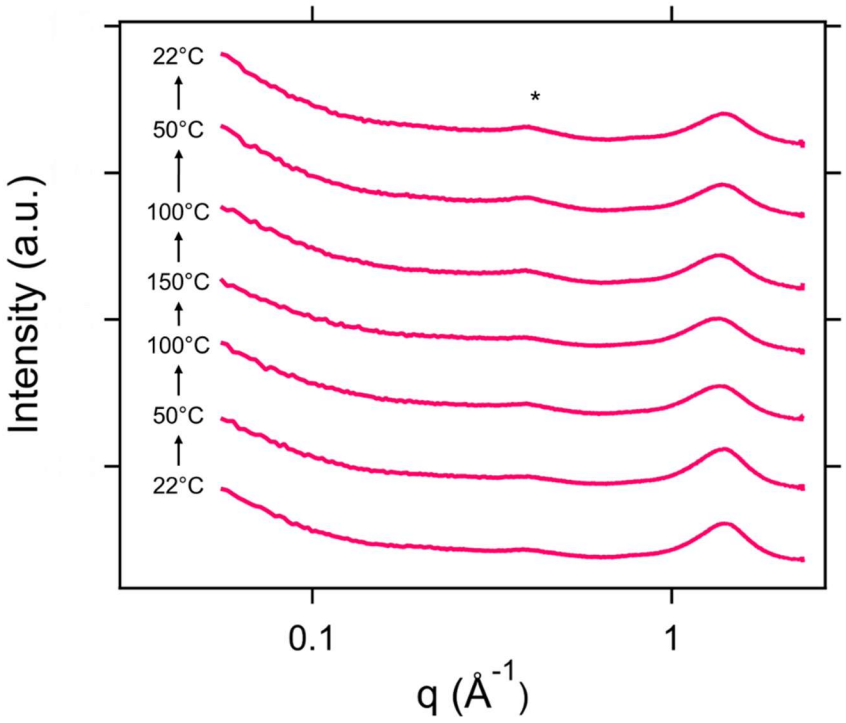

Figure S3.15: Temperature-dependent wide angle x-ray scattering spectra of **4-Eu** heated across a range of temperature from 22 °C to 150 °C and back to 22 °C. The feature at q = 0.38 $Å^{-1}$ (d = 16.5 Å) indicated by an asterisk corresponds to the polyimide tape used to seal the samples.

3.7 References

[1] T. Kato, J. Uchida, T. Ichikawa, B. Soberats, *Polym. J.* **2018**, *50*, 149.

[2] X. Lyu, A. Xiao, D. Shi, Y. Li, Z. Shen, E. Q. Chen, S. Zheng, X. H. Fan, Q. F. Zhou, *Polymer (Guildf).* **2020**, *202*, 122740.

[3] P. G. De Gennes, *C. R. Acad. Sci. B* **1975**, *281*, 101.

[4] H. Finkelmann, H.-J. Kock, G. Rehage, *Die Makromol. Chemie, Rapid Commun.* **1981**, *2*, 317.

[5] M. Warner, E. M. Terentjev, *International Series of Monographs on Physics: Liquid Crystal Elastomers*, Oxford University Press, Oxford, **2007**.

[6] J. Gao, Y. He, X. Cong, H. Yi, J. Guo, *ACS Appl. Mater. Interfaces* **2022**, *14*, 53348.

[7] L. D. C. de Castro, T. A. P. Engels, O. N. Oliveira, A. P. H. J. Schenning, *ACS Appl. Mater. Interfaces* **2024**, *16*, 14144.

[8] K. R. Schlafmann, M. S. Alahmed, H. M. Pearl, T. J. White, *ACS Appl. Mater. Interfaces* **2024**, 23780.

[9] K. A. Burke, P. T. Mather, *J. Mater. Chem.* **2010**, *20*, 3449.

[10] B. Jin, J. Liu, Y. Shi, G. Chen, Q. Zhao, S. Yang, *Adv. Mater.* **2022**, *34*, 2107855.

[11] W. Feng, Q. He, L. Zhang, *Adv. Mater.* **2024**, 2312313.

[12] C. Luo, C. Chung, N. A. Traugutt, C. M. Yakacki, K. N. Long, K. Yu, *ACS Appl. Mater. Interfaces* **2021**, *13*, 12698.

[13] D. Mistry, N. A. Traugutt, B. Sanborn, R. H. Volpe, L. S. Chatham, R. Zhou, B. Song, K. Yu, K. N. Long, C. M. Yakacki, *Nat. Commun.* **2021**, *12*, 6677.

[14] H. Guo, A. Terentjev, M. O. Saed, E. M. Terentjev, *Sci. Rep.* **2023**, *13*, 10035.

[15] Q. He, Z. Wang, Y. Wang, A. Minori, M. T. Tolley, S. Cai, *Sci. Adv.* **2019**, *5*, eaax574.

[16] Y. Yao, E. He, H. Xu, Y. Liu, Z. Yang, Y. Wei, Y. Ji, *Nat. Commun.* **2023**, *14*, 3518.

[17] R. H. Volpe, D. Mistry, V. V. Patel, R. R. Patel, C. M. Yakacki, *Adv. Healthc. Mater.* **2020**, *9*, 1901136.

[18] S. Tasmim, Z. Yousuf, F. S. Rahman, E. Seelig, A. J. Clevenger, S. N. VandenHeuvel, C. P. Ambulo, S. Raghavan, P. E. Zimmern, M. I. Romero-Ortega, T. H. Ware, *Biomaterials* **2023**, *292*, 121912.

[19] P. A. Pranda, A. Hedegaard, H. Kim, J. Clapper, E. Nelson, L. Hines, R. C. Hayward, T. J. White, *ACS Appl. Mater. Interfaces* **2024**, *16*, 6394.

[20] H. Gou, S. Hou, M. O. Saed, *Adv. Mater. Interfaces* **2024**, *2400488*.

[21] Y. Wu, B. D. Clarke, K. M. Liechti, Z. A. Page, *Chem. Mater.* **2024**, *36*, 8066.

[22] S. J. Rowan, S. J. Cantrill, G. R. L. Cousins, J. K. M. Sanders, J. F. Stoddart, *Angew. Chemie - Int. Ed.* **2002**, *41*, 898.

[23] R. J. Wojtecki, M. A. Meador, S. J. Rowan, *Nat. Mater.* **2011**, *10*, 14.

[24] N. Zheng, Y. Xu, Q. Zhao, T. Xie, *Chem. Rev.* **2021**, *121*, 1716.

[25] C. Valenzuela, Y. Chen, L. Wang, W. Feng, *Chem. – A Eur. J.* **2022**, *28*, e202201957.

[26] B. Jin, S. Yang, *Adv. Funct. Mater.* **2023**, *33*, 2304769.

[27] R. Lan, X. Hu, J. Chen, X. Zeng, X. Chen, T. Du, X. Song, H. Yang, *Responsive Mater.* **2024**, *2*, e20230030.

[28] Z. Pei, Y. Yang, Q. Chen, E. M. Terentjev, Y. Wei, Y. Ji, *Nat. Mater.* **2014**, *13*, 36.

[29] Z. Wang, H. Tian, Q. He, S. Cai, *ACS Appl. Mater. Interfaces* **2017**, *9*, 33119.

[30] J. Lee, J. Bae, J. H. Hwang, M. Choi, Y. S. Kim, S. Park, J. Na, D. Kim, S. Ahn, *Adv. Funct. Mater.* **2022**, *32*, 2110360.

[31] C. A. Lindberg, E. Ghimire, C. Chen, S. Lee, N. D. Dolinski, J. M. Dennis, S. Wang, J. J. de Pablo, S. J. Rowan, *J. Polym. Sci.* **2024**, *62*, 907.

[32] Z. Lei, H. Chen, S. Huang, L. J. Wayment, Q. Xu, W. Zhang, *Chem. Rev.* **2024**, *124*, 7829.

[33] E. Ghimire, C. A. Lindberg, T. D. Jorgenson, C. Chen, J. J. de Pablo, N. D. Dolinski, S. J. Rowan, *Macromolecules* **2024**, *57*, 682.

[34] K. M. Herbert, P. T. Getty, N. D. Dolinski, J. E. Hertzog, D. de Jong, J. H. Lettow, J. Romulus, J. W. Onorato, E. M. Foster, S. J. Rowan, *Chem. Sci.* **2020**, *11*, 5028.

[35] M. H. P. de Heer Kloots, S. K. Schoustra, J. A. Dijksman, M. M. J. Smulders, *Soft Matter* **2023**, 2857.

[36] N. R. Boynton, J. M. Dennis, N. D. Dolinski, C. A. Lindberg, A. P. Kotula, G. L. Grocke, S. L. Vivod, J. L. Lenhart, S. N. Patel, S. J. Rowan, *Science (80-.).* **2024**, *383*, 545.

[37] N. D. Dolinski, R. Tao, N. R. Boynton, A. P. Kotula, C. A. Lindberg, K. J. Petersen, A. M. Forster, S. J. Rowan, *ACS Macro Lett.* **2024**, 174.

[38] S. Sivakova, D. A. Bohnsack, M. E. Mackay, P. Suwanmala, S. J. Rowan, *J. Am. Chem. Soc.* **2005**, *127*, 18202.

[39] M. Burnworth, L. Tang, J. R. Kumpfer, A. J. Duncan, F. L. Beyer, G. L. Fiore, S. J. Rowan, C. Weder, *Nature* **2011**, *472*, 334.

[40] Y. Chen, A. M. Kushner, G. A. Williams, Z. Guan, *Nat. Chem.* **2012**, *4*, 467.

[41] R. J. Wojtecki, A. Nelson, *J. Polym. Sci. Part A Polym. Chem.* **2016**, *54*, 457.

[42] J. -M Lehn, *Angew. Chemie Int. Ed. English* **1990**, *29*, 1304.

[43] L. Brunsveld, B. J. B. Folmer, E. W. Meijer, R. P. Sijbesma, *Chem. Rev.* **2001**, *101*, 4071.

[44] T. F. A. De Greef, M. M. J. Smulders, M. Wolffs, A. P. H. J. Schenning, R. P. Sijbesma, E. W. Meijer, *Chem. Rev.* **2009**, *109*, 5687.

[45] T. Aida, E. W. Meijer, S. I. Stupp, *Science (80-.).* **2012**, *335*, 813.

[46] K. M. Herbert, S. Schrettl, S. J. Rowan, C. Weder, *Macromolecules* **2017**, *50*, 8845.

[47] L. Hammer, N. J. Van Zee, R. Nicolaÿ, *Polymers (Basel).* **2021**, *13*, 396.

[48] U. S. Schubert, C. Eschbaumer, *Angew. Chemie - Int. Ed.* **2002**, *41*, 2892.

[49] S. J. Rowan, J. B. Beck, *Faraday Discuss.* **2005**, *128*, 43.

[50] M. Burnworth, D. Knapton, S. J. Rowan, C. Weder, *J. Inorg. Organomet. Polym. Mater.* **2007**, *17*, 91.

[51] G. R. Whittell, M. D. Hager, U. S. Schubert, I. Manners, *Nat. Mater.* **2011**, *10*, 176.

[52] A. Winter, U. S. Schubert, *Chem. Soc. Rev.* **2016**, *45*, 5311.

[53] S. Ghiassinejad, K. Mortensen, M. Rostamitabar, J. Malineni, C. A. Fustin, E. Van Ruymbeke, *Macromolecules* **2021**, *54*, 6400.

[54] S. Coulibaly, C. Tchambaga Etienne, A. Koné, A. F. Kouassi, C. Siomenan, *Adv. Polym. Technol.* **2024**, 1782876.

[55] F. Biedermann, H. J. Schneider, *Chem. Rev.* **2016**, *116*, 5216.

[56] Y. L. Rao, A. Chortos, R. Pfattner, F. Lissel, Y. C. Chiu, V. Feig, J. Xu, T. Kurosawa, X. Gu, C. Wang, M. He, J. W. Chung, Z. Bao, *J. Am. Chem. Soc.* **2016**, *138*, 6020.

[57] Y. L. Rao, V. Feig, X. Gu, G. J. Nathan Wang, Z. Bao, *J. Polym. Sci. Part A Polym. Chem.* **2017**, *55*, 3110.

[58] L. N. Neumann, I. Gunkel, A. Barron, E. Oveisi, A. Petzold, T. Thurn-Albrecht, S. Schrettl, C. Weder, *Macromolecules* **2020**, *53*, 5068.

[59] Y. Li, C. Pyromali, F. Zhuge, C.-A. Fustin, J.-F. Gohy, D. Vlassopoulos, E. van Ruymbeke, *J. Rheol. (N. Y. N. Y).* **2022**, *66*, 1203.

[60] R. D. Mukhopadhyay, A. Ajayaghosh, *Chem. Soc. Rev.* **2023**, *52*, 8635.

[61] P. N. Johnson, Y. Yao, X. Huang, I. Kevlishvili, S. Schrettl, C. Weder, H. J. Kulik, S. L. Craig, *Polymer (Guildf).* **2023**, *285*, 126337.

[62] H. Park, T. Kang, H. Kim, J.-C. Kim, Z. Bao, J. Kang, *Nat. Commun.* **2023**, *14*, 5026.

[63] B. T. Michal, B. M. McKenzie, S. E. Felder, S. J. Rowan, *Macromolecules* **2015**, *48*, 3239.

[64] C. Zhang, G. Fei, X. Lu, H. Xia, Y. Zhao, *Adv. Mater.* **2024**, *36*, 2307210.

[65] S. J. A. Houben, S. J. D. Lugger, R. J. H. Van Raak, A. P. H. J. Schenning, *ACS Appl. Polym. Mater.* **2022**, *4*, 1298.

[66] R. Liang, H. Yu, L. Wang, D. Shen, *Adv. Funct. Mater.* **2023**, *33*, 2211914.

[67] J. B. Beck, S. J. Rowan, *J. Am. Chem. Soc.* **2003**, *125*, 13922.

[68] J. B. Beck, J. M. Ineman, S. J. Rowan, **2005**, 5060.

[69] J. R. Kumpfer, J. J. Wie, J. P. Swanson, F. L. Beyer, M. E. MacKay, S. J. Rowan, *Macromolecules* **2012**, *45*, 473.

[70] S. Coulibaly, C. Heinzmann, F. L. Beyer, S. Balog, C. Weder, G. L. Fiore, *Macromolecules* **2014**, *47*, 8487.

[71] L. N. Neumann, E. Oveisi, A. Petzold, R. W. Style, T. Thurn-Albrecht, C. Weder, S. Schrettl, *Sci. Adv.* **2021**, *7*, eabe4154.

[72] C. Piguet, J. C. G. Bünzli, G. Bernardinelli, G. Hopfgartner, A. F. Williams, *J. Alloys Compd.* **1995**, *225*, 324.

[73] M. Enamullah, W. Linert, *J. Coord. Chem.* **1996**, *40*, 193.

[74] H. J. Hong, S. Y. Park, *J. Ind. Eng. Chem.* **2022**, *110*, 424.

[75] J. Sautaux, L. M. De Espinosa, S. Balog, C. Weder, *Macromolecules* **2018**, *51*, 5867.

[76] F. Marx, M. Beccard, A. Ianiro, A. Dodero, L. N. Neumann, G. Stoclet, C. Weder, S. Schrettl, *Macromolecules* **2023**, *56*, 7320.

[77] M. T. Sims, L. C. Abbott, R. M. Richardson, J. W. Goodby, J. N. Moore, *Liq. Cryst.* **2019**, *46*, 11.

[78] J. J. Hermans, P. H. Hermans, D. Vermaas, A. Weidinger, *Recl. des Trav. Chim. des Pays-Bas* **1946**, *65*, 427.

[79] H. Guo, M. O. Saed, E. M. Terentjev, *Macromolecules* **2023**, *56*, 6247.

[80] C. Heinzmann, C. Weder, L. M. De Espinosa, *Chem. Soc. Rev.* **2016**, *45*, 342.

[81] P. Sun, B. Qin, J. Xu, X. Zhang, *Macromol. Chem. Phys.* **2023**, *224*, 2200332.

[82] H. J. Farre-Kaga, M. O. Saed, E. M. Terentjev, *Adv. Funct. Mater.* **2022**, *32*, DOI 10.1002/adfm.202110190.

[83] T. Ohzono, M. O. Saed, E. M. Terentjev, *Adv. Mater.* **2019**, *31*, 1902642.

[84] P. Froidevaux, J. M. Harrowfield, A. N. Sobolev, *Inorg. Chem.* **2000**, *39*, 4678.

[85] C. Jagadeeswara Rao, K. A. Venkatesan, K. Nagarajan, T. G. Srinivasan, P. R. Vasudeva Rao, *Electrochim. Acta* **2009**, *54*, 4718.

[86] M. C. Wilkinson, M. Higson, *Org. Process Res. Dev.* **2017**, *21*, 75.

[87] Y. Barre, M. Simon, R. Neige, R. Duval, *UREIDO OR CARBAMATE DERIVATIVES OF CROWN ETHERS AND OF SILICON USABLE FOR PREPARING SUPPORTS INTENDED FOR THE SEPARATION BY CHROMATOGRAPHY OF METAL CATIONS AND OF ORGANIC MOLECULES COMPRISING AMINE FUNCTIONAL GROUPS*, **2007**, US7230123B2.

[88] S. V. Arehart, C. Pugh, *J. Am. Chem. Soc.* **1997**, *119*, 3027.

CHAPTER 4

STUCK ON REPEAT: DYNAMIC LIQUID CRYSTAL ELASTOMERS AS (RE)TRAINABLE ADHESIVES

4.1 Summary

Polymeric networks whose performance can be trained as a function of mechanical inputs provide materials with additional possibilities as they offer an opportunity to further modulate a material's properties post synthesis and processing. Herein, disulfide-containing dynamic liquid crystal elastomer (LCE) adhesives exhibiting (re)trainable multistage adhesive character are reported. Synthetic tailoring of the lateral substituent size and ordering of the constituent mesogenic units allows for direct tuning of the thermal properties (T_g and T_{NI}) of the network. Despite conventional adhesive benchmarking (Dahlquist criterion and viscoelastic window) predicting poor adhesive quality for these dynamic LCEs, the materials exhibit pressure tunable adhesive behavior as a result of their inherent soft elasticity and stimuli-responsive dynamic bonds. Furthermore, higher strength hot melt adhesive joints can be formed through the activation of the incorporated dynamic disulfide bonds at high temperatures (> 150 °C). General adhesive performance can be tuned through mesogen structure while multi-cycle probe-tack tests show that their adhesion increases with each cycle, demonstrating the trainability of the pressure tunable adhesive response with repeated use. Thermal disruption of the LC phase resets the adhesive character which can be subsequently reattained through mechanical training.

4.2 Introduction

From consumer electronics to arts and crafts, adhesives have cemented their status as an integral class of materials with a broad range of industrial applications that include construction,[1–3] dentistry,[4–6] and packaging.[7–9] State of the art adhesive materials incorporate a wide array of fillers and chemistries to impart additional functionalities such as biocompatibility,[10–12] conductivity,[8,13–15] stimuli-responsive character,[16–20] and wet adhesion.[21–23] Adhesives are traditionally divided into two categories, reactive and physically setting, depending on whether a chemical reaction occurs during the application of the adhesive.[24] Typically, reactive adhesives include formulations comprised of low viscosity small molecules capable of forming higher molecular weight species upon the polymerization of a chemically active functional handle (cyanoacrylates, epoxies, etc.). Physically setting adhesives, in contrast, are composed of higher molecular weight polymers that exhibit adhesive character upon experiencing a physical stimulus such as melting, solvent evaporation, or the application of a mechanical force. As this category encompasses a wide array of physical transitions, this class of adhesives includes materials ranging from hot melt adhesives (HMAs), that are applied at elevated temperatures and tend to serve as higher strength structural adhesives, to pressure sensitive adhesives (PSAs) which include the lower viscosity polymer films that exhibit removable and replaceable fast adhesion with mild pressure.[25] As the property profiles of the materials within this class of adhesives vary dramatically due to the vast range of physical stimuli that can be employed, a unique challenge exists for creating trainable multistage adhesives (MSAs) whose response can be tuned/enhanced through the nature and intensity of the stimulus being employed. By incorporating multiple tunable stimuli-responsive moieties into the design of trainable MSA materials, a single adhesive with leveled modes of adaptive adhesion can be realized. This material has the potential to operate as a high-strength structural adhesive under one set of stimuli or as a temporary replaceable adhesive under another set, with the ability to interconvert between these two states.[18,26–28]

As a high surface area is essential for the formation of a robust interface between two substrates, a material's ability to effectively wet a surface is a critical parameter to consider when designing an adhesive.[29] One recent advent to confer enhanced surface wettability into adhesive network materials is the inclusion of dynamic covalent bonds.[13,18,26,30] Dynamic bonds are chemical bonds that can be controllably formed, broken, and reformed (ideally without side reactions)[31,32] and include chemistries such as disulfides,[16,17] thia/aza-Michael reactions,[18,33,34] and boronic esters.[10,35] In a sense, the addition of dynamic bonds to adhesive materials blurs the traditional delineation between reactive adhesives and physically setting adhesives as many dynamic adhesive materials exist as high molecular weight polymer systems while leveraging a reactive dynamic chemistry *in situ* to facilitate bonding or debonding. The disulfide bond is a multi-responsive moiety that can be activated through thermal,[39–41] photo,[26,42] redox,[43] mechanical,[44,45] or chemical[46] stimuli. In particular, disulfides have the ability to undergo either an associative or dissociative dynamic pathway depending on the stimulus of choice (Figure 4.1A) and its relatively high activation energy of 60 kcal mol^{-1} (251 kJ mol^{-1})[47] for aliphatic disulfides, the latter resulting in the disulfide requiring high activation temperatures (T > 150 °C) to achieve the formation of a significant number of active dynamic species *in situ*.[40,42] These useful properties have led to several studies investigating disulfides in adhesive applications.[13,18,26,27,36–38] One example of work incorporating disulfides into adhesives by Michal et al.[26] demonstrated the utility of a disulfide chemistry in a material that exhibited leveled adhesive behavior. These materials consisted of semi-crystalline polymers crosslinked by disulfide bonds where the melting of the crystalline domains and the thermal activation of the disulfides afforded different levels of adhesive performance. By melting the crystalline domains (~80 °C) and applying pressure, hot melt joints of a moderate strength were formed. However, the semicrystalline nature of the materials prevented their use as pressure sensitive adhesives under room temperature conditions. An ideal system would utilize a material that operates effectively across a broader range of application temperatures and offers tunability to achieve a robust yet controllable adhesive property.

Recent work has shown that liquid crystal elastomers (LCEs) can exhibit pressure sensitive adhesive (PSA) behavior.[48–53] LCEs are elastomeric polymer networks whose constituent polymers contain liquid crystal (LC) mesogens capable of forming locally ordered microscopic domains throughout the bulk elastomer.[54,55] LCEs exhibit a unique set of thermomechanical properties on account of their liquid crystallinity, which include thermally induced mechanical and optical transformations, as well as soft elasticity via stress dissipation through the rotational modes of their mesogens.[56–58] While these materials have mainly been studied in contexts relating to complex shape memory, modelling work by Corbett et al. predicted that LCEs would possess adhesive character and a high tack energy due to their dissipative nature.[59] Recently, works by Ohzono et al. directly explored the experimental tack behavior of LCEs and demonstrated that LCEs do in fact possess stimuli-responsive adhesive character with a strong dependence on the thermal stability of the nematic to isotropic liquid crystalline transition.[48,60] Further work by Farre-Kaga et al.[49] and others[51,52] have shown that LCEs display PSA character that is both rate and pressure dependent, the latter takeaway being akin to observations made by Deneke et al.[61] in their separate study of systems they have termed "pressure *tunable* adhesives".

A natural extension of these prior works would leverage the dual modalities of a mesogenic transition and a dynamically exchangeable bond toward a singular stimuli-responsive adhesive material (Figure 4.1B). The incorporation of dynamic covalent bonds into LCEs has been well studied and extended to a wide range of chemistries.[62–66] However, these studies have typically focused on the utility of dynamic chemistries as a means to facilitate reprocessability and post-synthetic alignment within LCEs leaving the study of these materials as stimuli-responsive adhesives largely overlooked. Reported herein are studies on the adhesive abilities of a series of dynamic LCE to explore how the LCE thermomechanical property profiles impacts the overall adhesive character of the material.

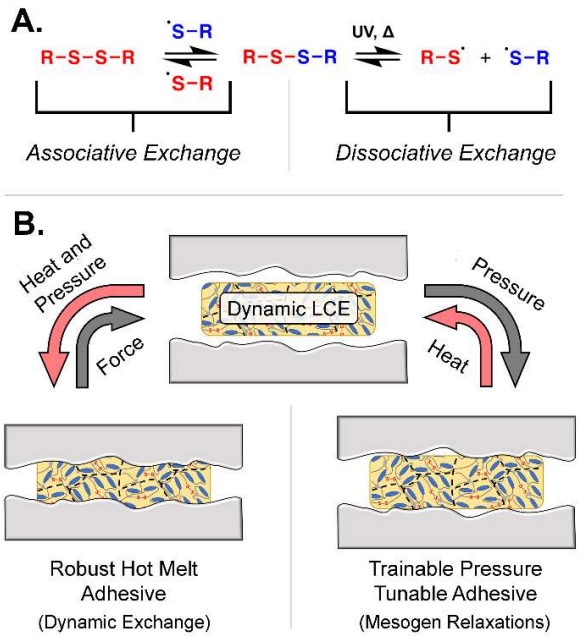

Figure 4.1 A) Scheme of the dual associative and dissociative dynamic exchange mechanisms of disulfide bond; B) Schematic depicting how a dynamic LCE can access multiple modes of adhesion through choice of stimulus.

4.3 Results and Discussion

4.3.1 Design and Synthesis

To design dynamic LCEs capable of exhibiting stimuli-responsive adhesive character, a modular approach was utilized that allows for variation in material properties through component selection (Figure S4.4.2). A key feature of this synthetic strategy is the isolation of domain stability as a variable while holding constant other parameters, such as crosslink density, average network density of liquid crystal unit, and chain extender packing, which have the potential to coincidentally alter mechanical properties, change the accessible phase of the LC domains, or induce crystallinity, respectively.[67–70] As such, this approach allows for an exploration of phase transition's impact on the adhesive properties of dynamic LCE materials. As the packing of the mesogens is directly related to the liquid crystal transition temperatures,[71] a series of phenyl ester mesogenic monomers (**1-R**) was prepared with different sized substituents, namely methyl (**1-Me**), methoxy (**1-OMe**), and *tert*-butyl (**1-*t*Bu**), bonded to the mesogens' central aromatic ring (full synthetic details are available in the Supporting Information).[72] Additionally, an allyl functionalized

monomer containing a disulfide bond (**2**) was utilized as the dynamic component for this system following a preparation from the literature (full synthetic details are available in the Supporting Information).[73] Using **1-R**, **2**, the dithiol chain extenders 1,6-hexanedithiol (**HDT**) and 2,2′-(ethylenedioxy)diethanethiol (**PDT**), and the tetrathiol crosslinker pentaerythritol tetrakis(3-mercaptopropionate) (**PETMP**) in ratios calculated using a simplified version of Carother's equation[74] to target a molecular weight between crosslinks of approximately 5,000 g mol^{-1}, a series of dynamic LCE networks (**3-Me**, **3-OMe**, and **3-*t*Bu**) was synthesized using a one-pot thiol-ene click reaction. The bulk materials were washed through a swelling and deswelling process (alternating between methylene chloride and methanol) and dried to ensure the removal of unreacted components as confirmed by thermogravimetric analysis (TGA) (Figure S4.4.1). The gel fractions of these materials were measured to be between 85 – 88 wt.% indicating a consistently high conversion of the monomers across the different systems. To determine the processing conditions required

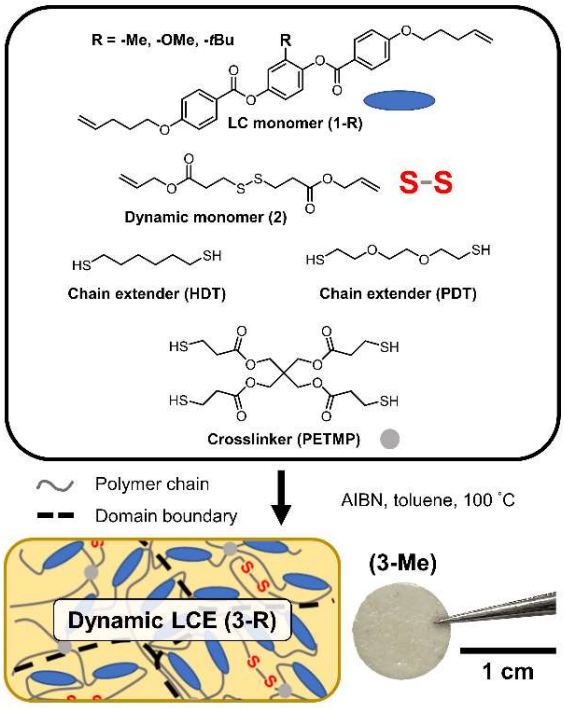

Figure 4.2. Synthesis of a representative dynamic LC network from the reaction of LC monomers (**1-R**), disulfide monomer (**2**), chain extenders (**HDT** and **PDT**), and crosslinker (**PETMP**).

for the effective thermal processing of these materials into films, high temperature stress relaxation experiments were carried out from 150 – 180 °C (Figure S4.2). The stress relaxation curves showed that the materials did not dissipate the majority of its stress within an hour until exposed to a temperature of 180 °C. Using this high temperature to facilitate the disulfide exchange in conjunction with compression molding led to the conditions (1 h, 180 °C, 4 tons) used to access polydomain LCE films.

4.3.2 Thermomechanical Characterization

To understand how the sterics of the mesogens' aryl-substituent affects the thermal transitions of dynamic LCEs, the series of materials (**3-Me**, **3-OMe**, and **3-*t*Bu**) was first studied using differential scanning calorimetry (DSC) to measure the T_g and the T_{NI} of the materials (Figure S4.3A). As expected, the T_{NI} of the materials decreased with an increase in the size of the substituent attached to the mesogen[71] with **3-Me**, **3-OMe**, and **3-*t*Bu** exhibiting T_{NI}'s of 105 °C, 77 °C, and 28 °C respectively as measured by the location of the minima of the endotherms present in the DSC thermogram. Conversely, the T_g's of the materials, taken as the midpoint of the step in the DSC thermogram, increases with increasing aryl-substituent size and were measured to be –14 °C, –1 °C, and 11 °C for **3-Me**, **3-OMe**, and **3-*t*Bu** respectively. The differences in the measured T_{NI}'s are in line with literature precedent and provides a straightforward method for achieving a wide range of transition temperatures.[72,75]

To determine how this modification impacts the mechanical properties of the dynamic LCEs, thermomechanical characterization was performed using small angle oscillatory shear (SAOS) rheometry (Figure S4.3B). For all measured samples, dynamic temperature ramps displayed three thermal transitions, characteristic of LCE materials.[76] The first transition, which appears as a step in the storage modulus curve and a peak in the tan(δ) curve, is indicative of the glass transition temperature and occurs at –1 °C for **3-Me**, 12 °C for **3-OMe**, and 19 °C for **3-*t*Bu** (in agreement with DSC measurements). The second transition is indicated by a broader lower intensity peak in tan(δ) that occurs around 45 °C for **3-Me** and **3-OMe** and

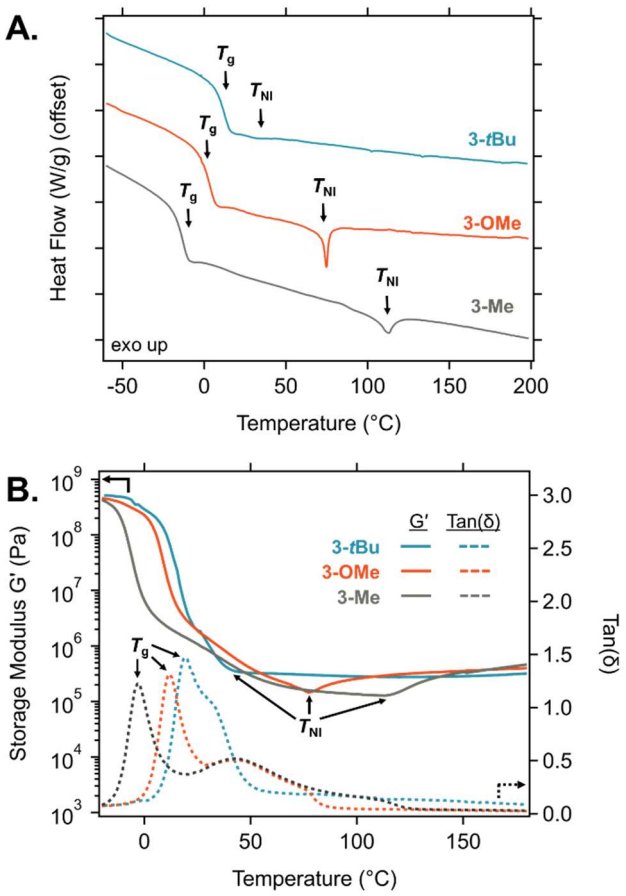

Figure 4.3: A. Differential scanning calorimetry (DSC) thermograms of dynamic LCE materials; B. Small angle oscillatory shear (SAOS) rheology dynamic temperature ramps of storage modulus (solid lines) and tan(δ) (dashed lines) for dynamic LCE materials

around 30 °C for **3-*t*Bu** (although convoluted by its proximity to T_g) and corresponds to the dynamic soft elastic behavior characteristic of LCE networks.[76] The third transition presents as a minimum in storage modulus and a step in the tan(δ) signal indicating the transition from the liquid crystalline to isotropic state. Importantly, while the thermal transitions of these dynamic LCEs are different, the modulus of these materials in both the glassy and isotropic states are similar, suggesting that the nature of mesogen does not significantly impact the network properties beyond those directly corresponding to the thermal transitions.

4.3.3 Adhesive Testing

It is worth noting that under the conditions used for the SAOS rheology experiments, there is no evidence of bulk flow in these dynamic LCE materials (Figure 4.3B) which indicates their robustness at shorter

timescales (1 Hz) even at temperatures where the disulfide typically shows significant cleavage (T > 150 °C) in polymer networks.[26,39,40] While it has been demonstrated that dynamic covalent bonds contribute to the network relaxation of dynamic LCE materials at longer timescales (~ 1 h) in general,[34,77–79] this modality has yet to be leveraged in the context of adhesive applications for dynamic LCEs particularly as higher strength HMAs. To test the performance of dynamic LCEs as HMA materials, 5 mm diameter discs of dynamic LCE were used to form two types of adhesive joints: one in a stud-pull geometry between two aluminum I-bars and one in a lap-shear geometry between two rectangular aluminum fixtures (Figure S4.4A-B). The surfaces of the aluminum fixtures were prepared via etching following a literature preparation to clean the surface.[80] These adhesive joints were held together with binder clips (25 N) and heated for an hour to 180 °C. Upon cooling to room temperature, the set adhesive joints were loaded into the clamps of a uniaxial tensile testing instrument and strained until failure to measure the adhesive strength of the dynamic LCE HMA joints (Figure 4.4C). All three dynamic LCEs formed robust HMA adhesive joints where the stud-pull tests for **3-Me**, **3-OMe**, and **3-*t*Bu** produced adhesive strengths of 2.5 ± 0.1 MPa, 2.9 ± 0.2 MPa, and 3.1 ± 0.4 MPa while lap-shear tests produced adhesive strengths of 0.8 ± 0.1 MPa, 1.4 ± 0.1 MPa, and 2.0 ± 0.1 MPa respectively. The reduced strength seen in lap shear is explained by the debonding stress perpendicular to loading stress inducing mesogen surface realignment that results in a failure mode at the interface.[51] Based on these adhesive strength values, it can be observed that materials possessing bulkier mesogens and a higher T_g correlate with higher hot-melt adhesive strengths. Another observation of note is that both geometries of adhesive joint for all materials tested resulted in adhesive failure (Figure 4.4D, Figure S4.3) indicating a higher cohesive strength of the material when compared to the interfacial strength of the joint. Overall, these materials performed impressively in an HMA context reaching adhesive strengths about one- third that of average commercial HMA materials (~3–4 MPa in shear)[81] despite the fact that these materials do not achieve observable macroscopic flow at the temperatures and timescales of application which is the typical mechanism by which HMAs wet a surface.[82] This surprising adhesive performance is attributed to the high-temperature processing conditions

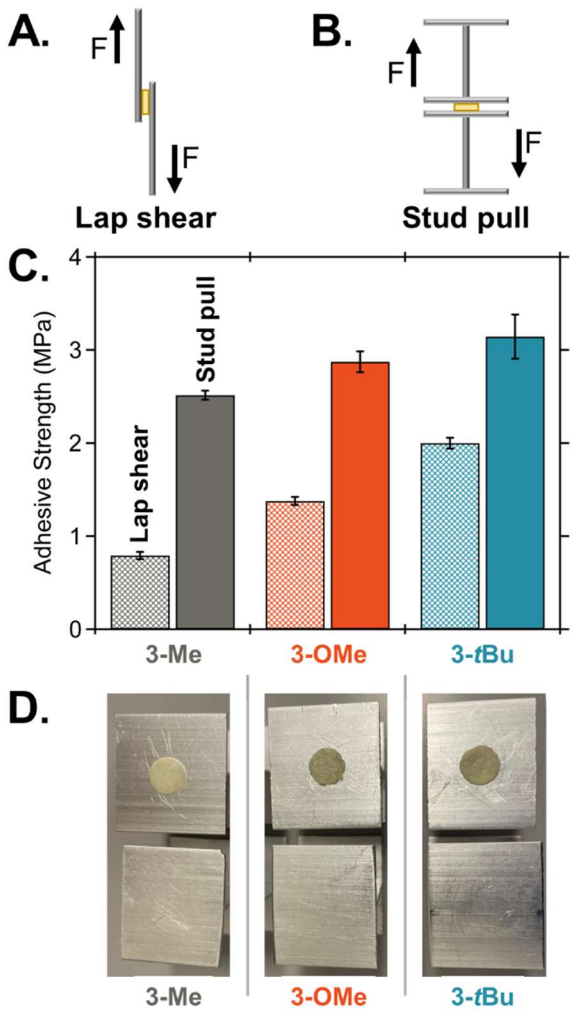

Figure 4.4: A. General schematic detailing the geometry of lap shear fixtures used in hot melt adhesive (HMA) testing; B. General schematic detailing the geometry of stud pull fixtures used in HMA testing; C. Comparison of HMA strengths between **3-Me**, **3-OMe**, and **3-*t*Bu** in both lap shear and stud pull geometries; D. Representative images of stud pull hot melt joints after strength testing all demonstrating adhesive failure.

inducing both the high mobility of the polymer chains in the isotropic state and the active exchange of the disulfide bond allowing stress relaxation within the network.

With the HMA properties measured, the PSA performance of these materials was evaluated using cyclic probe-tack adhesion testing. It is important to note that this is not the first use of probe tack testing to study the adhesive character of LCE materials as a number previous studies have investigated the effects of debonding rate, contact time, and temperature on the adhesive force generated by LCE PSAs.[48,49,51,52,60] The mechanism for general PSA behavior is well-debated in the field with multiple theories as to the root

cause of the phenomenon,[29] a recent study by Guo et al.[51] puts forward a mechanism by which LCEs exhibit robust PSA character through both their anomalously high viscoelastic dissipation and the local director rotation brought on by the of application of a compressive stress in forming an adhesive bond. Guo et al. further propose that debonding in lap shear LCE specimens imposes alignment of the mesogens at the adhesive interface in the same direction as the debonding event.[51] If this is correct then it stands to reason that repeated cycling of an LCE adhesive in a probe-tack geometry could increase the amount of imposed alignment and hypothetically produce an enhanced adhesive response.

To test this hypothesis, cyclic probe-tack test experiments were carried out on a shear rheometer setup. Samples were prepared by punching 10 mm diameter discs from dynamic LCE films and heating them through their T_{NI}'s to remove any temporary deformation resulting from the punching process. The samples were mounted in the center of a stainless-steel lower rheometer geometry (25 mm diameter circular plate) with double sided tape. For a single representative probe-tack cycle, the top plate (8 mm diameter circular plate) was brought into contact with the dynamic LCE disc at room temperature at a constant axial force (0.1 N, 1 N, or 10 N) for 60 s after which the top plate was removed from the disc at a rate of 0.1 mm s^{-1} (Figure 4.5A). This contact and removal process was repeated for a total of 25 cycles to determine the effect of repeated cycling on the adhesive force generated by the dynamic LCEs. The resulting force curves were then analyzed to determine the peak force of each cycle (Figure 4.5B), defined as the maximum force attained over the course of the cycle. The pull-off peak force was then analyzed as a function of cycle number to determine how repeated adhesion and debonding affected the performance of the adhesive.

Remarkably, rather than deteriorating or remaining constant as is typically expected of conventional PSA materials, the pull off strength was found to increase with cycle number for all materials and load forces (F_{load}) tested (Figure 4.6, Figure S4.5-S6). This mechanically induced cyclic enhancement presents as a predictable monotonic response suggesting that it would be possible to "train-in" a desired adhesive

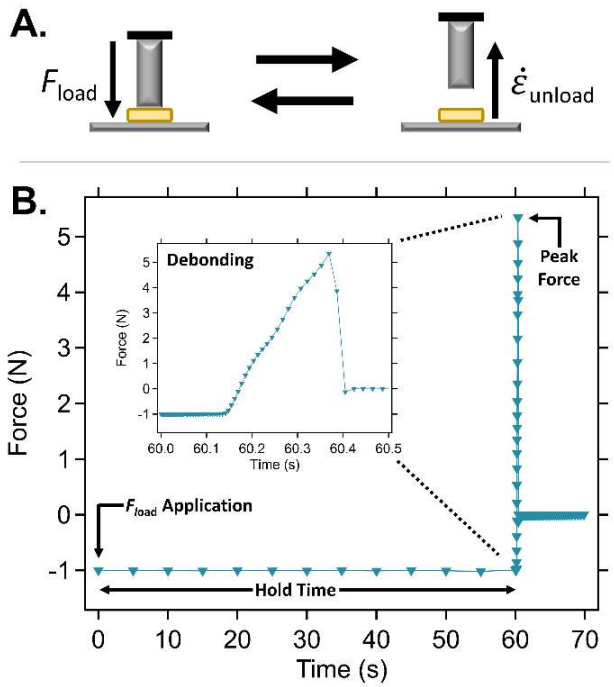

Figure 4.5: A. General schematic detailing the process of cyclic tack experiments performed on a shear rheometry setup; B. A representative force curve for a single probe tack cycle indicating the peak force value utilized in the analysis of cyclic experiments.

response with an appropriate mechanical input. Another observation of note is that decreases in T_{NI} result in increased adhesive performance with **3-*t*Bu** consistently having the largest pull-off strengths for a given applied load while **3-Me** had the lowest across the three load forces tested. As has been shown for non-dynamic LCEs,[49] increased force applied to the dynamic LCE also resulted in increased pull off strength proportional to the applied load force which is demonstrative of the pressure-tunable adhesive behavior (Figure 4.6).[61]

To rule out wetting effects stemming from a change in the surface roughness of the dynamic LCE potentially conforming to the surface of the probe tack geometry, profilometry measurements (Figure 4.3) were performed on a representative material (**3-*t*Bu**) where increasing numbers of cycles had been performed on it. While cycling produces a significant drop from the initial roughness of the material, the roughness values are within error across 25 cycles and overall remain higher than the roughness of the probe itself. As temperature has been previously shown to have a large effect on the general PSA behavior of

LCEs, a temperature series was performed on a single material system (**3-*t*Bu**, 1 N load) at T < T_g (–10 °C), T > T_{NI} (50 °C), and T_g < T < T_{NI} (22 °C) (Figure 4.6) to determine how the trainability of adhesion in dynamic LCEs responds to changes in temperature. At 22 °C, **3-*t*Bu** is in its nematic state and demonstrates the cyclic enhancement as was seen previously. At 50 °C when **3-*t*Bu** is isotropic, both the adhesive response and the enhancement effect are significantly suppressed. As expected of the material at –10 °C, the glassy **3-*t*Bu** exhibits no adhesive behavior. These temperature studies are consistent with the LC phase being responsible for the enhancement effect that is observed in these materials. As these LCEs also contain disulfide bonds it was interest to explore their contribution to the adhesive quality of the material system. To probe this, in addition to the dynamic LCE **3-*t*Bu**, similar networks that contained mesogens and no

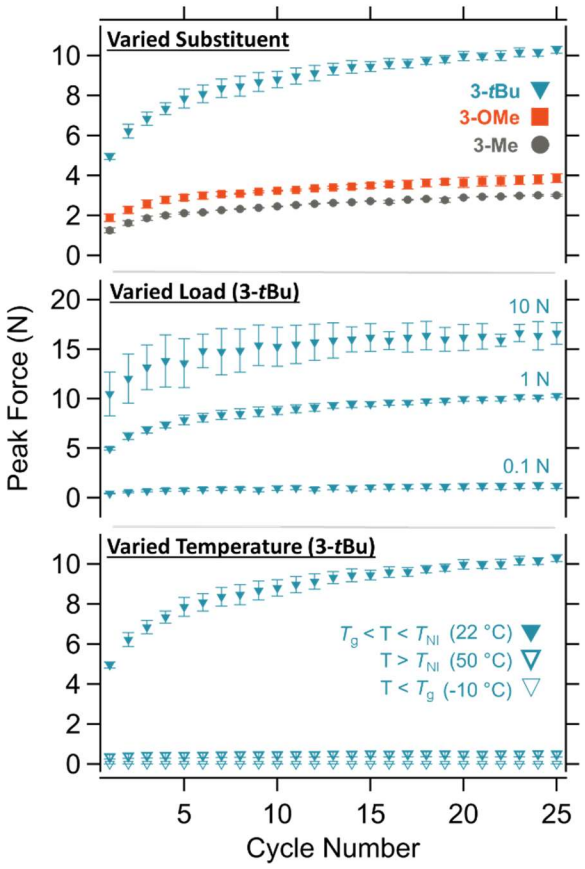

Figure 4.6: (top) Probe tack cycling data from experiments demonstrating the effect of the bulk of the mesogen used (**3-*t*Bu**, **3-OMe**, and **3-Me**) on the cyclic enhancement effect; (middle) Probe tack cycling data from experiments demonstrating the effect of variation in applied load on the cyclic enhancement effect; (bottom) Probe tack cycling data from experiments demonstrating the effect of variation in temperature on the cyclic enhancement effect.

disulfide (**3-mesogenic**, Fig S7A) or dynamic disulfides and no mesogens (**3-dynamic**, Fig S7B) were synthesized (full synthetic details available in SI). For **3-mesogenic**, the dynamic monomer (**2**) was swapped out with a nondynamic analogue (**2N**) of similar chemical structure where the disulfide was replaced with a carbon-carbon bond (Figure S4.6B). In the case of **3-dynamic**, the composition was identical to that of **3-*t*Bu** except for the use of **PDT** as the sole chain extender which results in a depression of the T_{NI} below room temperature effectively removing the nematic character of the material for room temperature probe tack testing (Figure S4.6C). Cyclic probe tack tests on **3-*t*Bu**, **3-mesogenic** and **3-dynamic** (Figure S4.7) were performed following the procedure previously outlined. Of the three materials, **3-dynamic** had the lowest relative performance in terms of both force output and rate of enhancement which is in line with the hypothesized importance of nematic character to the training effect. **3-mesogenic** fared better in both cases demonstrating noticeable enhancement with cycling in addition to an improved force of adhesion. However, it is interesting to note that when both functionalities are incorporated into a single material, a synergistic effect is observed resulting in a further improvement of adhesive character. This suggests that both the nematic character and dynamic bonds play a role in the PSA behavior exhibited by these materials.

All the studies above utilized polydomain LCEs films as the adhesive. If mesogen orientation is important in the adhesive properties of the LCE then it could be expected that monodomain films should exhibit very different adhesion characteristics. To this end stress relaxation experiments and cyclic probe tack tests were performed on both polydomain and monodomain **3-*t*Bu** films. Polydomain films were used as initially processed while the formation of a monodomain film of **3-*t*Bu** was achieved through a programming process where the film was strained to alignment and then exposed to UV-light to induce network rearrangement (Figure S4.8). This process locked in the alignment similar to what has been reported previously in the literature,[83] and the resulting adhesive films have the mesogens aligned parallel to the substrate. In addition, given the relatively low T_{NI} (~50 °C) it is possible to explore the isotropic **3-**

***t*Bu** film by slightly raising the temperature during testing to 50 °C. Each of the samples were then tested via shear stress relaxation (3% strain, 1 h) to determine the relative dissipative character of these three differently oriented materials (Figure 4.7A). After 60 s, the polydomain, monodomain, and isotropic materials had relaxed 91%, 89%, and 59% of their initial stress respectively confirming the importance of the liquid crystalline character as a relaxation mode in these materials. Subsequent tack testing (Figure 4.7B) yields results that follow a similar trend where the polydomain sample has the best adhesive performance followed by the monodomain and isotropic sample respectively. An observation of note is that while the trend is similar between the stress relaxation and probe tack data, the difference in adhesive quality between the polydomain and monodomain samples does not appear to be fully explained by the few percent

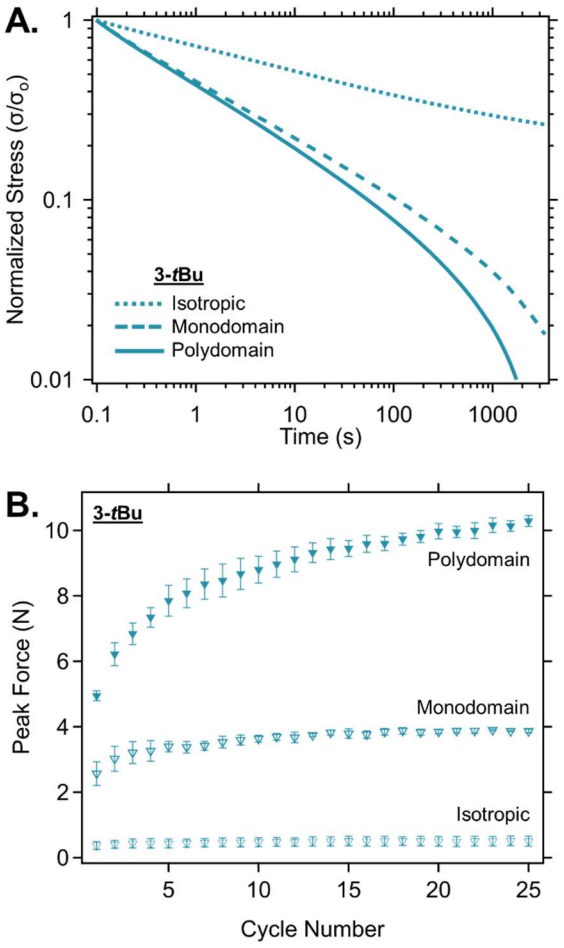

Figure 4.7: A. Shear stress relaxation experiments on **3-*t*Bu** under different orientations of the liquid crystalline; B. Probe tack cycling data from experiments demonstrating the effect of mesogen orientation polydomain and monodomain @ r.t. and isotropic @ 50 °C).

difference in their bulk stress relaxation values which suggests there may be additional mesogenic contributions beyond the dissipative character captured by these experiments that factor into the mechanism of adhesion for this system. As a means of further exploring the adhesive behavior of these dynamic LCEs, a series of rheological frequency studies were conducted to compare the samples against benchmarks for PSA character commonly employed in non-LC adhesives. Frequency sweeps from 0.01 to 100 rad s^{-1} were performed at temperatures near the desired operating temperature for the material of 22 °C (22 °C, 25 °C, 35 °C, and 45 °C). By applying the time-temperature superposition principle and the WLF fit, a master curve for each material was created from the frequency data (Figure 4.8A). Based on the generated master curves it is generally possible to predict the potential for PSA behavior of a polymeric material using two commonly employed metrics: the Dahlquist criterion and the Chang viscoelastic window (VW).[84,85] The Dahlquist criterion states that there exists, for a given material at its operating temperature, a critical storage modulus (3 x 10^5 Pa at 1.0 rad s^{-1}) above which materials lose a significant amount of tack rendering themnot useful as PSA materials.[84] The application of this metric to the master curves displayed in Figure 4.8A would suggest that all of the dynamic LCEs materials that were studied herein should possess poor PSA character as their storage moduli lie above the 3 x 10^5 Pa threshold despite what literature precedent has shown for nondynamic LCEs previously. As a further benchmark of the adhesive performance of these materials, the master curves can also be used to produce VWs for determining PSA character (see SI for full details). Based on the VWs formed for the dynamic LCEs (Figure 4.8B), all three materials overlap with the high shear PSA regime characterized by high G′ and G″. Interestingly, while the size of the LCE's viscoelastic window increases with increasing steric bulk of the mesogen's substituent the fraction of overlap with the traditional viscoelastic window decreases, suggesting that increasing the steric bulk of the mesogens should result in poorer adhesive properties. While the Dahlquist criterion and VW techniques are often reliably employed as measures of the PSA quality of a given material, their application to these LCE materials gives a counterintuitive result in this work. As such these traditional benchmarking techniques

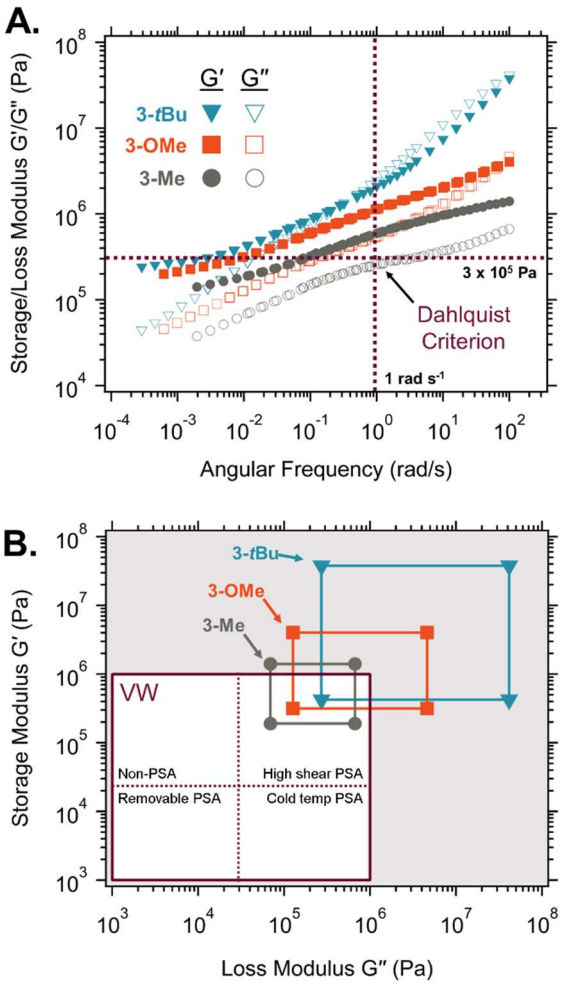

Figure 4.8: A. Master curves of storage modulus (solid shapes) and loss modulus (empty shapes) as a function of angular frequency for dynamic LCE materials with dashed lines to indicate the Dahlquist criterion (1 rad s^{-1} and 3 x 10^5 Pa); B. Viscoelastic windows of dynamic LCE materials plotted against the conventional viscoelastic window (10^3 – 10^6 in storage and loss modulus).

may not be generally appropriate for LCE materials as they do not directly account for the complex dissipative modalities stemming from the materials' mesogenic character. As a demonstration of the control that can be attained over the mechanical as both sets of benchmarking results contradict the existence of observed PSA behavior in LCE materials trainability of PSA character for the dynamic LCEs through applied force and temperature, sequential cycling experiments were carried out to determine the robustness of the cycling effect as it is erased and reengaged under different sets of conditions (Figure 4.9). Sequential cycling experiments were conducted in a similar fashion to the previous cycling tests at ambient conditions with the caveat that multiple sets of cycles at two alternating loading forces (F_{load} = 1 N or 0.1 N) were run

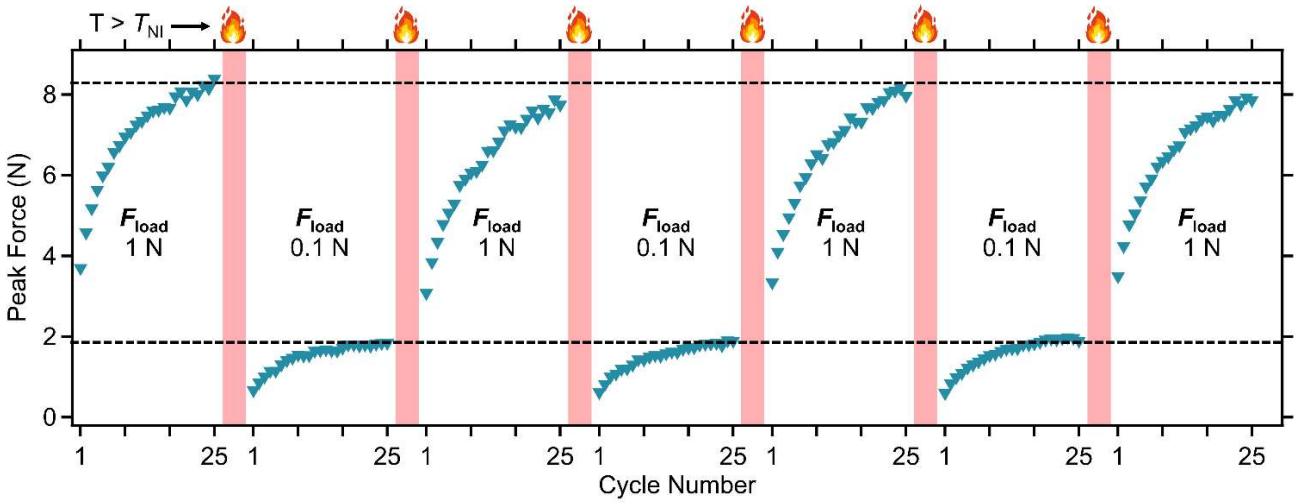

Figure 4.9: Multi-set experiment demonstrating the robustness of the cyclic enhancement of the PSA character of dynamic LCEs. Sets of 25 cycles were performed in series on a single sample of **3-tBu** with a thermal clearing above the T_{NI} in between sets demonstrating a recovery in performance that is proportional to the applied load.

in series on a single sample with a heating step (T > T_{NI}) in between each set to reset mesogen alignments that were mechanically induced by the compressive stresses applied to the dynamic LCE. As shown in Figure 4.6C heating above the T_{NI} allows for disruption of the LC interactions required for cyclic enhancement which implies that the adhesive behavior of a given material can be (re)trained for a different response under a new set of conditions

4.4 Conclusions

Dynamic LCEs comprised of mesogenic monomers with differing packing stabilities (**1-R**), a disulfide containing monomer (**2**), and di- and tetra-functional thiol components were shown to exhibit trainable stimuli-responsive MSA behavior. By activating dynamic disulfide bond exchange reactions in the bulk it is possible to induce network rearrangements that enable these materials to perform in a higher strength HMA context. Furthermore, despite what their viscoelastic behavior at room temperature would suggest via the Dahlquist criterion and viscoelastic windows, cyclic tack tests demonstrated that the dynamic LCEs were able to perform as robust PSAs with properties that can be (re)trained as a function of mechanical cycling and thermal clearing. This behavior is believed to be a result of engagement of the additional rotational mesogenic modes inherent to the polydomain liquid crystal phase present in LCE networks.

Additionally, varying the mesogens' structure has a pronounced effect on the adhesive properties, with LCEs with lower packing stabilities leading to improved PSA and HMA characteristics. As such, utilization of the relationships elucidated in this work between mesogenic character, dynamic bonds, and their effects on adhesion can be leveraged toward the development of the next generation of stimuli-responsive MSA materials.

4.5 Materials and Methods

4.5.1 Materials

Potassium carbonate was purchased from Fisher Scientific. 5-Bromo-1-pentene was purchased from Combi-Blocks. All other chemicals were purchased from Millipore-Sigma and were used as received unless noted otherwise. All solvents were purchased from Fisher Scientific and were used as received unless noted otherwise.

4.5.2 Methods

Synthesis of 4'-(Pent-1-enyloxy)benzoic acid

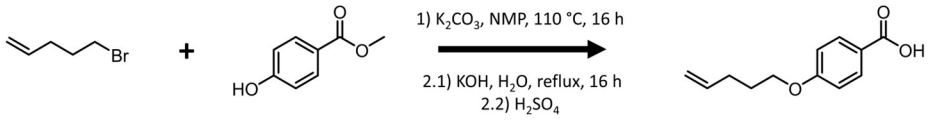

4′-(Pent-1-enyloxy)benzoic acid was synthesized using a modified version of previously published procedures.[1,2] 5-bromo-1-pentene (50 g, 0.336 mol, 1 eq), methyl-4-hyroxybenzoate (52.145 g, 0.342 mol, 1.02 eq), potassium carbonate (50.172 g, 0.362 mol, 1.08 eq) were all added to a flask containing N-methyl-2-pyrrolidone (150 mL, 3 vol). The flask was equipped with a condenser, and the reaction mixture was heated to 80°C while stirring. After observing an exotherm in the form of vigorous bubbling the temperature was raised to 110°C where the reaction was allowed to proceed for 16 h. The reaction mixture was then cooled to room temperature and added to a separatory funnel with toluene (300 mL) and water (100 mL).

The organic layer was washed three times with water whereafter the solvent was removed under vacuum. To the resulting oil was added 300 mL of 10 wt% aqueous potassium hydroxide solution. The reaction mixture was then heated to 110 °C and allowed to proceed for 16 h with stirring. After cooling to room temperature, the reaction mixture was extracted with ethyl ether (50 mL) three times. The aqueous layer was then diluted with water to a volume of 2 L while stirring whereupon concentrated sulfuric acid (25 mL) was added to adjust the solution to a pH of about 2. As the sulfuric acid is added, white solid began to precipitate from solution until the reaction mixture became a slurry that was difficult to stir magnetically. The solid was filtered from the aqueous solution using a Buchner funnel and recrystallized three times in hot ethanol yielding white crystals. (61 g, 88% yield) ^{1}H NMR (400 MHz, $CDCl_3$) δ 8.16 – 7.97 (m, 2H), 7.00 – 6.88 (m, 2H), 5.98 – 5.74 (m, 1H), 5.17 – 4.94 (m, 2H), 4.04 (t, J = 6.4 Hz, 2H), 2.25 (qd, J = 7.4, 1.4 Hz, 2H), 2.03 – 1.82 (m, 2H).

Synthesis of liquid crystal monomer (1-R)

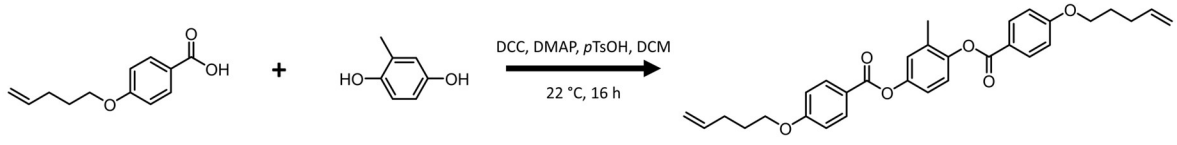

Liquid crystal monomer (**1**) was prepared using a previously reported procedure.[3] 4′-(Pent-1-enyloxy)benzoic acid (24.3 g, 0.118 mol, 1.95 eq), an R-substituted hydroquinone (~7.5 g, 0.060 mol, 1 eq), dicyclohexylcarbodiimide (28.692g, 0.139 mol, 2.4 eq), 4-dimethylaminopyridine (14.050g, 0.115 mol, 1.9 eq), and *p*-toluenesulfonic acid monohydrate (21.875 g, 0.115 mol, 1.9 eq) were added to a flask containing 400 mL of dichloromethane. The reaction mixture was stirred at room temperature (22 °C) for 16 hours. A solid white urea byproduct was then filtered out of the reaction mixture, and the solvent was then removed from the filtrate under vacuum. The remaining solid was then recrystallized three times in hot ethanol to afford white powdery crystals. (44.25 g, 75% yield) ^{1}H NMR (400 MHz, $CDCl_3$) δ 8.29 –

8.04 (m, 4H), 7.22 – 7.04 (m, 3H), 7.04 – 6.92 (m, 4H), 5.96 – 5.77 (m, 2H), 5.17 – 4.97 (m, 4H), 4.07 (td, J = 6.4, 2.0 Hz, 4H), 2.35 – 2.20 (m, 7H), 2.01 – 1.87 (m, 4H).

Synthesis of dynamic monomer (2)

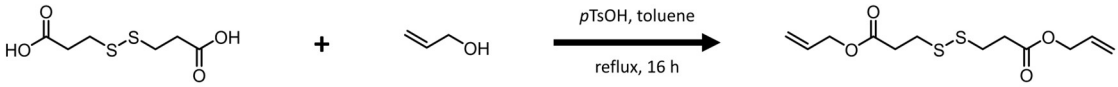

Dynamic monomer (**2**) was prepared using a modified version of a previously reported procedure.[4] 3,3′-Dithiodipropionic acid (10 g, 0.048 mol, 1 eq), allyl alcohol (6.911 g, 0.119 mol, 2.5 eq), and *p*-toluenesulfonic acid (0.913 g, 0.005 mol, 0.1 eq) were added to a flask containing 200 mL of toluene. The flask was equipped with a Dean-Stark apparatus, and the reaction mixture was stirred under reflux for 16 h. Upon cooling to room temperature, the reaction mixture was transferred to a separatory funnel and washed with an aqueous solution saturated with sodium bicarbonate three times and then water three times. The organic layer was isolated and had the solvent removed from it under vacuum. The resulting product was a yellow oil. (12.824 g, 92% yield) ^{1}H NMR (400 MHz, $CDCl_3$) δ 5.92 (ddt, J = 17.1, 10.4, 5.8 Hz, 2H), 5.40 – 5.20 (m, 4H), 4.61 (dt, J = 5.8, 1.4 Hz, 4H), 2.94 (td, J = 7.2, 0.7 Hz, 4H), 2.77 (td, J = 7.1, 0.7 Hz, 4H).

Synthesis of covalent monomer (2N)

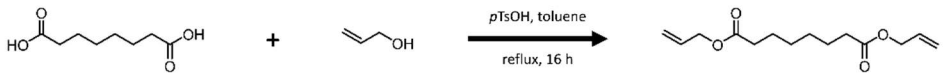

Nondynamic monomer (**2N**) was prepared using a modified version of a previously reported procedure.[4] Suberic acid (10 g, 0.057 mol, 1 eq), allyl alcohol (8.305 g, 0.143 mol, 2.5 eq), and *p*-toluenesulfonic acid (1.141 g, 0.006 mol, 0.1 eq) were added to a flask containing 200 mL of toluene. The flask was equipped with a Dean-Stark apparatus, and the reaction mixture was stirred under reflux for 16 h. Upon cooling to room temperature, the reaction mixture was transferred to a separatory funnel and washed with an aqueous

solution saturated with sodium bicarbonate three times and then water three times. The organic layer was isolated and had the solvent removed from it under vacuum. The resulting product was a yellow oil. (12.322 g, 85% yield) ^{1}H NMR (400 MHz, $CDCl_3$) δ 5.92 (ddt, J = 17.2, 10.4, 5.7 Hz, 2H), 5.37 – 5.15 (m, 4H), 4.57 (dt, J = 5.8, 1.4 Hz, 4H), 2.33 (t, J = 7.5 Hz, 4H), 1.73 – 1.54 (m, 4H), 1.43 – 1.28 (m, 4H).

Preparation of dynamic LCE networks (3-tBu, 3-OMe, 3-Me)

Dynamic LCE networks were prepared as follows utilizing a 1:1 ratio of thiol:alkene to ensure a stoichiometric number of functionalities. For example, synthesis of **3-*t*Bu** with a target molecular weight between crosslinks of 5,000 g/mol consisted of adding **1-*t*Bu** (2.032 g, 0.004 mol), **HDT** (0.282 g, 0.002 mol), **PDT** (0.342 g, 0.002 mol), **2** (0.363 g, 0.002 mol), **PETMP** (0.301 g, 0.0006 mol), and a catalytic amount of the thermal radical initiator azobisisobutyronitrile (AIBN) (0.049 g, 0.0003 mol) to a vial containing toluene (4 mL). The reaction mixture was thoroughly mixed and sonicated until all components were well dissolved in solution. The vial containing the reaction mixture was then heated to 100 °C for 16 h to initiate the polymerization and form a solid LCE plug.

Preparation of covalent LCE network (3-mesogenic)

Nondynamic LCE network (**3-mesogenic**) was prepared as follows utilizing a 1:1 ratio of thiol:alkene to ensure a stoichiometric number of functionalities. Synthesis of **3-mesogenic** consisted of adding **1-*t*Bu** (2.032 g, 0.00 mol), **HDT** (0.283 g, 0.002 mol), **PDT** (0.343 g, 0.002 mol), **2N** (0.317 g, 0.001 mol), **PETMP** (0.415 g, 0.002 mol), and a catalytic amount of photoinitiator 2,2-dimethoxy-2-phenylacetophenone (DMPA) (0.092 g, 0.0004 mol) to a vial containing tetrahydrofuran (4 mL). The reaction mixture was thoroughly mixed and sonicated until all components were well dissolved in solution. The reaction mixture was then transferred to a Teflon dish where it was exposed to UV light (320-390 nm, 2 x 30 s, 50 mW cm^{-2}) to initiate the polymerization and form a solid LCE film.

Preparation of amorphous network (3-dynamic)

Amorphous network (**3-dynamic**) was prepared as follows utilizing a 1:1 ratio of thiol:alkene to ensure a stoichiometric number of functionalities. Synthesis of **3-dynamic** consisted of adding **1** (2.033 g, 0.004 mol), **PDT** (0.679 g, 0.004 mol), **2** (0.363 g, 0.001 mol), **PETMP** (0.312 g, 0.0006 mol), and a catalytic amount of the thermal radical initiator azobisisobutyronitrile (AIBN) (0.049 g, 0.0003 mol) to a vial containing toluene (4 mL). The reaction mixture was thoroughly mixed and sonicated until all components were well dissolved in solution. The vial containing the reaction mixture was then heated to 100 °C for 16 h to initiate the polymerization and form a solid LCE plug.

Processing of dynamic LCE networks

Freshly cured dynamic LCE networks were cut into pieces and swelled in methylene chloride and deswelled in methanol three times each. The washed LCE pieces were then dried under vacuum at 60 °C for 16 h. Teflon with a thickness of 0.5 mm was cut into 5 cm x 5 cm square molds and used to set the thickness of the LCE films. Pieces of the washed and dried LCE were then thermally processed in the molds to make uniform films using a hot melt press at 180 °C for 1 h under 4 tons of pressure. The as-pressed films were then used as is for subsequent characterization.

Processing of nondynamic LCE network

Freshly cured nondynamic LCE network was washed by allowing the as-cured film to swell in a gently stirring mixture of tetrahydrofuran and methanol that was changed once every hour for 6 hours. The film was then dried in a vacuum oven at 60 °C under vacuum for 16 h. The washed and dried film was then used for subsequent characterization.

4.5.3 Instrumentation

All nuclear magnetic resonance (NMR) spectra were collected on a Bruker Avance III HD nanobay 400 MHz spectrometer.

All differential scanning calorimetry (DSC) thermograms were collected on a TA Instruments Discovery 2500 differential scanning calorimeter. Experiments were run following a (22/200/-90/200) ramp using heating and cooling rates of 10 °C min^{-1}. All curves shown are from the second heating.

All shear mechanical testing including dynamic temperature ramps and stress relaxation data were collected on TA Instruments ARES-G2 shear rheometer. Shear rheology experiments were performed on using a disk-shaped sample. (diameter = 8 mm, thickness = 0.43 mm)

All tensile mechanical testing of stud-pull and lap-shear adhesive joints were collected on a Zwick-Roell zwickiLine Z0.5 materials testing instrument. Tensile tests were performed on at 22 °C at a strain rate of 5 mm min^{-1} until failure.

All cyclic probe-tack testing was performed on a TA Instruments ARES-G2 shear rheometer. Probe-tack experiments were performed using a circular stainless-steel geometry (diameter = 8 mm) pressed into disk-shaped samples (diameter = 10 mm, thickness = 0.43 mm) affixed to the lower geometry with double sided tape.

All profilometry experiments were performed with a Bruker Dektak XT Stylus Profilometer. The system was equipped with a 12.5 μm radius tip and an applied stylus force of 3 mg was employed. Height profiles were collected across a 6000 μm scan over a duration of 30 s and an average roughness was calculated via the default software setup.

All wide-angle x-ray scattering (WAXS) data were collected on a SAXSLAB GANESHA 300XL utilizing a Cu Kα source ($\lambda = 0.154$ nm) at a voltage and power of 40 kV and 40 mA, respectively. Films were affixed to a stage with Kapton tape and shot directly and measured for 5 min at $q = 0.05 – 0.25$.

4.6 Supporting Information

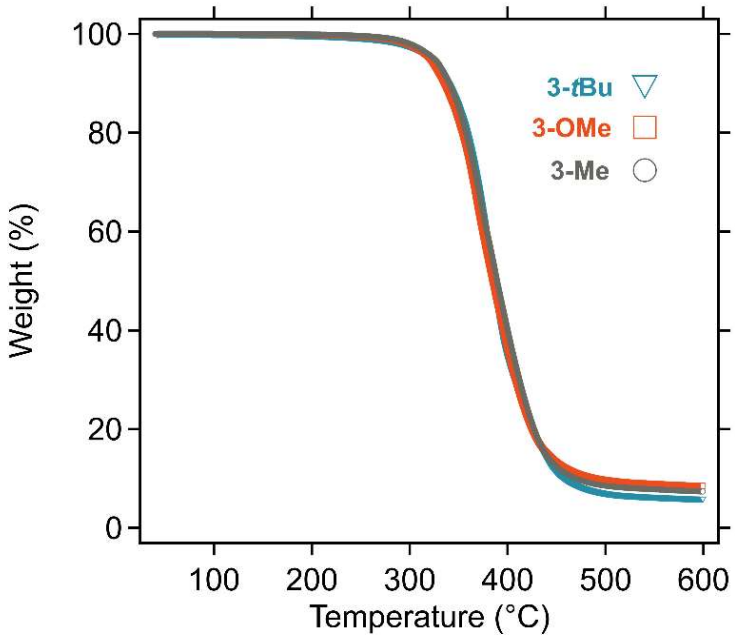

Figure S4.1: Thermogravimetric analysis (TGA) curves of **3-Me**, **3-OMe**, and **3-*t*Bu** indicating an onset of degradation for all three materials studied around 300°C.

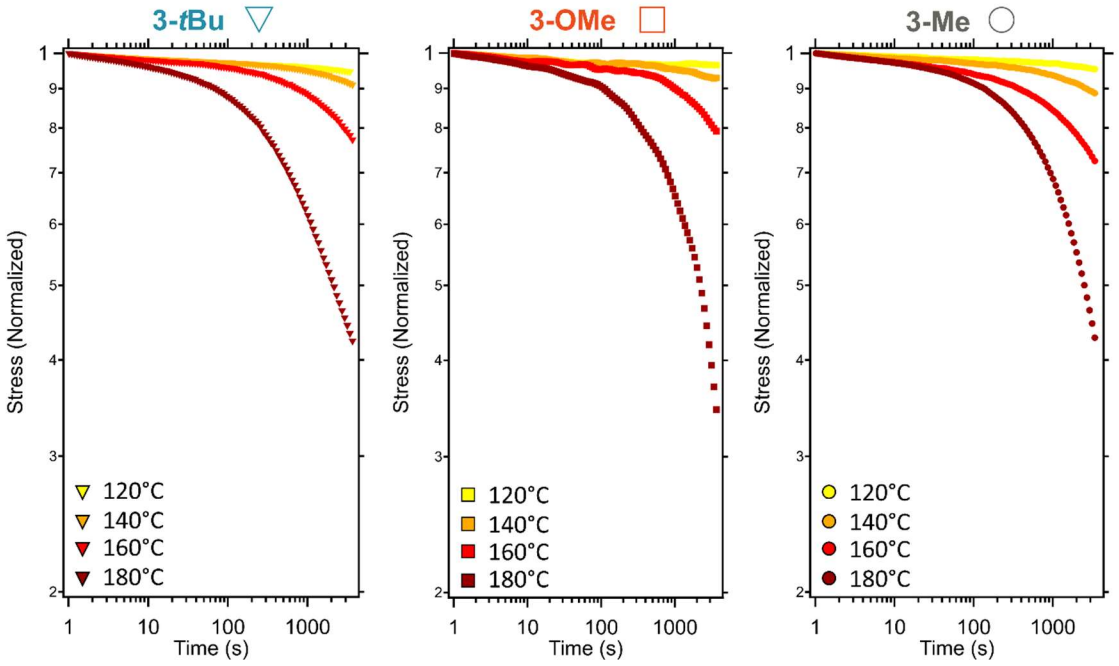

Figure S4.2: Stress relaxation of **3-Me**, **3-OMe**, and **3-*t*Bu** as a function of temperature demonstrating a lack of influence of LC domain stability on stress relaxation performed at temperatures above T_{NI}

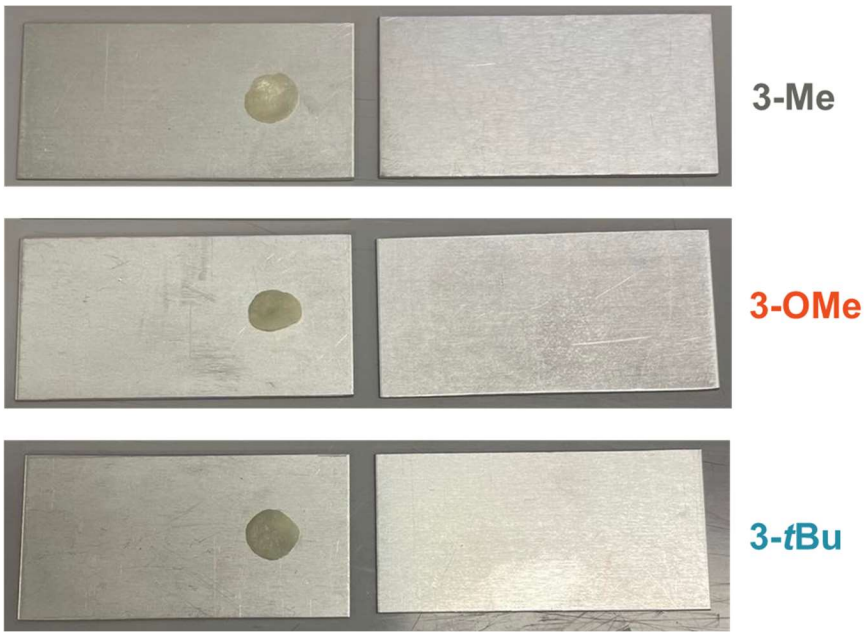

Figure S4.3: Representative images of lap shear hot melt joints after strength testing all demonstrating adhesive failure.

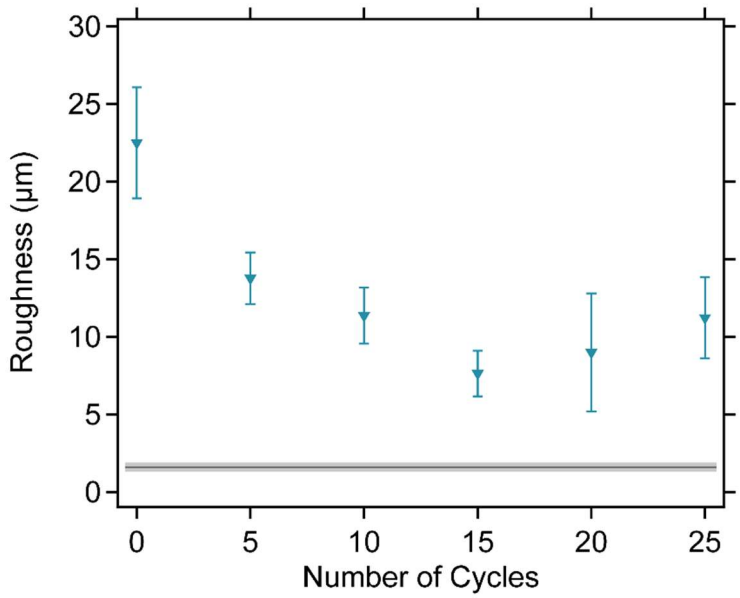

Figure S4.4: Average roughness values as a function of adhesive cycle number performed on films of **3-*t*Bu** compared to the average measured roughness of the tack geometry (grey bar).

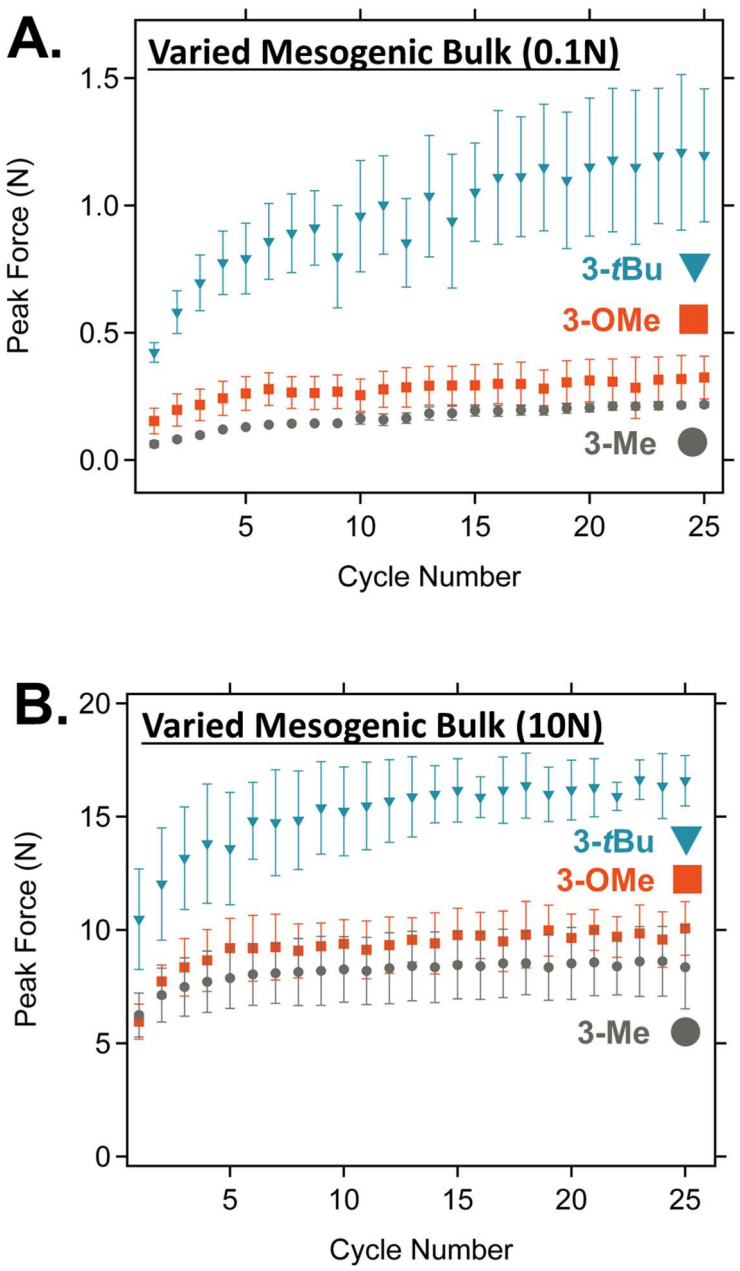

Figure S4.5: Probe tack cycling data from experiments demonstrating the effect of the bulk of the mesogen used (**3-tBu**, **3-OMe**, and **3-Me**) on the cyclic enhancement effect load forces of **A.** 0.1N; and **B.** 10N

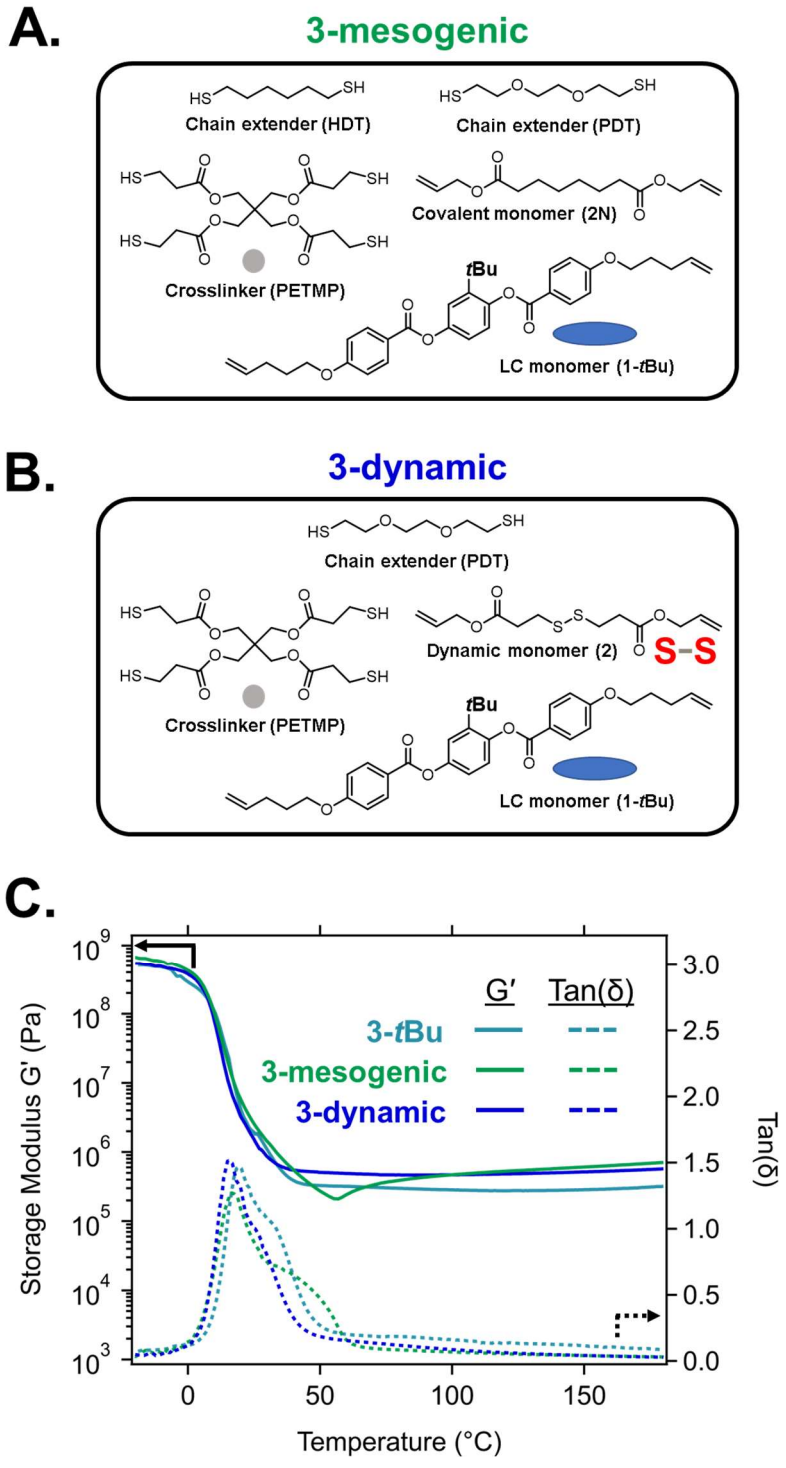

Figure S4.6: **A.** Synthetic composition of **3-mesogenic**; **B.** Synthetic composition of **3-dynamic**;and **C.** Shear rheology dynamic temperature ramps of storage modulus (solid lines) and tan(δ) (dashed lines) for dynamic LCE materials

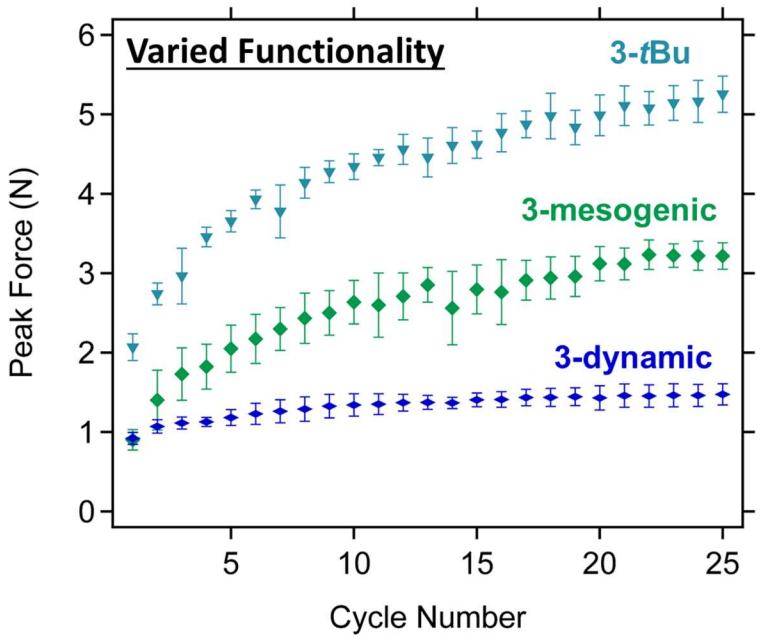

Figure S4.7: Probe tack cycling data from experiments demonstrating the effect of functionality used (**3-tBu**, **3-mesogenic**, and **3-dynamic**) on the cyclic enhancement effect

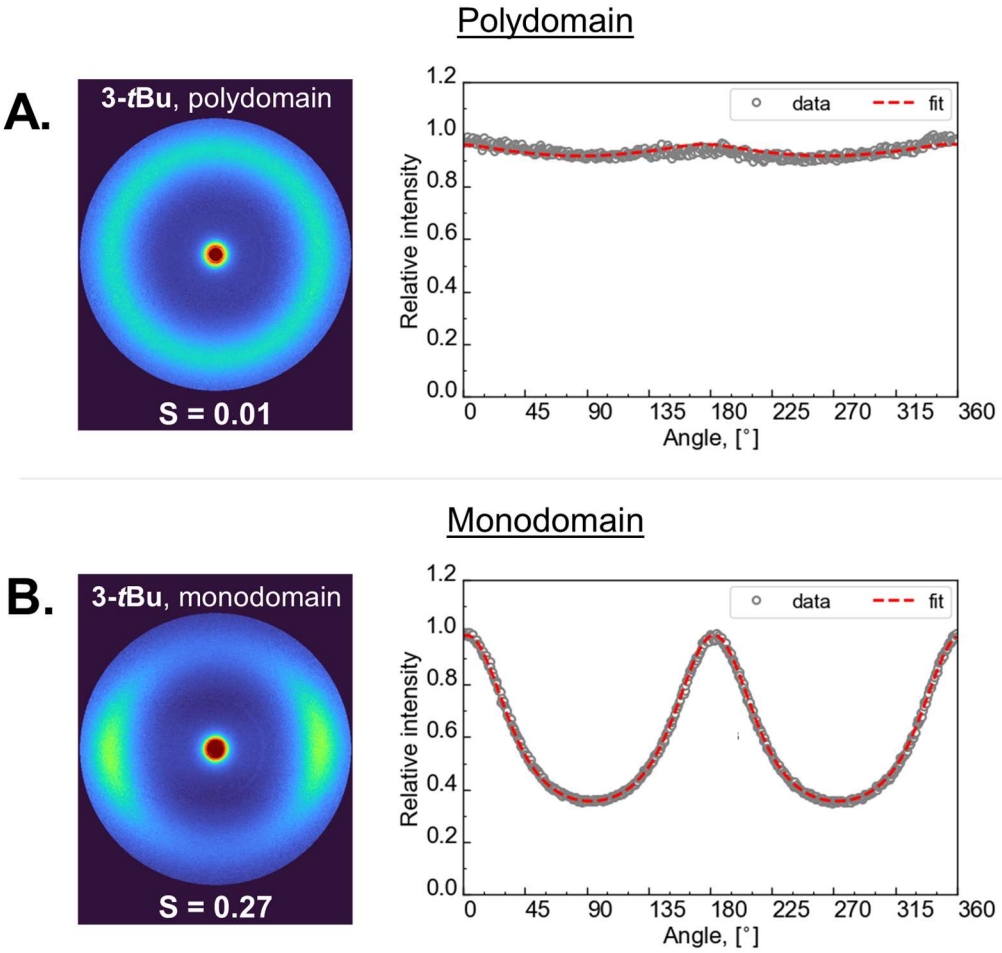

Figure S4.8: Wide angle x-ray scattering experiments quantifying the amount of alignment in **3-*t*Bu** in a **A.** polydomain state and **B.** monodomain state.

4.7 References

[1] D. Gonçalves, J. M. Bordado, A. C. Marques, R. Galhano dos Santos, *Polymers (Basel).* **2021**, *13*, 4086.

[2] P. Zuo, A. P. Vassilopoulos, *Int. Mater. Rev.* **2021**, *66*, 313.

[3] J. Michalak, *Ceramics* **2021**, *4*, 378.

[4] K. L. Van Landuyt, J. Snauwaert, J. De Munck, M. Peumans, E. Coutinho, K. Suzuki, Y. Yoshida, P. Lambrechts, B. Van Meerbeek, **2007**, *28*, 3757.

[5] S. Nagarkar, N. Theis-Mahon, J. Perdigão, *J. Biomed. Mater. Res. Part B Appl. Biomater.* **2019**, *107*, 2121.

[6] D. Dressano, M. V Salvador, M. Tavares, G. Maria, B. M. Fronza, M. Hadis, W. M. Palin, A. Fonseca, *J. Mech. Behav. Biomed. Mater.* **2020**, *110*, 103875.

[7] R. V. I. Gadhave, C. R. Gadhave, *Open J. Polym. Chem.* **2022**, *12*, 55.

[8] K. George, *Int. J. Res. Appl. Sci. Eng. Technol.* **2021**, *9*, 440.

[9] A. Emblem, M. Hardwidge, in *Packag. Technol.*, Elsevier, **2012**, pp. 381–394.

[10] M. Chen, Y. Wu, B. Chen, A. M. Tucker, A. Jagota, S. Yang, *Proc. Natl. Acad. Sci.* **2022**, *119*, 1.

[11] A. Tzagiollari, H. O. McCarthy, T. J. Levingstone, N. J. Dunne, *Bioengineering* **2022**, *9*, 250.

[12] B. Xue, J. Gu, L. Li, W. Yu, S. Yin, M. Qin, Q. Jiang, W. Wang, Y. Cao, *Nat. Commun.* **2021**, *12*, 7156.

[13] R. Kato, P. Mirmira, A. Sookezian, G. L. Grocke, S. N. Patel, S. J. Rowan, *ACS Macro Lett.* **2020**, *9*, 500.

[14] R. Aradhana, S. Mohanty, S. Kumar, *Int. J. Adhes. Adhes.* **2020**, *99*, 102596.

[15] Y. Ko, J. Oh, K. T. Park, S. Kim, W. Huh, B. J. Sung, J. A. Lim, S. S. Lee, H. Kim, *ACS Appl. Mater. Interfaces* **2019**, *11*, 37043.

[16] B. T. Michal, E. J. Spencer, S. J. Rowan, *ACS Appl. Mater. Interfaces* **2016**, *8*, 11041.

[17] E. Cudjoe, K. M. Herbert, S. J. Rowan, *ACS Appl. Mater. Interfaces* **2018**, *10*, 30723.

[18] K. M. Herbert, N. D. Dolinski, N. R. Boynton, J. G. Murphy, C. A. Lindberg, S. J. Sibener, S. J. Rowan, *ACS Appl. Mater. Interfaces* **2021**, *13*, 27471.

[19] A. Bratek-Skicki, *Appl. Surf. Sci. Adv.* **2021**, *4*, 100068.

[20] C. Li, M. Li, Z. Ni, Q. Guan, B. R. K. Blackman, E. Saiz, *J. R. Soc. Interface* **2021**, *18*, 20210162.

[21] Q. Guo, J. Chen, J. Wang, H. Zeng, J. Yu, *Nanoscale* **2020**, *12*, 1307.

[22] Q. Peng, J. Chen, T. Wang, L. Gong, X. Peng, M. Wu, Y. Ma, F. Wu, D. Yang, H. Zhang, H. Zeng, *J. Mater. Chem. A* **2021**, *9*, 12988.

[23] Z. Wang, L. Guo, H. Xiao, H. Cong, S. Wang, *Mater. Horizons* **2020**, *7*, 282.

[24] G. Habenicht, *Applied Adhesive Bonding*, Wiley, **2008**.

[25] T. P. Lecompte, M. P. Bernimoulin, *Innovations in Pressure-Sensitive Adhesive Products*, **2015**.

[26] B. T. Michal, E. J. Spencer, S. J. Rowan, *ACS Appl. Mater. Interfaces* **2016**, *8*, 11041.

[27] E. Cudjoe, K. M. Herbert, S. J. Rowan, *ACS Appl. Mater. Interfaces* **2018**, *10*, 30723.

[28] C. A. Lindberg, A. E. Roberson, E. Ghimire, J. E. Hertzog, N. R. Boynton, G. Liu, D. K. Schneiderman, S. N. Patel, S. J. Rowan, *Chem. – A Eur. J.* **2025**, *31*, e202404672.

[29] I. Benedek, M. M. Feldstein, *Fundamentals of Pressure Sensitivity*, CRC Press, **2008**.

[30] Z. Liu, Y. Tang, Y. Chen, Z. Lu, Z. Rui, *Chem. Eng. J.* **2024**, *497*, 154710.

[31] R. J. Wojtecki, M. A. Meador, S. J. Rowan, *Nat. Mater.* **2011**, *10*, 14.

[32] S. J. Rowan, S. J. Cantrill, G. R. L. Cousins, J. K. M. Sanders, J. F. Stoddart, *Angew. Chemie - Int. Ed.* **2002**, *41*, 898.

[33] K. M. Herbert, P. T. Getty, N. D. Dolinski, J. E. Hertzog, D. de Jong, J. H. Lettow, J. Romulus, J. W. Onorato, E. M. Foster, S. J. Rowan, *Chem. Sci.* **2020**, *11*, 5028.

[34] E. Ghimire, C. A. Lindberg, T. D. Jorgenson, C. Chen, J. J. de Pablo, N. D. Dolinski, S. J. Rowan, *Macromolecules* **2024**, *57*, 682.

[35] Y. Yang, F. S. Du, Z. C. Li, *ACS Appl. Polym. Mater.* **2020**, *2*, 5630.

[36] L. Li, X. Chen, J. M. Torkelson, *ACS Appl. Polym. Mater.* **2020**, *2*, 4658.

[37] H. Y. Tsai, Y. Nakamura, W. H. Hu, T. Fujita, M. Naito, *Mater. Adv.* **2021**, *2*, 5047.

[38] S. Luo, N. Wang, Y. Pan, B. Zheng, F. Li, S. Dong, *Small* **2024**, *20*, 1.

[39] L. Zhang, L. Chen, S. J. Rowan, *Macromol. Chem. Phys.* **2017**, *218*, 1600320.

[40] L. Imbernon, E. K. Oikonomou, S. Norvez, L. Leibler, *Polym. Chem.* **2015**, *6*, 4271.

[41] L. Chen, L. Zhang, P. J. Griffin, S. J. Rowan, *Macromol. Chem. Phys.* **2020**, *221*, 1900440.

[42] B. T. Michal, C. A. Jaye, E. J. Spencer, S. J. Rowan, *ACS Macro Lett.* **2013**, *2*, 694.

[43] G. L. Grocke, H. Zhang, S. S. Kopfinger, S. N. Patel, S. J. Rowan, *ACS Macro Lett.* **2021**, *10*, 1637.

[44] J. M. A. Carnall, C. A. Waudby, A. M. Belenguer, M. C. A. Stuart, J. J.-P. Peyralans, S. Otto, *Science (80-.).* **2010**, *327*, 1502.

[45] U. F. Fritze, M. Von Delius, *Chem. Commun.* **2016**, *52*, 6363.

[46] Y. Li, Y. Zhang, O. Rios, J. K. Keum, M. R. Kessler, *RSC Adv.* **2017**, *7*, 37248.

[47] S. Patai, Z. Rappoport, *Sulphur-Containing Functional Groups (1993)*, John Wiley & Sons, Inc., Chichester, UK, **1993**.

[48] T. Ohzono, M. O. Saed, E. M. Terentjev, *Adv. Mater.* **2019**, *31*, 1902642.

[49] H. J. Farre-Kaga, M. O. Saed, E. M. Terentjev, *Adv. Funct. Mater.* **2022**, *32*, 2110190.

[50] J. Cui, D. M. Drotlef, I. Larraza, J. P. Fernández-Blázquez, L. F. Boesel, C. Ohm, M. Mezger, R. Zentel, A. Del Campo, *Adv. Mater.* **2012**, *24*, 4601.

[51] H. Guo, M. O. Saed, E. M. Terentjev, *Macromolecules* **2023**, *56*, 6247.

[52] R. Annapooranan, S. Suresh Jeyakumar, R. J. Chambers, R. Long, S. Cai, *Adv. Funct. Mater.* **2024**, *34*, 2309123.

[53] Y. Wu, B. D. Clarke, K. M. Liechti, Z. A. Page, *Chem. Mater.* **2024**, *36*, 8066.

[54] P. G. De Gennes, *C. R. Acad. Sci. B* **1975**, *281*, 101.

[55] H. Finkelmann, H.-J. Kock, G. Rehage, *Die Makromol. Chemie, Rapid Commun.* **1981**, *2*, 317.

[56] M. Warner, E. M. Terentjev, *International Series of Monographs on Physics: Liquid Crystal Elastomers*, Oxford University Press, Oxford, **2007**.

[57] K. M. Herbert, H. E. Fowler, J. M. McCracken, K. R. Schlafmann, J. A. Koch, T. J. White, *Nat. Rev. Mater.* **2021**, *0123456789*, DOI 10.1038/s41578-021-00359-z.

[58] T. J. White, D. J. Broer, *Nat. Mater.* **2015**, *14*, 1087.

[59] D. R. Corbett, J. M. Adams, *Soft Matter* **2013**, *9*, 1151.

[60] T. Ohzono, Y. Norikane, M. O. Saed, E. M. Terentjev, *ACS Appl. Mater. Interfaces* **2020**, *12*, 31992.

[61] N. Deneke, A. L. Chau, C. S. Davis, *Soft Matter* **2021**, *17*, 863.

[62] Z. Wang, S. Cai, *J. Mater. Chem. B* **2020**, *8*, 6610.

[63] M. O. Saed, A. Gablier, E. M. Terentjev, *Chem. Rev.* **2022**, *122*, 4927.

[64] C. Valenzuela, Y. Chen, L. Wang, W. Feng, *Chem. – A Eur. J.* **2022**, *28*, e202201957.

[65] D. Mistry, N. A. Traugutt, K. Yu, C. M. Yakacki, *J. Appl. Phys.* **2021**, *129*, DOI 10.1063/5.0044533.

[66] R. Lan, X. Hu, J. Chen, X. Zeng, X. Chen, T. Du, X. Song, H. Yang, *Responsive Mater.* **2024**, *2*, e20230030.

[67] H. J. Hong, S. Y. Park, *J. Ind. Eng. Chem.* **2022**, *110*, 424.

[68] M. Barnes, S. Cetinkaya, A. Ajnsztajn, R. Verduzco, *Soft Matter* **2022**, 5074.

[69] M. O. Saed, R. H. Volpe, N. A. Traugutt, R. Visvanathan, N. A. Clark, C. M. Yakacki, *Soft Matter* **2017**, *13*, 7537.

[70] H. Kim, J. M. Boothby, S. Ramachandran, C. D. Lee, T. H. Ware, *Macromolecules* **2017**, *50*, 4267.

[71] D. J. Broer, G. P. Crawford, S. Žumer, *Cross-Linked Liquid Crystalline Systems: From Rigid Polymer Networks to Elastomers*, CRC Press, Boca Raton, **2011**.

[72] M. A. Qaddoura, K. D. Belfield, *Int. J. Mol. Sci.* **2009**, *10*, 4772.

[73] Y.-K. Lee, K. Onimura, H. Tsutsumi, T. Oishi, *Polym. J.* **2000**, *32*, 395.

[74] W. H. Carothers, *Trans. Faraday Soc.* **1936**, *32*, 39.

[75] I. A. Rousseau, H. Qin, P. T. Mather, *Macromolecules* **2005**, *38*, 4103.

[76] M. O. Saed, A. H. Torbati, C. A. Starr, R. Visvanathan, N. A. Clark, C. M. Yakacki, *J. Polym. Sci. Part B Polym. Phys.* **2017**, *55*, 157.

[77] Z. Wen, M. K. McBride, X. Zhang, X. Han, A. M. Martinez, R. Shao, C. Zhu, R. Visvanathan, N. A. Clark, Y. Wang, K. Yang, C. N. Bowman, *Macromolecules* **2018**, *51*, 5812.

[78] D. W. Hanzon, N. A. Traugutt, M. K. McBride, C. N. Bowman, C. M. Yakacki, K. Yu, *Soft Matter* **2018**, *14*, 951.

[79] C. A. Lindberg, E. Ghimire, C. Chen, S. Lee, N. D. Dolinski, J. M. Dennis, S. Wang, J. J. de Pablo, S. J. Rowan, *J. Polym. Sci.* **2024**, *62*, 907.

[80] B. Chen, D. A. Dillard, J. G. Dillard, R. L. Clark, *J. Adhes.* **2001**, *75*, 405.

[81] S. Ebnesajjad, Ed., *Adhesives Technology Handbook*, William Andrew Inc., Norwich, **2009**.

[82] A. Pizzi, K. Mittal, Eds., *Handbook of Adhesive Technology, Third Edition*, CRC Press, Boca Raton, **2017**.

[83] Z. Wang, H. Tian, Q. He, S. Cai, *ACS Appl. Mater. Interfaces* **2017**, *9*, 33119.

[84] C. A. Dahlquist, *Pressure Sensitive Adhesives*, Marcel Dekker, Inc., **1969**.

[85] E. P. Chang, *J. Adhes.* **1991**, *34*, 189.

CHAPTER 5
SUMMARY AND OUTLOOK

5.1 Summary

As polymer scientists gain a more complete understanding of the mechanisms that govern fundamental polymer phenomena, it becomes more straightforward to effectively engineer these concepts into the next generation of functional materials. By incorporating multiple active modalities into individual polymeric materials, the potential appears for classes of materials with large property profiles whose useful lifetimes can be extended by their widened application scope. The work in this thesis builds upon this paradigm by studying the design of adaptive polymeric materials with multiple levels of action through the incorporation of multiple independently accessible stimuli-responsive moieties.

While there are many dynamic bond-containing liquid crystal elastomers (LCEs) that have been studied to date, there is a host of understanding that still needs to be developed about the interactions that these different moieties have with one another and how to best leverage them toward materials with useful properties. As such, these materials serve as an effective platform for studying multiple stimuli-responsive moieties within the context of a single polymeric material. The first aim of this work was to develop systems that allowed for the systematic study of dynamic bond placement to better understand how molecular control over dynamic topology relative to the molecular network architecture of the material translates to the tailorability of the bulk properties of the material. The second aim studied herein demonstrated that the incorporation of physical crosslinking through phase-separation into LC polymers (despite using labile metallosupramolecular interactions) was able to produce robust functional materials capable of

acting as adhesives with different levels of performance. The final aim of this work looked to modify the strength of the LC interactions themselves and determine how mechanical perturbations of these materials could produce adaptive training responses that could be imparted and erased solely through thermal manipulation of the LC phase.

5.2 Outlook

One obstacle to overcome with the widespread adoption of next-generation LC polymers, even in performance applications, is the cost. LC building blocks are significantly more expensive and intensive to produce than the monomers currently isolated and used in the production of today's commodity polymers. Further advancements in the development of cheaper feedstocks for LC materials or utilizing systems that can incorporate LC units at lower loadings while retaining their desirable properties could be promising alternatives to make this class of materials more viable. Further study of materials that combine LC interactions with other morphological features like phase separation or spontaneous self-assembly could also be a route for producing materials with novel sets of properties. Incorporating dynamic linkages into LC materials that can be switched on and off while maintaining material cohesion to allow for the reorganization of polymer strands into different morphologies is one potential avenue for the selective modulation of bulk properties. By furthering the study of LC polymers through the incorporation of additional stimuli-responsive moieties, this utility of this class of materials will only continue to grow into new and exciting application areas.